



8-2014

## Structure, Function and Regulation of Two Isoforms of Glutamine Synthetase from Soybean Root Nodules

Pintu Daulatrao Masalkar

*University of Tennessee - Knoxville*, pmasalka@vols.utk.edu

Follow this and additional works at: [https://trace.tennessee.edu/utk\\_graddiss](https://trace.tennessee.edu/utk_graddiss)

 Part of the [Biochemistry Commons](#)

---

### Recommended Citation

Masalkar, Pintu Daulatrao, "Structure, Function and Regulation of Two Isoforms of Glutamine Synthetase from Soybean Root Nodules. " PhD diss., University of Tennessee, 2014.  
[https://trace.tennessee.edu/utk\\_graddiss/2842](https://trace.tennessee.edu/utk_graddiss/2842)

This Dissertation is brought to you for free and open access by the Graduate School at TRACE: Tennessee Research and Creative Exchange. It has been accepted for inclusion in Doctoral Dissertations by an authorized administrator of TRACE: Tennessee Research and Creative Exchange. For more information, please contact [trace@utk.edu](mailto:trace@utk.edu).

To the Graduate Council:

I am submitting herewith a dissertation written by Pintu Daulatrao Masalkar entitled "Structure, Function and Regulation of Two Isoforms of Glutamine Synthetase from Soybean Root Nodules." I have examined the final electronic copy of this dissertation for form and content and recommend that it be accepted in partial fulfillment of the requirements for the degree of Doctor of Philosophy, with a major in Biochemistry and Cellular and Molecular Biology.

Daniel M. Roberts, Major Professor

We have read this dissertation and recommend its acceptance:

Elizabeth Howell, Gladys Alexandre, Beth Mullin, Feng Chen

Accepted for the Council:

Carolyn R. Hodges

Vice Provost and Dean of the Graduate School

(Original signatures are on file with official student records.)

**Structure, Function and Regulation of Two  
Isoforms of Glutamine Synthetase from Soybean  
Root Nodules**

A Dissertation Presented for the

Doctor of Philosophy

Degree

The University of Tennessee, Knoxville

Pintu Daulatrao Masalkar  
August 2014

## **ACKNOWLEDGEMENTS**

It was my privilege to work with Dr. Daniel M Roberts, my PhD adviser. I would like to thank him for making me what I am today. I like his approach of following the results and not chasing a hypothesis. I am sure his constant suggestions about paying attention to details will help me in my future endeavors. He is not only a good scientist, he is also a very good person. I am thankful to him for keeping patience and helping me to get through difficult times.

I would like to thank my committee members Elizabeth Howell, Gladys Alexandre, Beth Mullin and Feng Chen for their guidance and insightful recommendations. They were very accessible, helpful and provided constructive criticism of my research. I would like to thank Dr. Howell for giving insightful recommendations for my binding studies and analytical ultracentrifugation experiments.

I would like to thank Ian Wallace for his guidance at the beginning of my PhD work. I liked his dedication towards work and his critical thinking. He influenced me in a big way during my early days in Dr. Roberts lab which played a big role in my decision of joining the lab. I thank him for trusting me to continue his work in this lab and hope that I worked to his expectations. I would also like to thank Eric Vincill, Won-Gyu Choi and Jin Ha Hwang for providing me the knowledge, good company and all the support during my early days at UT.

I would also like to thank a number of people in the lab for giving me joyous times. Ansul Lokdarshi is like a brother to me and was always available for good scientific conversations. He has a critical mind which will help him to



achieve big scientific goals. Tian Li is an all-rounder student in the lab. I always admired her dedication and hard working nature and wished to be more like her. She has this ability to do things without any hesitation which always amused me. I had the pleasure of working with Craig Conner, the nicest person I know of. Words are not enough to thank Craig Conner for being such a sport and being so kind. If it wasn't for him, my English would have been a big problem for my committee. His attention to details will help him to succeed in his scientific carrier. I would also like to thank Dr. Pratyush Routray for having insightful conversations about plant transformation, nodulation and life after PhD. All these people are my friends for life and I will cherish all the time I spent with them.

I would also like to thank my friends and family for being with me during this whole time. I would like to thank Sumit Goswami and Ritin Sharma for their support. I would like to specially thank my wife Pradnya for putting up with me and getting through the last few years of my PhD. I truly could not have done this without her and I thank her from the bottom of my heart. I would finally like to dedicate this dissertation to my parents who managed to get me to the position where I can follow my dreams.

## ABSTRACT

Glutamine synthetase (GS) is a major ammonia assimilatory enzyme in soybean nodules. The four isoforms of cytosolic glutamine synthetase (GS<sub>1</sub>[glutamine synthetase 1] $\beta$ [beta]1, GS<sub>1</sub> $\beta$ 2, GS<sub>1</sub> $\gamma$ [gamma]1 and GS<sub>1</sub> $\gamma$ 2) present in soybean nodules are 80% identical with respect to amino acid sequence, and share similar kinetic properties. It is shown all major GS<sub>1</sub> isoforms interact with nodulin 26, a member of the aquaporin family of membrane channels. Nodulin 26 is the major protein component of the symbiosome membrane (SM), where it serves a function as an ammonia and water channel. The site of interaction of GS on nodulin 26 is the cytosolic C-terminus, where it binds with 1:1 stoichiometry. The binding of GS is proposed to dock the enzyme to the cytosolic surface of the SM. This would promote efficient assimilation of fixed nitrogen, as well as prevent potential ammonia toxicity, by futile cycling of ammonia/ammonium across the SM. Quantitative PCR analysis of the transcripts of all the isoforms from soybean tissues shows that GS<sub>1</sub> $\gamma$  are the nodule-specific isoforms, but that the GS<sub>1</sub> $\beta$  isoforms are highly expressed and the highest transcripts in nodules is GS<sub>1</sub> $\beta$ 1. Further investigation of GS<sub>1</sub> isoforms showed that they are subjected to differential regulation by thiol based disulfide bond formation. Specifically, GS<sub>1</sub> $\gamma$ 1 is sensitive to inhibition by reversible oxidation whereas the GS<sub>1</sub> $\beta$ 1 is not sensitive to oxidizing conditions. Site-directed mutagenesis of the GS<sub>1</sub> $\gamma$ 1 isoform showed that the oxidation observed is due to reversible disulfide bond formation through intersubunit cys92 and cys159 across the shared active site. Analytical ultracentrifugation studies

showed a difference in the native oligomeric molecular weight of the two isoforms, with GS<sub>1</sub>β1 forming a decamer and GS<sub>1</sub>γ1 forming a dodecamer. It is hypothesized that these differences in quaternary structure is linked to their different sensitivities to thiol based regulation, possibly due to distinct positioning of the intersubunit cysteine sulfhydryls. The reversible oxidation observed for GS<sub>1</sub>γ1 is unique to this isoform and may serve as an additional level of regulation in response to oxygen tension in the infected cell, as well as in response to reactive oxygen production during stress responses.

## TABLE OF CONTENTS

<b>CHAPTER I Introduction.....</b>	<b>1</b>
<b>1.1. Nitrogen: A major macronutrient of plants .....</b>	<b>1</b>
<b>1.2. Endosymbiotic nitrogen fixation .....</b>	<b>3</b>
I. Establishment of symbiosis.....	4
i. The role of flavonoids and nod factors in initiation of symbiosis .....	4
ii. Entry of rhizobia into a host plant .....	7
II. Nodule morphology and physiology .....	9
III. Transport of metabolites through symbiosome membrane.....	11
IV. Nodulin 26 as an ammonia channel on the symbiosome membrane .....	14
V. Assimilation of ammonia in the plant cytosol .....	18
<b>1.3. Glutamine synthetase.....</b>	<b>20</b>
I. The central role of glutamine synthetase in plant nitrogen metabolism .....	26
II. Types of glutamine synthetases in plants .....	28
<b>1.4. Goal of the research work.....</b>	<b>30</b>
<b>CHAPTER II Materials and methods.....</b>	<b>33</b>
<b>2.1. Plant growth conditions .....</b>	<b>33</b>
<b>2.2. RNA extraction and cDNA synthesis .....</b>	<b>34</b>
<b>2.3. Molecular cloning of cytosolic glutamine synthetase isoforms from</b> nitrogen-fixing soybean root nodules .....	35
<b>2.4. Q- PCR expression analysis .....</b>	<b>39</b>
<b>2.4. Site directed mutagenesis of GS.....</b>	<b>41</b>
<b>2.5. Purification of native nodule and recombinant soybean GS<sub>1</sub> isoforms from</b> <i>E. coli</i> expression clones .....	47

2.6. Glutamine synthetase (GS) activity assay .....	48
2.7. Determination of free cysteinyl residues in reduced and oxidized GS <sub>1γ1</sub> ..	51
2.8. Affinity chromatography on peptide resins .....	52
2.9. Mass spectrometry .....	55
2.10. Two-dimensional electrophoresis .....	56
2.11. Symbiosome membrane binding assays .....	57
2.12. Fluorescence binding assays .....	59
2.13. <i>In vitro</i> kinase assay and effect of phosphorylation on GS activity .....	60
2.14. Crosslinking methods .....	61
2.15. Bimolecular fluorescence complementation (BiFC) assay .....	62
2.16. Protein analytical techniques .....	66
2.17. Molecular modeling techniques .....	69
<b>CHAPTER III Results .....</b>	<b>70</b>
3.1. Interaction of glutamine synthetase with nodulin 26 .....	70
I. Isolation of proteins interacting with the C-terminus of nodulin 26 .....	70
II. Identification of the 40 kDa protein interacting with nodulin 26 .....	73
III. Determination of the K <sub>d</sub> for the interaction of glutamine synthetase with the C-terminal peptide of nodulin 26 .....	79
IV. Interaction of glutamine synthetase with full-length nodulin 26. ....	82
V. Interaction of glutamine synthetase with native nodulin 26 on symbiosome membrane .....	92
VI. Effect of phosphorylation of nodulin 26 on interaction with glutamine synthetase .....	95
VII. Determination of the interaction site for nodulin 26 on glutamine synthetase. ....	97

<b>3.2. Differential regulation of cytosolic glutamine synthetase isoforms from soybean root nodules by reversible oxidation .....</b>	<b>110</b>
I. Selective inhibition of cytosolic glutamine synthetase isoforms from soybean root nodules by oxidation. ....	113
II. Reversibility of cysteine-specific oxidation of GS <sub>1</sub> γ1.....	117
III. Intersubunit disulfide bond formation in GS monomers results in inhibition of GS <sub>1</sub> γ1.....	121
IV. GS <sub>1</sub> γ1 and GS <sub>1</sub> β1 form distinct oligomeric structures. ....	127
<b>CHAPTER IV Discussion .....</b>	<b>139</b>
<b>4.1. Interaction of glutamine synthetase with nodulin 26 .....</b>	<b>139</b>
<b>4.2. Regulation of glutamine synthetase by reversible oxidation .....</b>	<b>149</b>
<b>4.3. Potential role of thiol regulation in nodule GS function .....</b>	<b>151</b>
<b>LIST OF REFERENCES.....</b>	<b>158</b>
<b>Vita.....</b>	<b>200</b>

## LIST OF TABLES

Table 2.1: - Oligonucleotide primers used for cloning of soybean glutamine synthetase isoforms. ....	36
Table 2.2: - Oligonucleotide primers used for Q-PCR analysis. ....	40
Table 2.3: - Oligonucleotide primers used for generating site-directed GS <sub>1</sub> mutants. ....	43
Table 2.4: - Oligonucleotide primers used for chimera cloning. ....	46
Table 2.5: - Sequences of nodulin 26 C-terminal peptides. ....	53
Table 2.6: - Oligonucleotide primers used for generation of BiFC interaction plasmid constructs. ....	63
Table 3.1.1: - Mass of 40 kDa protein tryptic peptides determined by MALDI-TOF. ....	77
Table 3.1.2: - List of GS tryptic peptides involved in crosslinking with CK-25. ....	103
Table 3.1.3: - Effect of interaction of peptide on kinetic properties of GS <sub>1</sub> β1. ....	109
Table 3.2.1: Kinetic properties of GS <sub>1</sub> isoforms for each substrate. ....	112

## LIST OF FIGURES

Figure 1.2.1: Nodule formation. ....	5
Figure 1.2.2: Bidirectional exchange of metabolites between host and symbiont. ....	13
Figure 1.2.3: Assimilation of ammonia in soybean nodules. ....	19
Figure 1.3.1: Mechanism of action of glutamine synthetase. ....	24
Figure 1.3.2: The central role of glutamine synthetase in plant nitrogen metabolism. ....	27
Figure 1.3.3: Sequence alignment analysis of cloned soybean glutamine synthetase isoforms. ....	31
Figure 2.1: pET28a-GS <sub>1</sub> vector map. ....	38
Figure 2.2: Strategy for PCR-based site-directed mutagenesis. ....	42
Figure 2.3: Chimera synthesis. ....	45
Figure 2.4: Vector maps of BiFC constructs. ....	64
Figure 3.1.1: Isolation of soybean nodule proteins interacting with the C- terminus of nodulin 26. ....	71
Figure 3.1.2: Identification of the 40 kDa CK-25 interacting protein as cytosolic glutamine synthetase (GS). ....	75
Figure 3.1.3: Interaction of purified NGS with the C-terminal domain of nodulin 26. ....	78
Figure 3.1.4: Binding of fluorescent NBD-labeled CK-25 with purified GS. ....	80
Figure 3.1.5: Quantitation of the interaction between GS <sub>1</sub> and the C- terminal peptide of soybean nodulin 26 (CK-25). ....	81



Figure 3.1.6: Split-ubiquitin yeast two-hybrid methodology.....	83
Figure 3.1.7: Analysis of interactions between soybean glutamine synthetase isoforms and nodulin 26 <i>in vivo</i> using the yeast split- ubiquitin system. ....	86
Figure 3.1.8: Bimolecular fluorescence complementation assay methodology. ....	89
Figure 3.1.9: Visualization of the interaction of nodulin 26 with soybean nodule GS <sub>1</sub> $\beta$ 1 by BiFC in onion cells. ....	90
Figure 3.1.10: Interaction of GS with isolated soybean symbiosome membranes.....	93
Figure 3.1.11: Quantitation of the interaction between GS <sub>1</sub> and the phosphorylated C-terminal peptide of soybean nodulin 26 (CK-25P). .	96
Figure 3.1.12: Effect of nodulin 26 phosphorylation on its interaction with GS <sub>1</sub> $\beta$ 1. ....	98
Figure 3.1.13: Crosslinking of <sup>32</sup> P-CK-25 with GS <sub>1</sub> $\beta$ 1. ....	101
Figure 3.1.14: MALDI-TOF spectra of tryptic digest of CK-25 cross-linked with GS <sub>1</sub> $\beta$ 1. ....	102
Figure 3.1.15: Homology model of GS <sub>1</sub> $\beta$ 1.....	105
Figure 3.1.16: Predicted interaction site of CK-25 on the GS. ....	107
Figure 3.1.17: Effect of C-terminal nodulin 26 peptide on recombinant GS activity. ....	108
Figure 3.2.1: Q-PCR analysis of GS <sub>1</sub> isoforms from soybean root and root nodules. ....	111

Figure 3.2.2: Sensitivity of GS <sub>1</sub> isoforms to oxidation. ....	114
Figure 3.2.3: Effect of oxidizing and reducing agents on the activity of GS <sub>1</sub> isoforms.....	116
Figure 3.2.4: Cysteine specific reversible oxidation of GS <sub>1</sub> γ1.....	118
Figure 3.2.5: Sequence alignment of soybean GS <sub>1</sub> isoforms. ....	119
Figure 3.2.6: Determination of free cysteine in oxidized and reduced GS1γ1.....	120
Figure 3.2.7: Location of cysteine residues on GS <sub>1</sub> γ1. ....	122
Figure 3.2.8: Identification of a cysteine residue in GS <sub>1</sub> γ1 that is involved in disulfide bond formation.....	125
Figure 3.2.9: Activity analysis of GS <sub>1</sub> γ1SQ-PE mutant.....	128
Figure 3.2.10: Chimeric constructs of GS <sub>1</sub> β1 and GS <sub>1</sub> γ1.....	129
Figure 3.2.11: Effect of oxidation on the activity of GS <sub>1</sub> chimeric proteins. .....	130
Figure 3.2.12: Native PAGE analysis of GS <sub>1</sub> β1 and GS <sub>1</sub> γ1 isoforms. ....	132
Figure 3.2.13: Sedimentation velocity AUC studies of GS <sub>1</sub> isoforms. ....	133
Figure 3.2.14: Sedimentation velocity analysis of GS <sub>1</sub> isoforms. ....	135
Figure 3.2.15: Recombinant GS <sub>1</sub> protein analysis using sedimentation equilibrium AUC.....	136
Figure 4.1.1: Metabolic model for interaction of nodulin 26 and glutamine synthetase and its effect on nitrogen assimilation in nitrogen-fixing nodules. ....	144
Figure 4.1.2: Futile cycle prevention by nodulin 26/GS interaction. ....	147

<b>Figure 4.3.1: Proposed model to integrate the oxidative regulation of GS</b>	
<b>within the context of root nodule metabolism. ....</b>	<b>156</b>

# CHAPTER I

## INTRODUCTION

### 1.1. Nitrogen: A major macronutrient of plants

The availability of mineral nutrients controls the growth of all organisms and among the most important is nitrogen (Graham and Vance 2000; Socolow 1999), which is essential for the biosynthesis of proteins, nucleic acids, and other cellular constituents necessary for life. Although 80% of the atmosphere is nitrogen gas, this dinitrogen is not directly usable by most organisms and must first be transformed into more accessible chemical forms (Gutierrez 2012). One of the sources of usable soil nitrogen is through atmospheric reactions during lightning discharge which convert molecular nitrogen into nitric acid and nitrous acid, which accumulates as nitrite ( $\text{NO}_2^-$ ) and nitrate ( $\text{NO}_3^-$ ) in the soil. Plants use soil  $\text{NO}_2^-$  and  $\text{NO}_3^-$  and convert it to reduced ammonia by the activity of nitrite reductase and nitrate reductase for further incorporation into organic compounds (Ireland and Lea 1999; Sanchez et al. 2009; Sivasankar and Oaks 1996; Stitt 1999). An additional source of reduced nitrogen comes from industrial or biological fixation of molecular nitrogen. Commercial fertilizers are a major source of usable nitrogen for plants. One percent of the world's energy production is utilized to generate the high temperature and pressure conditions needed for the production of nitrogen fertilizers by the Haber-Bosch process (Gruber and Galloway 2008). Comparatively, nitrogen-fixing bacteria carry out the same reaction under atmospheric temperature and pressure using an

enzyme known as nitrogenase. Biological nitrogen fixation contribute ~40 million tones of reduced nitrogen to the biosphere. (Herridge et al. 2008).

In 1901, Beijerinck discovered that a specialized group of prokaryotes (diazotrophs) perform nitrogen fixation by converting molecular dinitrogen to ammonia (Beijerinck 1901; Franche et al. 2009; Lam et al. 1996; Wagner 2011). Free living heterotrophic soil bacteria such as *Azotobacter*, *Bacillus*, *Clostridium* and *Klebsiella* fix nitrogen without any interaction with other organisms by using organic molecules released from other organisms as an energy source. However, other bacterial species such as the *Azospirillum* perform nitrogen fixation by forming close associations with plant species of the *Poaceae* family, such as rice, wheat, corn, oats and barley.

While biological nitrogen fixation is vastly more energetically efficient than industrial nitrogen fixation, it still represents a large metabolic cost to the organism. Some nitrogen-fixing bacteria solve this problem by entering into a symbiotic relationship with plants. Some microorganisms such as *rhizobia*, *Actinobacteria*, *Frankia* and cyanobacteria fix nitrogen by forming a symbiotic relationship with a host plant, where they depend on the plant for a carbon source which provides energy for nitrogen fixation with the fixed ammonia then released and assimilated by the plant host (Postgate 1998; Postgate 1982; Stal et al. 2010; Vessey et al. 2005). Symbiotic nitrogen fixation is a highly specific interaction and the most efficient process for nitrogen fixation. Endosymbiotic

nitrogen fixation is the closest of these symbiotic relationships. The characteristics of legume-rhizobia symbioses are summarized below.

## **1.2. Endosymbiotic nitrogen fixation**

*Leguminosae* are second only to *Gramineae* as the major component of food, and feed for livestock and raw materials for industry (Graham and Vance 2003). To circumvent the problem of limited nitrogen availability in soil, a number of leguminous plants perform nitrogen fixation by entering into an endosymbiotic association with *rhizobia* bacterium as discussed above (Atkins 1987). Nitrogen fixing bacteria of the *Rhizobiaceae* family are able to enter into a symbiotic relationship with legumes by invading the plant root leading to induction of a developmental pathway forming specialized organs on roots called nodules (Atkins 1987) where they produce ammonia by using atmospheric nitrogen and carbon fuels from the host plant. The structure of nodules provides a microaerobic environment required for efficient bacterial nitrogen fixation by restricting the free flow of oxygen, a potent inactivator of nitrogenase. This microaerobic zone is maintained by the unique anatomy of the nodule which forms an oxygen gas diffusion barrier within the cortical layers of the nodule that surround the infected zone, and by using a high affinity oxygen binding protein leghemoglobin as an oxygen carrier produced by host plant within infected zones (Ott et al. 2005).

## ***I. Establishment of symbiosis***

Establishment of the rhizobia-legume symbiosis, which ultimately leads to the formation of infected root nodules, involves an intricately orchestrated interplay between *Rhizobiaceae* bacteria and legume roots (reviewed in Kereszt et al. 2011; Oldroyd 2013). An overview of the process of rhizobial infection of legume roots and nodule formation is shown in figure 1.2.1.

### ***i. The role of flavonoids and nod factors in initiation of symbiosis***

The association of nitrogen fixing bacteria with their host plant is initiated through chemical signaling between the host plant root and the rhizobiaceae bacteria present in the rhizosphere surrounding the host plant root (reviewed in Oldroyd 2013). The symbiosis process is initiated under limiting conditions of nitrogen, by the release of flavonoid compounds by the legume roots into the rhizosphere. These flavonoid compounds are sensed by rhizobia through the NodD receptor present on the cytoplasmic side of the membrane of rhizobia, leading to induction of *nod* genes (Barnett and Fisher 2006; Perret et al. 2000). Once activated by flavonoids, NodD dissociates from the membrane and binds to nod boxes present upstream of nod operons and activates transcription of *nod* genes. There are two types of *nod* genes in bacteria, common and host-specific *nod* genes. The common *nodABC* genes, which are found in all the nitrogen-fixing bacteria studied so far, are usually expressed from a single operon. These genes are required for the establishment of symbiosis and the loss of these genes abolishes various processes required for symbiosis

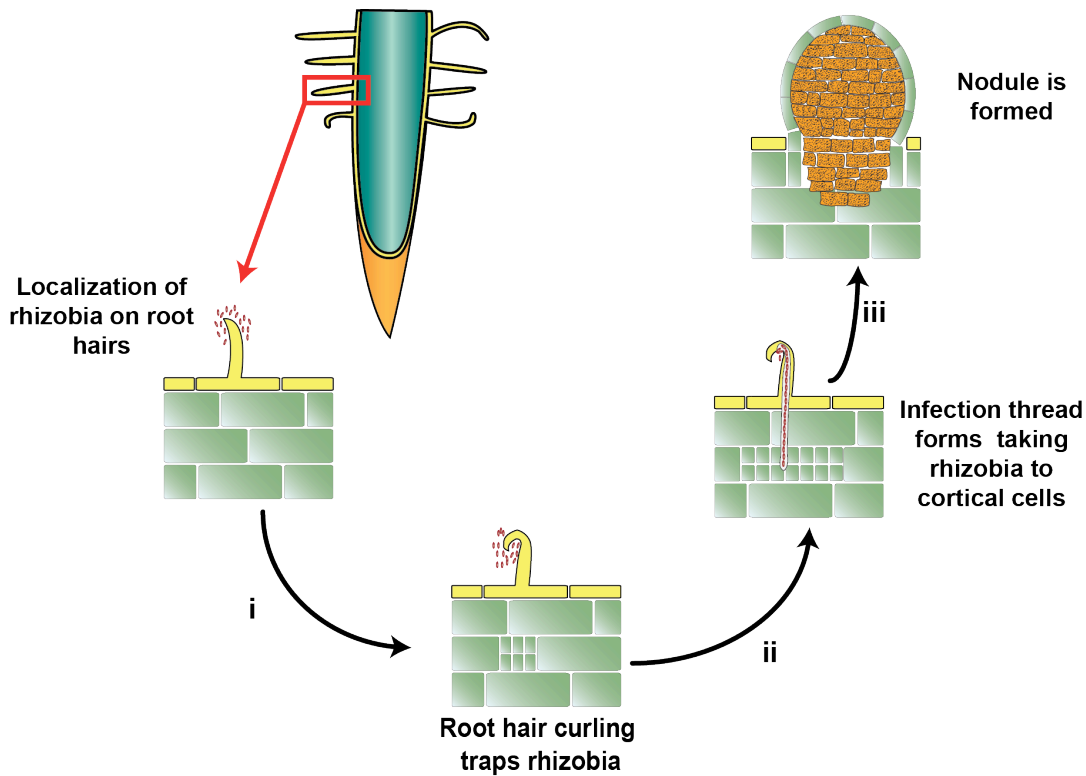


**Figure 1.2.1: Nodule formation.** Nodulation is the coordinated process of establishment of bacterial infection and nodule organogenesis. Nod factors released by rhizobia in response to plant flavonoids, initiate cell division in the cortex. Bacteria are entrapped in a curled root hair, and from this site an infection thread (IT) is initiated. ITs progress into the inner cortex where the nodule primordium has formed through a series of cell divisions. Once at the cortical cells, bacteria are endocytosed and surrounded by plant-derived membrane where bacteria undergo morphological changes leading to the formation of their nitrogen fixing form known as bacteroids.



(Long 1989; Martinez et al. 1990). On the other hand, host-specific *nod* genes are structurally and functionally diverse among rhizobia, and are necessary for host-specific nodulation (Kondorosi et al. 1984). Mutation in those genes alters the specificity of rhizobia towards the host plant (Faucher et al. 1989; Horvath et al. 1986).

Induction of rhizobial *nod* genes results in the production of enzymes that synthesize lipo-oligosaccharide nod factors, which are signaling molecules perceived by the plant host, and which play a crucial role in rhizobia-legume symbiosis. Bacterial mutants defective in the production of nod factors or legume mutants defective in nod factor recognition fail to produce functional symbiosis (Denarie et al. 1996; Downie and Walker 1999; Oldroyd and Downie 2008). Nod factor lipo-chitooligosaccharides consists of a backbone which is generally made up of four or five N-acetylglucosamine residues linked by beta1-4 glycosidic bonds, with further substitutions by various groups such as methyl, fucosyl, acetyl and sulphate groups (Denarie et al. 1996; Miller and Oldroyd 2012). The decorations on nod factors differ depending on the rhizobial species and plays an important role in maintaining host-symbiont specificities (Denarie et al. 1996; Roche et al. 1991). Nod factors produced by rhizobia are recognized in epidermal and root hair cells of their host plants through nod factor receptors which initiates a signaling pathway resulting in the formation of nodules (Downie 1998; Oldroyd et al. 2011; Oldroyd and Downie 2004).

## ***ii. Entry of rhizobia into a host plant***

Nod factors are recognized by receptors present on plant root epidermal cells which initiate various responses required for the establishment of symbiosis between rhizobia and its host legume (Oldroyd and Downie 2004). Nod factor receptors are receptor-like kinases containing a lysine motif (LysM) on the extracellular side which contain binding sites for nod factors with dissociation constants in nanomolar-range (Broghammer et al. 2012; Buist et al. 2008; Mulder et al. 2006; Radutoiu et al. 2007). Binding of rhizobial nod factors to plant nod factor receptors initiates a signaling program that induces changes in the intracellular calcium concentrations of plant epidermal and root hair cells. Mechanistically, binding of nod factors induces the autophosphorylation and activation of the intracellular kinase domains of nod factor receptors (Ehrhardt et al. 1996; Kosuta et al. 2008). Although the intermediate steps are unknown, receptor activation leads to oscillations in nuclear calcium concentrations. These calcium oscillations activate  $\text{Ca}^{2+}$  calmodulin-dependent serine/threonine protein kinase (CCamK) in the nucleus (Levy et al. 2004; Mitra et al. 2004). In root hair cells, these events remodel the cytoskeleton and promote a polarized growth which causes root hairs to curl around associated rhizobial cells, trapping them, which is a precursor to infection (Cardenas et al. 2003; Emons and Mulder 2000; Esseling et al. 2003; Gage 2004; Sielberer et al. 2005; Timmers et al. 1999). Calcium oscillations in root hairs then lead to microtubule rearrangement along the root hair length and forms the pre-infection threads (Sieberer et al. 2005). These signaling events at the root surface are communicated by an unknown

mechanism through interior cell layers to the cortical cells resulting in CCamK activation within these cells. In these cells, CCamK activation promotes cell growth and division (Levy et al. 2004; Mitra et al. 2004).

The infection process begins with nod factor-mediated curling of root hairs around surface-attached rhizobia, forming infection pockets (Geurts et al. 2005). Once trapped in infection pockets, the rhizobia continue dividing and form the infection foci. The plant cell wall is remodeled at the infection foci allowing dividing bacteria to move into the root hair cell. The plasma membrane invaginates around the penetrating bacteria and cell wall continues to be synthesized and degraded, allowing the replicating bacteria to enter, leaving a long tube called an infection thread (Ridge and Rolfe 1985; Turgeon and Bauer 1985). The infection thread extends inward through the root hair into the cortical cells. The growth of the infection thread is guided by the movement of the nucleus and is sustained by a constant supply of membrane vesicles to the growing tip of the infection threads (Gage 2004). Also, reactive oxygen species (ROS) mediated crosslinking of plant proteins connected with infection thread helps in extension of infection thread into cortical cells (Rathbun et al. 2002).

Ultimately, the bacteria are released into specialized host cells inside the nodule, known as infected cells, by endocytosis. The bacteria are enclosed within a host-derived membrane and develop into specialized organelles known as “symbiosomes” (Roth et al. 1988). Symbiosomes are delimited by a host-derived membrane known as the symbiosome membrane (SM), which separates

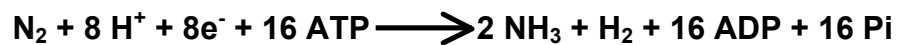
those symbiotic bacteria from the host cell cytosol (Oldroyd and Downie 2008; Verma and Hong 1996). The symbiosome membrane mediates all metabolic exchange between the plant host and enclosed endosymbiont, and also acts as a structural barrier that protects the endosymbiont from the host defense responses (Udvardi and Day 1997; Verma and Hong 1996). Bacteria present in symbiosomes undergo a profound change in cell morphology and are thereafter known as bacteroids, the functional form of nitrogen-fixing bacteria (Roth et al. 1988). A single infected plant cell may contain thousands of symbiosomes.

## ***II. Nodule morphology and physiology***

Nodules are bead-like structures on roots which can be divided into two morphological types; determinate (tropical region) and indeterminate (temperate region) (Oldroyd 2013). Mature indeterminate nodules have a persistent meristem and the nodule is divided into five distinct developmental zones. The outermost zone is the meristematic zone, which allows the nodule to grow throughout its development. The invasion zone lies below the meristematic zone and is where dividing rhizobia are present in infection threads. The interzone and fixation zone is where the bacteroids occupy symbiosomes and fix nitrogen to produce ammonia. The innermost zone is known as the senescence zone where senesced nodule cells are present. In contrast to indeterminate nodules, mature determinate nodules are devoid of a meristem and terminally differentiate into a defined spherical structure. Determinate nodules have a central infection zone surrounded by the nodule parenchyma and vascular bundles. The infection

zone consists mostly of infected cells, which contain symbiosomes, and companion uninfected cells lacking symbiosomes. Primary role of infected cells is assimilation of ammonia to produce amino acids, which are further processed in uninfected cells to produce allantoin and ureides that are transported out of the nodules (Ohyama et al. 2013). The focus of this research is on soybean nodules, which are determinate nodules.

The nitrogenase enzyme is produced by bacteroids within symbiosomes and catalyzes the conversion molecular nitrogen to ammonia (Hu and Ribbe 2011). The nitrogenase enzyme has two enzymatic components, dinitrogenase which is a heterotetrameric molybdenum-iron (MoFe) protein and homodimeric iron protein called dinitrogenase reductase (Dixon and Kahn 2004). The reaction performed by the nitrogenase is as follows.



The dinitrogenase reductase part of the nitrogenase provides the electrons required for the reaction and the dinitrogenase performs the catalysis of dinitrogen to produce ammonia by coordinating the FeMo cofactor active site (Dixon and Kahn 2004; Eady and Postgate 1974; Igarashi and Seefeldt 2003; Seefeldt et al. 2009; Yang et al. 2011). The energy and reducing power required for the nitrogenase action is produced from the carbon source provided by plant.

### ***III. Transport of metabolites through symbiosome membrane***

The symbiosome membrane has properties of both plasma and vacuolar membranes, along with features that are distinct from other endomembranes of plant cells (Roth et al. 1988; Verma and Hong 1996). As discussed earlier, the symbiosome membrane surrounding the bacteroids allows selective transport of metabolites between plant and bacteroids, which is important for maintenance of symbiosis (Udvardi and Day 1997; White et al. 2007). A number of “nodulins”, nod factor-activated, host-encoded genes are specifically targeted to the symbiosome membrane to perform the transport functions required for symbiosis (Fortin et al. 1985; Legocki and Verma 1980; White et al. 2007).

The major metabolite exchange which takes place through the symbiosome membrane, and which is central to the symbiosis, is the uptake of reduced carbon provided by the plant to bacteroids, and the efflux of fixed nitrogen in the form of ammonia from the bacteroids to the plant (Figure 1.2.2). Bacteroids in symbiosomes have a high demand of carbon sources from the plant in order to sustain the high energy cost of nitrogen fixation. Plants fulfill this demand by providing C<sub>4</sub> dicarboxylic acids in the form of malate and succinate to bacteroids, which is utilized by bacteroids for energy production through citric acid cycle (Ou yang et al. 1991; Ou Yang et al. 1990; reviewed in Udvardi and Poole 2013; Udvardi et al. 1988).

Energy produced in bacteroids is utilized in the process of nitrogen fixation by nitrogenase and the ammonia produced in this process diffuses into the

symbiosome space. The  $H^+$ -ATPase present on the symbiosome membrane pumps protons from the cytosol of the infected cell into the symbiosome space by using energy from ATP hydrolysis (Udvardi et al. 1991; Udvardi and Day 1989). This creates a positive membrane potential and an acidic pH in the symbiosome space (pH of 4.5 to 5 [(Pierre et al. 2013)]) which drives the continuous secondary transport of metabolites such as dicarboxylates and ammonia (Ou yang et al. 1991; Ou Yang et al. 1990; Roberts and Tyerman 2002; Tyerman et al. 1995). The low pH of the symbiosome space acid traps ammonia coming from bacteroids by protonating it. This provides counterbalance for the acidification of symbiosome space by the action of ATPase and respiration by bacteroids (Brewin 1991). Protonation of ammonia also prevents its backflow into bacteroids. Ammonia from the symbiosome space is transported into the cytosol by two pathways: ammonium ion ( $NH_4^+$ ) is transported through voltage activated, inwardly rectified non-selective cation channels (NSCC) (Roberts and Tyerman 2002; Tyerman et al. 1995); and ammonia ( $NH_3$ ) is transported by the nodulin 26 channel (Hwang et al. 2010). Both pathways are discussed below in detail.

The transport of  $NH_4^+$  across the symbiosome membrane was demonstrated by patch clamp recording of isolated symbiosomes (Tyerman et al. 1995). The presence of a similar transporter was shown in nodules from pea (Mouritzen and Rosendahl 1997) as well as *Lotus japonicus* (Roberts and Tyerman 2002). Due to gating by divalent cations or polyamines on the cytosolic

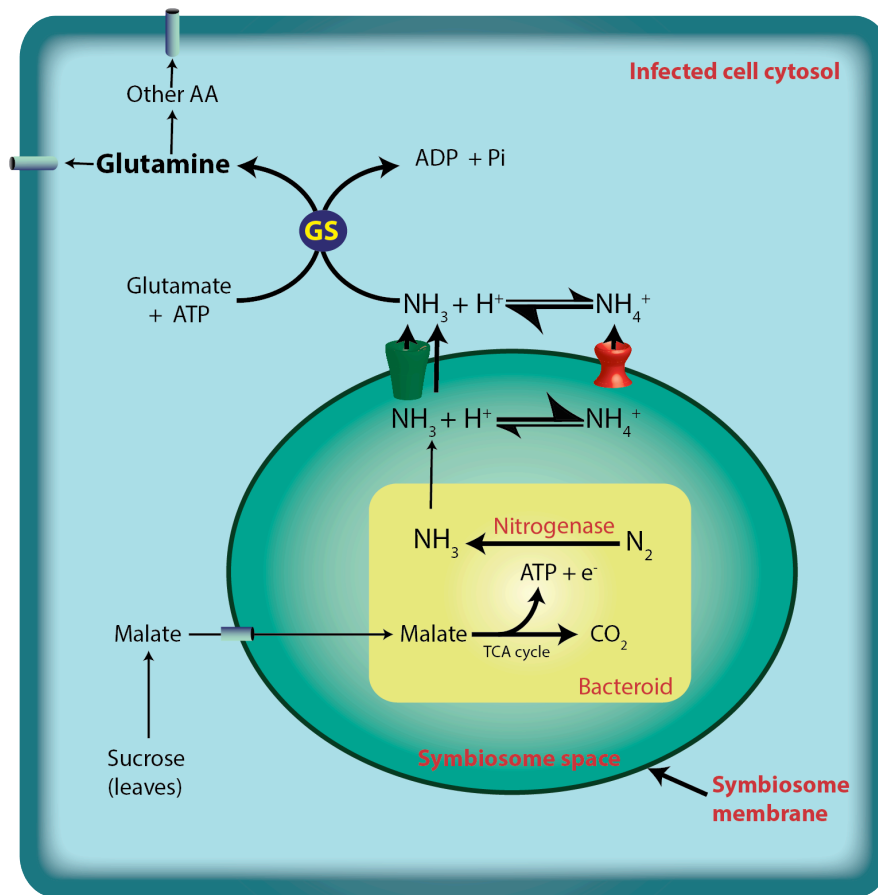


**Figure 1.2.2: Bidirectional exchange of metabolites between host and**

**symbiont.** Schematic representation of symbiotic nitrogen fixation in an infected cell with symbiosome is shown. The plant provides  $\text{C}_4$  dicarboxylates in the form of malate as a carbon source for bacteroids through transporters located on the symbiosome membrane. Bacteroids utilize this carbon source for energy production which is in turn utilized for nitrogen fixation by the action of nitrogenase. Ammonia produced through nitrogen fixation is transported into the cytosol of infected cell majorly through non-selective cation channel as ammonium ion and through nodulin 26 as ammonia.



side of the membrane, the channel is inwardly rectified and shows unidirectional transport of  $\text{NH}_4^+$  towards the cytosol (Obermeyer and Tyerman 2005; Roberts and Tyerman 2002; Whitehead et al. 1998; Whitehead et al. 2001). Activation of the channel is regulated by a voltage gradient across the membrane with channel opening occurring at negative voltage potentials established by the action of  $\text{H}^+$ -ATPase (Obermeyer and Tyerman 2005; Roberts and Tyerman 2002; Whitehead et al. 1998). Facilitated transport of uncharged ammonia occurs through nodulin 26 which is explained in detail in the following section.

#### ***IV. Nodulin 26 as an ammonia channel on the symbiosome membrane***

Genes that are expressed in a specific or enhanced manner during nodulation expressed are known as nodulins (Legocki and Verma 1980). Nodulin 26 is expressed during the biogenesis of symbiosome and is a major protein component of soybean symbiosome membrane (Fortin et al. 1987; Weaver et al. 1991). Expression of nodulin 26 is found to coincide with a rapid burst of membrane biosynthesis that precedes endocytosis and development of the symbiosome membrane (Fortin et al. 1987; Guenther et al. 2003). Nodulin 26 is shown to be specifically present on the symbiosome membrane where it accounts for more than 10% of the total protein (Dean et al. 1999; Weaver et al. 1994).

Nodulin 26 is one of the first discovered members of the major intrinsic protein (MIP)/aquaporin superfamily of water and solute channels in plants (Sandal and Marcker 1988). Nodulin 26 has the core structural feature of the

aquaporin superfamily, nodulin 26 has a conserved hour-glass fold with six trans-membrane  $\alpha$ -helical domains (H1-H6) joined by five loop regions (A-E) and has cytosol-exposed and hydrophilic N-terminal and C-terminal regions (Wallace and Roberts 2004). The aquaporin pore is formed by the packing of the six trans-membrane  $\alpha$ -helices with two loops (loop B and E) with short helical structure fold back into the pore of the protein forming a seventh pseudo trans-membrane  $\alpha$ -helix. The pore selectivity filter is formed by the confluence of four amino acids, two from loop E and one each from H2 and H5 helix which form narrowest constriction of pore referred to as the “aromatic-arginine” (ar/R) region. The ar/R is an important determinant of selectivity among the aquaporin channels (Fu et al. 2000; Stroud et al. 2001; Sui et al. 2001b; Wang et al. 2005).

Various roles for nodulin 26 on the symbiosome membrane have been discussed since the original identification of nodulin 26 over 25 years ago (Fortin et al. 1987). As mentioned earlier, nodulin 26 expression coincides with the synthesis of the symbiosome membrane after the initiation of nodule formation. Its timely expression and specific targeting to the symbiosome membrane led to the proposal that nodulin 26 has a symbiosis-supporting transport role. To investigate this role, functional analyses have been done by using nodulin 26-expressing *Xenopus laevis* oocytes, purified symbiosome membrane vesicles and recombinant nodulin 26 protein reconstituted in proteoliposomes. Studies using these systems showed that nodulin 26 is a multifunctional “aquaglyceroporin” that transports multiple substrates including water,

formamide, glycerol and ammonia (Dean et al. 1999; Hwang et al. 2010; Niemietz and Tyerman 2000; Rivers et al. 1997). These experiments showed that nodulin 26 has slow aquaporin activity, with a 30-fold lower single channel water conductance as compared to robust water-specific aquaporins such as mammalian aquaporin 1 (Rivers et al. 1997; Dean et al. 1999). It has also been shown that the symbiosome membranes have 50-fold higher osmotic water permeability than normal membrane bilayer diffusion rates (Rivers et al. 1997). Considering its high concentration on the symbiosome membrane, nodulin 26 has been proposed to serve as a low energy transport pathway for water within the infected cell, potentially to aid in cell volume regulation and to facilitate infected cell adaptation to osmotic stresses (Dean et al. 1999; Guenther et al. 2003; Rivers et al. 1997).

A facilitated ammonia transport role for nodulin 26 has also been proposed based on the demonstration that transport of ammonia is  $\text{Hg}^{2+}$  sensitive in isolated symbiosome vesicles (Niemietz and Tyerman 2000). Recent work by Hwang et al. showed that nodulin 26 can transport ammonia (Hwang et al. 2010). Stopped-flow fluorometric experiments using purified recombinant nodulin 26 reconstituted into proteoliposomes showed that nodulin 26 is a low energy facilitated transporter for ammonia with 4.9-fold preference over water. Also, the  $\text{Hg}^{2+}$  sensitive nature of the transport of ammonia through nodulin 26 suggests that the previously seen  $\text{Hg}^{2+}$  sensitive facilitated transport observed on soybean symbiosome membrane vesicles by Niemietz and Tyerman is through

nodulin 26 (Niemietz and Tyerman 2000). These findings suggest a metabolic function for nodulin 26 as a facilitated transport pathway for fixed  $\text{NH}_3$  efflux from the symbiosome to the plant cytosol for assimilation.

It has been shown that nodulin 26 is a target for phosphorylation by a symbiosome membrane-associated calcium-dependent protein kinase (CDPK) (Weaver et al. 1991) and the phosphorylation site, Ser 262, was found to be present on the C-terminus of the protein (Weaver and Roberts 1992). CDPK are protein kinases that have calcium-binding EF-hand domains which activate the kinase domain of the protein upon calcium binding (Harper and Harmon 2005). Increases in  $\text{Ca}^{2+}$  concentrations in the nodule possibly due to a stress condition or change in metabolic conditions (Guenther et al. 2003), activate CDPK resulting in the phosphorylation of their targets. Nodulin 26 is one of the first MIP proteins shown to be regulated through phosphorylation (Weaver et al. 1991), which has since been found to be a common regulatory mechanisms for MIPs.

The phosphorylation of nodulin 26 was detected 25 days post-infection, when the nitrogen fixation starts (Guenther et al. 2003). Enhancement of phosphorylation was observed under osmotic stress conditions such as salinity and drought, suggesting its role in osmoregulation in infected cells (Guenther et al. 2003). Guenther et al. also showed enhancement of the rate of water transport by phosphorylation.

## ***V. Assimilation of ammonia in the plant cytosol***

Ammonia is toxic to cells due to its effect on the ion concentration(s) and pH of the cell (Britto and Kronzucker 2002). Therefore, once ammonia is transported into the cytosol of infected cells, it needs to be assimilated quickly into an organic form. Plants do this by rapidly assimilating the ammonia into amino acids, thereby keeping the cytosolic ammonia levels low. Assimilation of ammonia is performed by the action of asparagine synthetase, glutamine oxoglutarate aminotransferase (GOGAT) or glutamate synthase, and glutamine synthetase (Antunes et al. 2008; Vance and Gantt 1992). All the reactions are shown in the figure 1.2.3. GOGAT (EC 1.4.1.14) along with glutamine synthetase form the GS/GOGAT cycle, which is a major ammonia assimilatory pathway in plants (Masclaux-Daubresse et al. 2006; Miflin and Lea 1980). Glutamine synthetase assimilates ammonia to produce glutamine, which can then be utilized by GOGAT to produce two molecules of glutamate. The glutamate produced can again be used for ammonia assimilation or can be converted into other amino acids by the action of aminotransferases (Forde and Lea 2007). In this manner the GS/GOGAT cycle assimilates nitrogen from ammonia to form a glutamate/glutamine pool, which serves as a molecular hub to provide nitrogen to various pathways. Asparagine synthetase and GOGAT performs a transamination reaction by using glutamine as the ammonia source, whereas glutamine synthetase directly assimilates ammonia onto glutamate. Amino acids produced in the cytosol of infected cells are transported into the

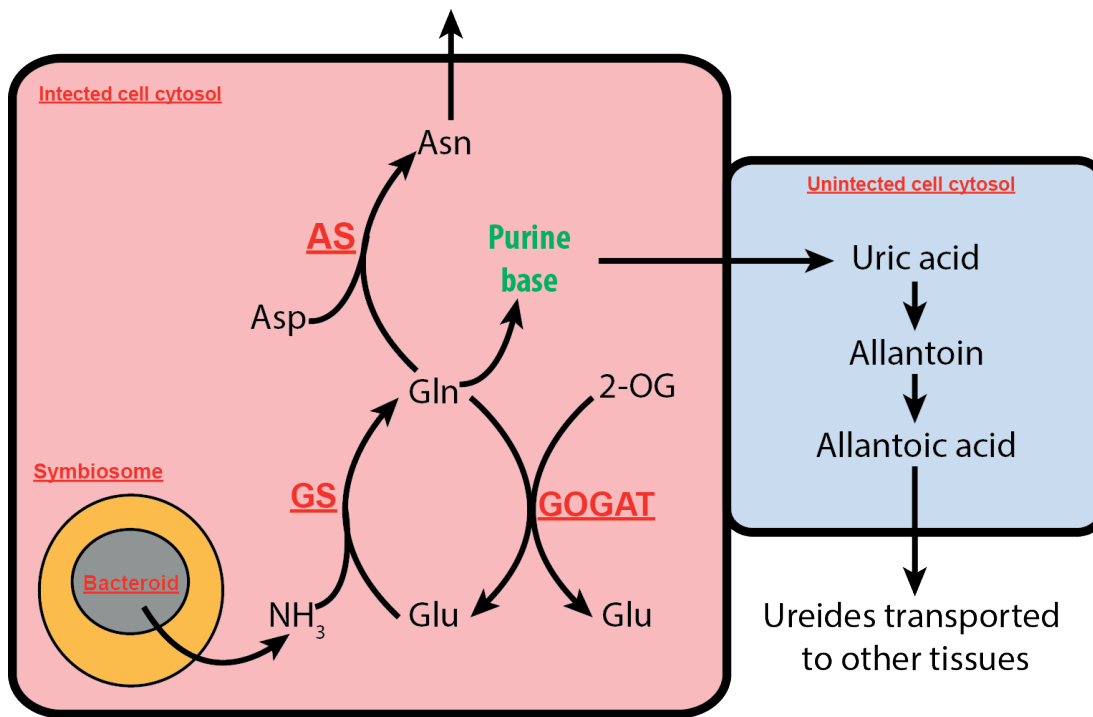
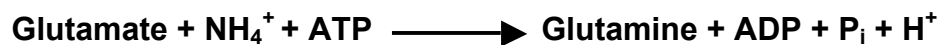


**Figure 1.2.3: Assimilation of ammonia in soybean nodules.** Ammonia produced by bacteroids is assimilated by GS and GOGAT cycle in the cytosol of infected cells. Gln produced after assimilation is further processed in uninfected cells to produce ureides (allantoin and allantoic acid) which are transported to other tissues of the plant. Gln is also used by asparagine synthase (AS) to produce asparagine (Asn) by transamination reaction. Asn produced is transported to other tissues for further utilization.

cytosol of uninfected cells where they are converted into ureides which are further transported to other tissues.

### 1.3. Glutamine synthetase

Glutamine synthetase (GS; EC 6.3.1.2) is among the most important enzymes in nitrogen metabolism that catalyzes the incorporation of ammonium onto glutamate at the expense of ATP, synthesizing glutamine (Mifflin and Habash 2002). The reaction is shown below.



Three different GS types have been identified among eukaryotes and prokaryotes. Among those, GS-I is found mostly in prokaryotes and is the most highly studied type of GS. GS-II is mostly found in eukaryotes, while GS-III is a another prokaryotic GS type. Based on sequence similarity, no GSIII could be found in plant genomes that have been fully sequenced.

Glutamine synthetase has two domains: an N-terminal domain which contains a beta-grasp domain, and the C-terminal domain, which is the catalytic domain. Earlier studies have shown that GS is not a monomeric enzyme (Stewart et al. 1980). Several atomic structures of GS-I from several bacteria have been determined (Almassy et al. 1986; Gill and Eisenberg 2001; Gill et al. 2002). In each case, GS-I been shown to assemble into a dodecamer made of two hexameric rings. The ~470 residue-long N-terminal domain of the GS-I monomer interacts with the C-terminal domain of the adjacent monomer to form

a hexameric ring, with two such rings stacked together to form a dodecamer that is maintained mainly by hydrophobic interactions between the two rings. The active site of GS-I is located between adjacent monomers and contains two  $\text{Mn}^{2+}$  ions. Therefore the GS-I holoenzyme possesses 12 active sites (Almassy et al. 1986).

GS-III is the least studied GS type and has been identified in cyanobacteria (Reyes and Florencio 1994) and two anaerobic bacteria (Goodman and Woods 1993; Southern et al. 1986). Initially, they were described as 75-83 kDa subunits arranged in a hexameric (Reyes and Florencio 1994) form until a single particle reconstruction model of GS-III from *Bacteroides fragilis* was generated which shows it to be a dodecamer similar to GS-I (van Rooyen et al. 2006).

The GS-II type enzymes are comparatively smaller than GS-I, with an average length of ~370 residues. Sequence analysis of bacterial (*M. tuberculosis*) and plant (*Zea mays* L.) GS revealed that the C-terminal residues (residues 393-478) contain an adenylation site in bacterial GS but not in plant GS (Unno et al. 2006). In addition to these C-terminal residues, the  $\beta$  loop residues (residues 143-154) which are involved in forming the interaction between the two hexamer rings are also absent in plant GS. For over two decades, the oligomeric state of the GS-II has been the subject of study, with models proposing it to be octameric or dodecameric. In the early low-resolution electron microscopic studies, it was believed that eukaryotic GS was an octamer with two tetrameric



rings with molecular weight of 350-400 kD (Boksha et al. 2002; Eisenberg et al. 2000; Llorca et al. 2006; Pushkin et al. 1985; Pushkin et al. 1981; Tsuprun et al. 1987). Subsequent single particle study of GS-II from human brain showed that GS-II has heptameric rings rather than tetrameric rings (Kiang 2001). However, sedimentation equilibrium studies conducted on human brain GS-II contradicted the previous finding by Kiang and showed that the GS-II, in fact, is an octamer containing two tetrameric rings (Boksha et al. 2002).

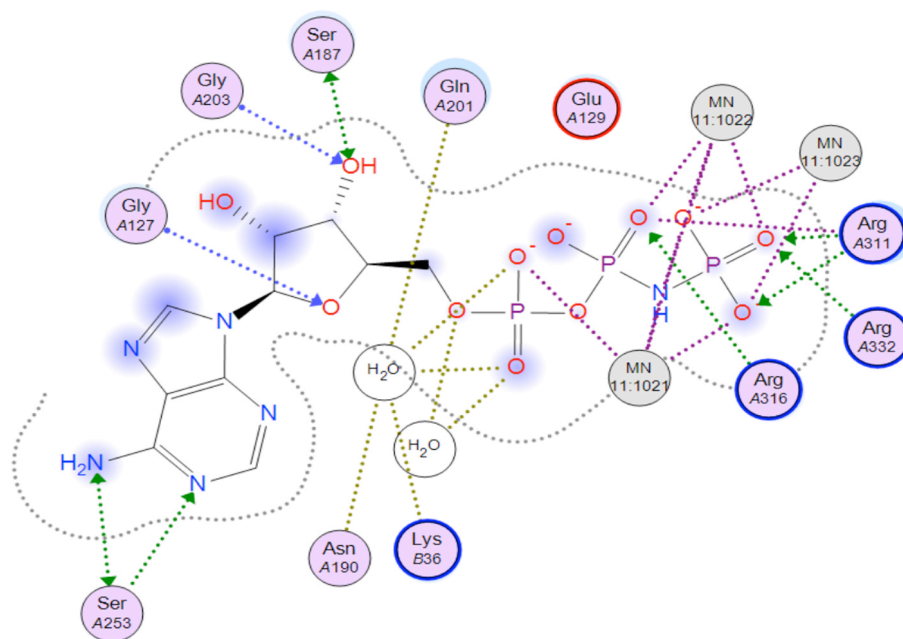
The first eukaryotic GS crystal structure determined was for maize GS (GS1a) in complex with ADP and a glutamate analogue in the presence of  $Mn^{2+}$  with resolutions of 2.63-3.8 Å (Unno et al. 2006). Similar structures have since been reported for yeast (He et al. 2009) and *Medicago truncatula* (Seabra et al. 2009). Also, the first mammalian GS-II (CfGS) structure was generated by molecular replacement using the GS1a structure in complex with MnADP and MSO-P (PDB entry code 2D3A) (Krajewski et al. 2008). From this crystal structure, it is clear that GS is a decameric protein with dimensions of 115 Å X 115 Å X 95 Å. Five subunits form a ring by forming interactions between the N-terminal and the C-terminal domains of adjacent monomers and the two face-to-face pentameric rings are held together by hydrophobic interactions to form the decameric holoenzyme. More specifically, the crystal structure revealed that the two pentameric rings are held together by four hydrophobic and 2 hydrogen bonding interactions, and that the active site is formed at the interface of the N- and C-terminal domains of adjacent subunits (Unno et al. 2006). Therefore,

there are 10 active sites in a single decameric GS molecule that are formed between two neighboring subunits. Also, three  $\text{Mn}^{2+}$  ions are present in the cleft of each active site.  $\text{Mn}^{2+}$  molecules are important in stabilizing the  $\gamma$  phosphate of ATP. While several remarkable differences between bacterial and eukaryotic glutamine synthetases have been discussed, these structural studies have also revealed that the interface surface area between the two rings of GS<sub>1a</sub> is 17 times smaller as compared to bacterial GS-I.

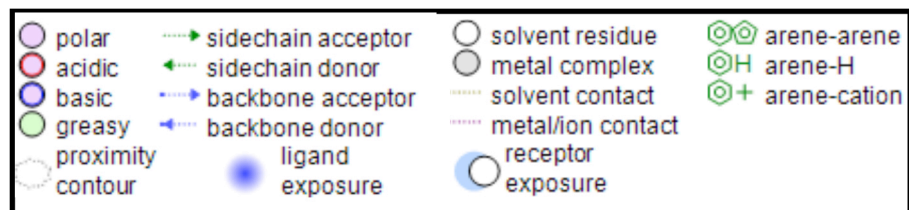
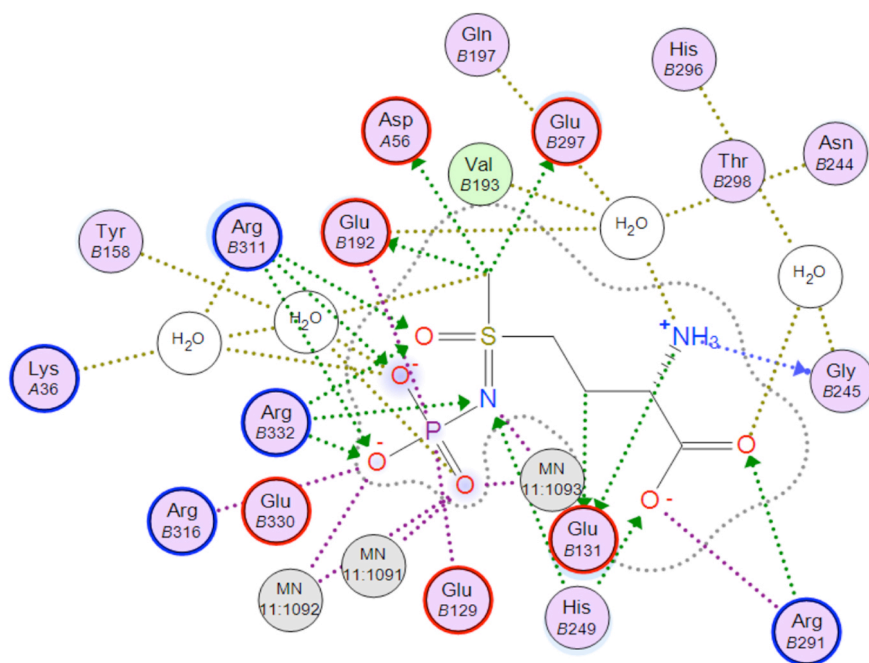
Liaw and Eisenberg (1994) have proposed a structural model for the reaction mechanism of glutamine synthetase. Their model is based on five different crystal structures of enzyme-substrate complexes of bacterial GS (Liaw and Eisenberg 1994). The model proposes a two-step mechanism with a tetrahedral intermediate:  $\gamma$ -glutamyl phosphate. According to their model, ATP binds to GS, which enhances binding of glutamate. Then, two of the three  $\text{Mn}^{2+}$  ions bound to the enzyme polarize the  $\gamma$ -phosphate of ATP, which allows glutamate to attack it and produce  $\gamma$ -glutamyl phosphate with the help of arg339 (arg311 in GS<sub>1</sub>). Following phosphoryl transfer, the presence of ADP in the active site induces movement of asp50, which then forms an ammonium binding site. The side chain of asp50 binds an ammonium ion and then accepts a proton from it producing the more reactive ammonia, which attacks  $\gamma$ -glutamyl phosphate and forms a tetrahedral intermediate. The positively charged  $\gamma$ -amino group from the tetrahedral intermediate forms a salt link with the negatively charged side chain of glu327 (glu297 in GS<sub>1</sub>) resulting in the stabilization of the

**Figure 1.3.1: Mechanism of action of glutamine synthetase.** GS has three substrates, glutamate, ammonia and ATP. Substrates shown in the figures are the substrate analogs (AMP-PNP for ATP and MetSox for glutamate) used in crystallization of GS. (A) AMP-PNP bound in GS active site is shown. Two of the three  $Mn^{2+}$  ions along with arg311 polarize the  $\gamma$ -phosphate of ATP. (B) shows the substrate glu bound in the active site of GS. Substrate glu attacks the polarized  $\gamma$ -phosphate of ATP and acquires it leading to formation of  $\gamma$ -glutamyl phosphate. Ammonia bound to asp50 attacks  $\gamma$ -glutamyl phosphate and forms the tetrahedral intermediate. The salt link of tetrahedral intermediate with glu297 stabilizes the flexible region from 294-298 blocking the exit of glutamate. When ammonia attacks the  $\gamma$ -glutamyl phosphate, phosphate group is released leading to formation of glutamine.

**A**



**B**



flexible region from 324-328 which blocks the substrate glutamate from exiting the active site. In the final step, the phosphate group from the tetrahedral intermediate leaves and a proton from the  $\gamma$ -amino group of the tetrahedral intermediate is accepted by glu327, which completes the formation of glutamine. GS sequences from animals, plants and bacteria show that all amino acid residues involved in catalysis (asp50, glu129, glu131, glu212, glu220, gly265, his 269, arg321, glu327, arg339, arg344, glu357, and arg359) are conserved. Also the residues involved in interaction with the metal ions are conserved among these species. This suggests that a similar mechanism is present in plant GS.

### ***1. The central role of glutamine synthetase in plant nitrogen metabolism***

Figure 1.3.2 shows the central role of glutamine synthetase in the complex network of plant nitrogen metabolism. Besides the assimilation of ammonia produced from the reduction of  $\text{NO}_3^-$ ,  $\text{NO}_2^-$  and  $\text{N}_2$ , there are additional biological reactions including transaminations and photorespiration which produce ammonia in plants. Other contributors to this pool of  $\text{NH}_3$  are secondary metabolites, transport compounds like allantoin, ureide, and asparagine. Most of the  $\text{NH}_3$  produced in plants is assimilated by glutamine synthetase. Glutamine produced in this reaction is a mobile form of assimilated nitrogen that is transported to different tissues, cells and sub-cellular compartments where it is converted to other amino acids and nitrogenous compounds. Once in different locations, these compounds can be used for the synthesis of different proteins in those locations. These observations suggest that glutamine synthetase has a

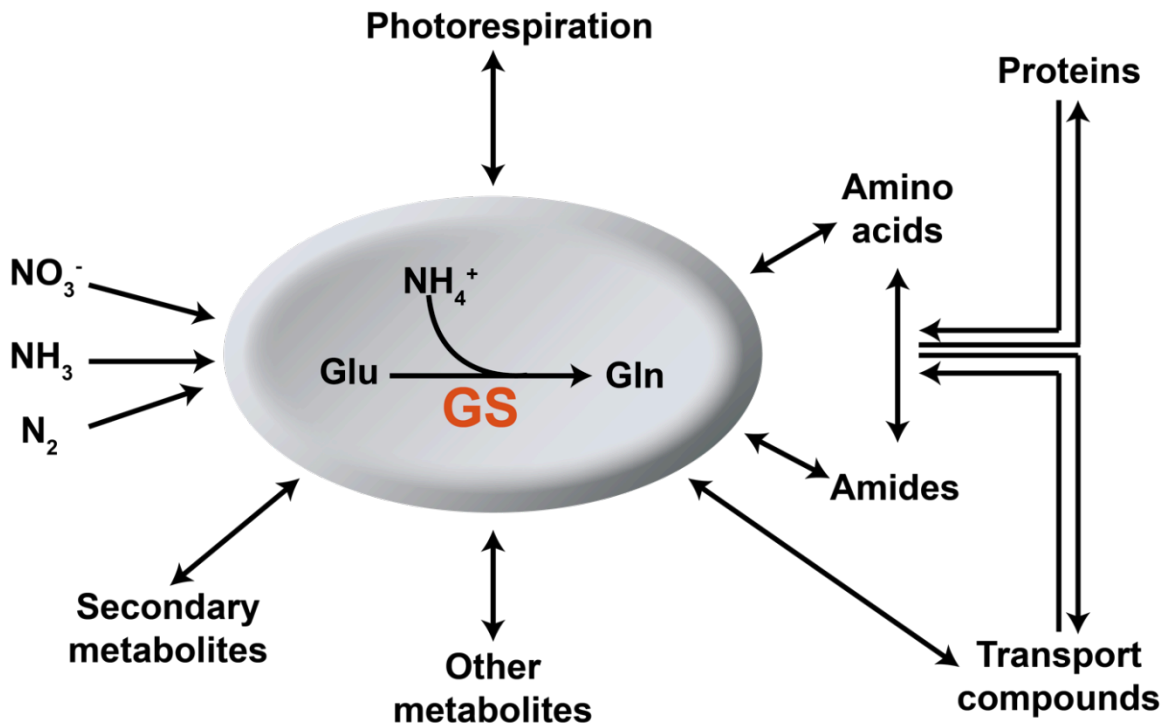


**Figure 1.3.2: The central role of glutamine synthetase in plant nitrogen**

**metabolism.** In plants, glutamine synthetase assimilates ammonia ( $\text{NH}_3$ ) from a variety of sources.  $\text{NH}_3$  is produced from cellular processes such as photorespiration, metabolism of nitrogenous compounds and from soil nitrates and nitrites. Ultimately, this ammonia is assimilated by glutamine synthetase (GS) to produce glutamine (gln). Gln can be further utilized for the production of other nitrogenous compounds that can be transported to other tissues.

central role in nitrogen metabolism in plants.

## ***II. Types of glutamine synthetases in plants***

In plants, two major isoform classes of GS (GS<sub>1</sub> and GS<sub>2</sub>) are present that are distinguished by their subcellular location (Forde and Woodall 1995; Hirel and Gadal 1980; Lam et al. 1996; Marquez et al. 2005; McNally et al. 1983; Miflin and Habash 2002) where GS<sub>2</sub> is more abundant in leaves while the cytosolic form GS<sub>1</sub> is predominately expressed in roots (Orea et al. 2002; Walls-grove et al. 1987). GS<sub>2</sub> is usually expressed by a single gene. Reassimilation of ammonia released in photorespiration is considered the primary role of GS<sub>2</sub> (Blackwell et al. 1987; Kozaki and Takeba 1996; Orea et al. 2002; Walls-grove et al. 1987). However, presence of GS<sub>2</sub> has also been seen in non-photosynthetic tissues such as roots (Woodall and Forde 1996) and nodules (Marquez et al. 2005; Melo et al. 2003). Its primary role in those tissues remains to be identified.

In contrast to GS<sub>2</sub>, GS<sub>1</sub> are generally encoded by a small gene family and each gene member is regulated differentially (Bennett et al. 1989; Gebhardt et al. 1986; Sakamoto et al. 1989; Tingey et al. 1988; Tingey et al. 1987) (Bernard et al. 2008; Goodall et al. 2013; Ishiyama et al. 2004a; Ishiyama et al. 2004c; Lara et al. 1983; Li et al. 1993; Martin et al. 2006; Morey et al. 2002; Nogueira et al. 2005; Stanford et al. 1993; Swarbreck et al. 2011; Teixeira et al. 2005; Tingey et al. 1987). Immunolocalization studies in different plant species have shown that GS<sub>1</sub> is predominantly localized to the vascular cells of different organs (Brugiere et al. 1999; Canovas et al. 2007; Edwards et al. 1990; Masclaux et al. 2000;

Sakurai et al. 1996; Tabuchi et al. 2005) where it is known to be involved in assimilation of external ammonium as well as ammonia derived from nitrogen fixation, protein degradation and other sources such as senescence (Tabuchi et al. 2007; Teixeira et al. 2005). In roots, its major role is to assimilate ammonia derived directly from soil, whereas in cotyledons, its major role is to assimilate ammonia released during germination. In root nodules, GS<sub>1</sub> assimilates ammonia produced during nitrogen fixation and prevents the harmful effects of high concentrations of ammonia on plant tissues. Consistent with its central role in nitrogen assimilation, it has been shown that the GS<sub>1</sub> activity increases after the onset of nitrogen fixation in the nodules of leguminous plants (Vance and Gantt 1992).

In legumes there are three major GS<sub>1</sub> isoforms, that are distinguished based on their tissue expression, molecular weight and apparent pI (Morey et al. 2002). In the common bean *Phaseolus vulgaris*, there are three functional GS<sub>1</sub> genes (GS $\alpha$ , GS $\beta$  and GS $\gamma$ ) and one pseudogene. GS $\alpha$  is expressed in early stages of leaf development, and GS $\beta$  is expressed more widely in leaves, roots and nodules, whereas the third gene, GS $\gamma$  expressed in nodules (Forde et al. 1989). A similar pattern was observed for GS<sub>1</sub> isoforms from soybean. There are five GS<sub>1</sub> genes ( $\alpha$ ,  $\beta_1$ ,  $\beta_2$ ,  $\gamma_1$ ,  $\gamma_2$ ) found in soybean. GS<sub>1</sub> $\alpha$  is shown to be specifically expressed in above ground tissues, GS<sub>1</sub> $\beta$  isoforms are expressed in roots and root nodules, and GS<sub>1</sub> $\gamma$  is specifically expressed in root nodules (Morey et al. 2002). Morey et al. (2002) found that there are 4 isoforms ( $\beta_1$ ,  $\beta_2$ ,



$\gamma_1$ ,  $\gamma_2$ ) of cytosolic GS present in the soybean root nodule and that these isoforms are subject to regulation by developmental and environmental cues. GS<sub>1</sub> isoforms from soybean nodules share more than 88% amino acid sequence identity (Figure 1.3.3). The identity increases to 96% within the GS<sub>1</sub> $\beta$  and GS<sub>1</sub> $\gamma$  isoform subfamily.

#### **1.4. Goal of the research work**

To understand the significance of different GS<sub>1</sub> isoforms in nitrogen fixation, the structure, function and regulation of cytosolic GS<sub>1</sub> isoforms from soybean root nodules were investigated. In addition, it is shown that the GS<sub>1</sub> interacts with symbiosome membranes through its binding with nodulin 26. The significance of these observations in the fixation, transport and assimilation of ammonia is discussed.

**Figure 1.3.3: Sequence alignment analysis of cloned soybean glutamine**

**synthetase isoforms.** The sequences of *Glycine max* (soybean) GS<sub>1</sub>β1 (Glyma11g33560.1), GS<sub>1</sub>β2 (Glyma18g04660.1), GS<sub>1</sub>γ1 (Glyma14g39420.1) and GS<sub>1</sub>γ2 (Glyma02g41120.1) were aligned using the Clustal W alignment algorithm and the BioEdit software version 5.0.6 ([www.mbio.ncsu.edu/BioEdit/BioEdit.html](http://www.mbio.ncsu.edu/BioEdit/BioEdit.html) ). Residues are colored according to the following scheme: green; hydrophobic, blue; basic, red; acidic, salmon; serine/ threonine, yellow; proline, and purple; glycine. Overall sequence identity is 88%. Within GS<sub>1</sub>β isoforms sequence identity is 96%. GS<sub>1</sub>γ isoforms also shows the similar identity.

GS1beta1	1	MSLLSDLINLNLSDTTEKVIAEYIWIGGSCMDLRSKARTLPGFVSDPSEL	50
GS1beta2	1	MSLLSDLINLNLSDTTEKVIAEYIWIGGSCMDLRSKARTLPGFVSDPSKL	50
GS1gamma1	1	MSLLSDLINLNLSDTITDFVIAEYIWVGGSCMDMRSKARTLSGFVSDPSKL	50
GS1gamma2	1	MSLLSDLINLNLSDTITDFVIAEYIWVGGSCMDMRSKARTLSGLVNDPSKL	50
GS1beta1	51	PKWNYDGSSTGQAPGEDSEVILYPQAIKRDFFRRGNNILVICDAYTEAGE	100
GS1beta2	51	PKWNYDGSSTGQAPGEDSEVILIPQAIKRDFFRRGNNILVICDAYTEAGE	100
GS1gamma1	51	PKWNYDGSSTGQAPGQDSEVILYPQAIKRDFFRRGNNILVMCLDAYTEAGE	100
GS1gamma2	51	PKWNYDGSSTGQAPGQDSEVILYPQAIKRDFFRRGNNILVMCLDAYTEAGE	100
GS1beta1	101	PIPTNKRHDAARVFSHPDVVAEEFWYGLEQEYTLQKDIQWPLGWVGGF	150
GS1beta2	101	PIPTNKRHDAARVFSHPDVVAEEFWYGLEQEYTLQKDIQWPLGWVGGF	150
GS1gamma1	101	PIPTNKRNNAAKIFCHPDVAAEEFWYGLEQEYTLQKDVQWPLGWPLGGF	150
GS1gamma2	101	PIPTNKRNNAAKIFSNPDVAAEEFWYGLEQEYTLQKDVQWPLGWPLGGF	150
GS1beta1	151	PGPQGPYYCGVGADKAFGRDIVDAHYKACIYAGINISGINGEVMPGQWEF	200
GS1beta2	151	PGPQGPYYCGVGADKAFGRDIVDAHYKACIYAGINISGINGEVMPGQWEF	200
GS1gamma1	151	PGPQGPYYCGTGANKAFGRDIVDSHYKACIYAGINISGINGEVMPGQWEF	200
GS1gamma2	151	PGPQGPYYCGTGANKAFGRDIVDSHYKACIYAGINISGINGEVMPGQWEF	200
GS1beta1	201	CVGPSVGISAGDEIWAARYILERITEIACVVVSFDPKPIQGDWNCACAH	250
GS1beta2	201	CVGPSVGISAGDEVWAARYILERITEIACVVVSFDPKPIQGDWNCACAH	250
GS1gamma1	201	CVGPSIGISAADIELWARYILERITEIACVVLVSFDPKPIQGDWNCACAH	250
GS1gamma2	201	CVGPSVGISAADIELWARYILERITEIACVVLVSFDPKPIQGDWNCACAH	250
GS1beta1	251	NYSTKSMRNDGGYEVIKAIADKLGRKHKEHIAAYGEGNERRLTGRHEIAD	300
GS1beta2	251	NYSTKSMRNDGGYEVIKAIADKLGRKHKEHIAAYGEGNERRLTGRHEIAD	300
GS1gamma1	251	NYSTKSMRNDGGYEVIKAIADKLGRKHKEHIAAYGEGNERRLTGRHEIAD	300
GS1gamma2	251	NYSTKSMRNDGGYEVIKAIADKLGRKHKEHIAAYGEGNERRLTGRHEIAD	300
GS1beta1	301	INTFLWGVANRGASVVFVGRDTEKAGKGYFEDRRFASNMDFYVVTSMIADT	350
GS1beta2	301	INTFLWGVANRGASVVFVGRDTEKAGKGYFEDRRFASNMDFYVVTSMIADT	350
GS1gamma1	301	MNTFLWGVANRGASIFVGRDTEKAGKGYFEDRRFASNMDFYVVTSMIAET	350
GS1gamma2	301	MNTFLWGVANRGASIFVGRDTEKAGKGYFEDRRFASNMDFYVVTSMIAET	350
GS1beta1	351	TIIWKP	356
GS1beta2	351	TIIWKP	356
GS1gamma1	351	TIIWKP	356
GS1gamma2	351	TIIWKP	356

## CHAPTER II

### MATERIALS AND METHODS

#### 2.1. Plant growth conditions

Soybean (*Glycine max* cv Bragg) were grown and nodulated with *Bradyrhizobium japonicum* USDA110 as described in (Guenther et al. 2003). Seeds were planted in vermiculite and watered with deionized water at the time of planting. *Bradyrhizobium japonicum* USDA 110 was grown in Bergersen's minimal medium (BMM)(270 mg/L  $\text{NaH}_2\text{PO}_4 \cdot 7\text{H}_2\text{O}$ ; 80 mg/L  $\text{MgSO}_4 \cdot 7\text{H}_2\text{O}$ ; 3 mg/L  $\text{FeCl}_3 \cdot 6\text{H}_2\text{O}$ ; 3.7 mg/L ferric monosodium EDTA; 30 mg/L  $\text{CaCl}_2 \cdot 2\text{H}_2\text{O}$ ; 0.0025 mg/L  $\text{MnSO}_4 \cdot 4\text{H}_2\text{O}$ ; 0.03 mg/L  $\text{H}_3\text{BO}_3$ ; 0.03 mg/L  $\text{ZnSO}_4 \cdot 7\text{H}_2\text{O}$ ; 0.00025 mg/L  $\text{NaMoO}_4 \cdot 2\text{H}_2\text{O}$ ; 0.1 mg/L biotin; 1 mg/L thiamine; 10 g/L mannitol; 0.5 g/L sodium glutamate; 0.5 g/L yeast extract; pH 6.8-7.1). Fifty ml of a mid log phase starter culture of *B. japonicum* (grown in BMM at 28°C with constant shaking) was used to inoculate a 500 ml culture. After 2 days of growth with constant shaking at 28°C, the culture was diluted 10 times in Herridge's solution and was used to inoculate the plants eight days after planting.

Inoculated plants were grown under long day conditions (16 hour day 25°C and 8 hour night 22°C) either in a growth chamber or a green house and were watered with Herridge's solution (Eskew et al. 1993) (22 mg/L  $\text{K}_2\text{HPO}_4$ ; 17 mg/L  $\text{KH}_2\text{PO}_4$ ; 250 mg/L  $\text{MgSO}_4 \cdot 7\text{H}_2\text{O}$ ; 37 mg/L  $\text{CaCl}_2 \cdot 2\text{H}_2\text{O}$ ; 9 mg/L ferric monosodium EDTA; 0.71 mg/L  $\text{H}_3\text{BO}_3$ ; 0.45mg /L  $\text{MnCl}_2 \cdot 4\text{H}_2\text{O}$ ; 0.03 mg/L  $\text{ZnCl}_2$ ;

0.01 mg/L  $\text{CuCl}_2 \cdot 2\text{H}_2\text{O}$ ; 0.005 mg/L  $\text{NaMoO}_4 \cdot 2\text{H}_2\text{O}$ ) on alternate weeks. Plants were grown for 26-36 days after inoculation before harvest of nodules.

## **2.2. RNA extraction and cDNA synthesis**

Soybean nodules and roots were frozen in liquid nitrogen and were then ground in a heat-baked mortar with a pestle. Heat baked mortar and pestle were pre-chilled in liquid nitrogen before using for tissue grinding. Chilled plant RNA reagent (Invitrogen) (500  $\mu\text{l}$ ) was added to ~200 mg of tissue powder. After incubation for 5 minutes at room temperature, the samples were centrifuged at 12,000 X g at room temperature for 2 minutes. The supernatant fraction was transferred to a new 1.5 ml tube containing 125  $\mu\text{l}$  of 4 M NaCl and 0.3 ml of chloroform, was vortexed, and then centrifuged at 12,000 X g at 4°C for 10 minutes. The upper aqueous phase was collected and an equal volume of isopropyl alcohol was added. After mixing by inversion, the samples were incubated at -20°C for 10 minutes and were centrifuged by centrifugation at 12,000 X g at 4°C for 10 minutes. The pellet was washed with 70% [v/v] ethanol and was centrifuged at 12,000 X g at room temperature for 1 minute. The washed pellet was air dried and was resuspended in diethylpyrocarbonate (DEPC) - treated water. The concentration and purity of RNA was determined spectrophotometrically at 260 and 280 nm. DNase I-treatment was performed in DNase I (New England Biolabs) buffer on 10  $\mu\text{g}$  of RNA using 2 units of DNase I at 37°C for 40 minutes. DNase inhibitor was added to the sample, and after 2 minutes incubation at room temperature. The sample was centrifuged at 14000

rpm in table top centrifuge for 1 minute. The supernatant fraction was collected, and the purity and integrity of the RNA was determined by electrophoresis on 1% [w/v] agarose gels in TAE buffer (40 mM Tris, 20 mM acetic acid, 1 mM EDTA, pH 8).

cDNA synthesis was performed using a Superscript III reverse transcription kit according to manufacturer's instructions (Invitrogen). For cDNA synthesis, 2 µg of DNase I-treated RNA was combined with 0.05 µg/µl oligo d(T) primer and 1 mM dNTP in a total volume of 20 µl, and was incubated at 65°C for 5-10 minutes. The mixture was then placed on ice for one minute and 18 µl of reverse transcriptase mixture (4 µl 10X reverse transcriptase buffer, 8 µl 25 mM MgCl<sub>2</sub>, 4 µl 100 mM dithiothreitol (DTT), 1 µl RNase out, 1 µl Superscript III enzyme [Invitrogen]) was added. The reverse transcription reaction was performed using the following amplification parameters in a Mastercycler (Eppendorf): 25°C for 15 minutes; 42°C for 90 minutes; 72°C for 15 minutes. The samples were then incubated with 1 µl of RNase H at 37°C for 30 minutes, and then stored at -20°C.

### **2.3. Molecular cloning of cytosolic glutamine synthetase isoforms from nitrogen-fixing soybean root nodules**

cDNA corresponding to cytosolic glutamine synthetase isoforms GS<sub>1</sub>β1, GS<sub>1</sub>β2, GS<sub>1</sub>γ1, and GS<sub>1</sub>γ2 (Morey et al. 2002) were isolated from soybean nodule cDNA by PCR amplification with primers specific for the 5' and 3' untranslated region (UTR) of each isoform (Table 2.1) based on sequences

**Table 2.1: - Oligonucleotide primers used for cloning of soybean glutamine synthetase isoforms.**

Primer Name <sup>b</sup>	Direction	Sequence (5'to 3') <sup>a</sup>
GS <sub>1</sub> β1 5' UTR	Forward	AGAATTCTCTAAAAGAGATCTTTTTC
GS <sub>1</sub> β1 3' UTR	Reverse	AGGCACCAACCATAGTACCA
GS <sub>1</sub> β2 5' UTR	Forward	AAGATTCTAAGAGAGATTTTGCTG
GS <sub>1</sub> β2 3' UTR	Reverse	CCTTGTTCCCTTGTTCCCTTGT
GS <sub>1</sub> γ1 5' UTR	Forward	AAGAGAAAAAATTCTCAGAAGA
GS <sub>1</sub> γ1 3' UTR	Reverse	AAGGCATGTGTGATTATTTTTG
GS <sub>1</sub> γ2 5' UTR	Forward	GAGAAAGAAATTGTTTCTCTCTAA
GS <sub>1</sub> γ2 3' UTR	Reverse	TGACCATCTAAACAACAATGC
GS <sub>1</sub> β1 NheI-For	Forward	CGAGCTAGCATGTCTCTGCTCTCAGATC
GS <sub>1</sub> β1 NotI-Rev	Reverse	CGAGCGGCCGCTCATGGCTTCCACAGAATGG
GS <sub>1</sub> β2 NheI-For	Forward	CGAGCTAGCATGTCGCTGCTCTCAGATCT
GS <sub>1</sub> β2 NotI-Rev	Reverse	CGAGCGGCCGCTCATGGCTTCCACAGAATGG
GS <sub>1</sub> γ1 NheI-For	Forward	CGAGCTAGCATGTCGTTGCTCTCCGAT
GS <sub>1</sub> γ1 NotI-Rev	Reverse	CGAGCGGCCGCTTATGGTTTCCAAAGAATGGT
GS <sub>1</sub> γ2 NheI-For	Forward	CGAGCTAGCATGTCGTTACTCTCCGA
GS <sub>1</sub> γ2 NotI-Rev	Reverse	CGAGCGGCCGCTTATGGTTTCCAAAGAATGGT

<sup>a</sup> All primer sequences are in the 5' to 3' direction. Underlined regions represent sequences coding for restriction sites *NotI* and *NheI* enzymes.

<sup>b</sup> 5' and 3' UTR indicates 5' untranslated region (UTR) and 3' untranslated region respectively. Primers are labeled with respective GS<sub>1</sub> isoform along with the restriction site.

available from genomic database Phytozome (<http://www.phytozome.net>). PCR reactions were performed using isoform-specific primers (0.5  $\mu$ M of each) and the Ex-Taq polymerase (TaKaRa) in Easystart Micro 50 (Molecular BioProducts, San Diego, CA) with the following amplification parameters: 94°C for 10 minutes; followed by 33 cycles of: 94°C for 30 seconds, 48°C for 40 seconds, 72°C for 200 seconds; and a final elongation cycle of 72°C for 15 minutes. PCR products were separated on a 1 % [w/v] low melting point agarose gel in TAE buffer, and were gel purified using the Qiaquick gel extraction kit (Qiagen). Purified PCR products were cloned into the pCR2.1-TOPO (Invitrogen) vector and were transformed into *E. coli* DH5 $\alpha$  by using the heat shock method (Sambrook et al. 2001). The identity of each isoform was verified by automated DNA sequence analysis in the Molecular Biology Resource Facility at The University of Tennessee, Knoxville.

For preparing protein expression constructs of GS<sub>1</sub> isoforms, cDNA containing the full length ORFs of GS<sub>1</sub> isoforms in pCR2.1-TOPO (Invitrogen) were amplified by using primers flanked by *NheI* and *NotI* restriction sites (Table 2.1). PCR products were separated by electrophoresis on a 1 % [w/v] low melting point agarose gel, and were gel purified using the Qiaquick gel extraction kit (Qiagen). Purified PCR products were digested with *NheI* and *NotI* restriction enzymes and were cloned into *NheI* and *NotI* digested bacterial expression vector pET28a (Novagen) in frame with an amino terminal his-tag linker. A map of the expression vector along with the cloned cDNA is shown in figure 2.1.



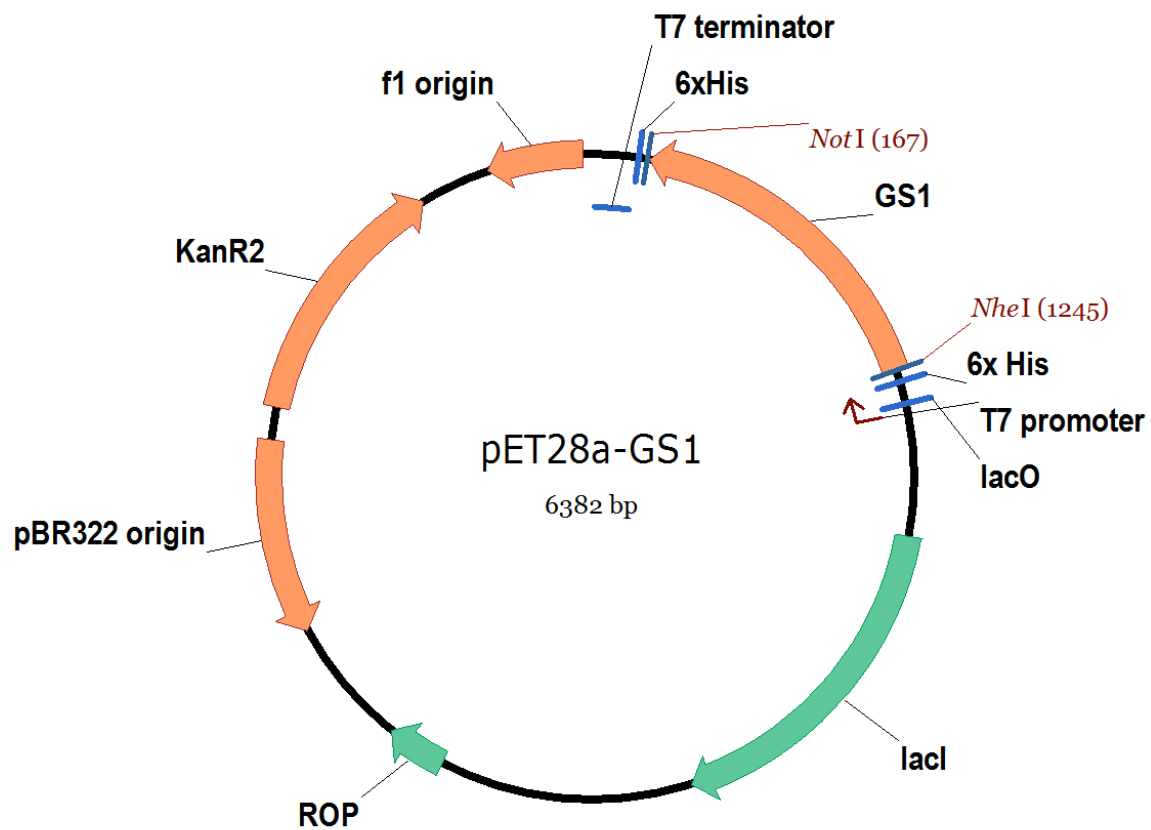


**Figure 2.1: pET28a-GS<sub>1</sub> vector map.** Schematic representation of *pET28a* expression vector (Invitrogen) used for expression of GS<sub>1</sub> isoforms is shown. The *NheI* and *NotI* restriction sites used for cloning GS<sub>1</sub> isoform are shown along with six histidine tag on 5' end.

## 2.4. Q-PCR expression analysis

Total RNA was extracted and cDNA was synthesized from 26-day-old soybean roots and nodules as described above. cDNA samples proportional to 10 ng of the starting RNA were analyzed by Q-PCR using an iQ5 Real-Time PCR detection system (Bio-Rad). *Glycine max* GS<sub>1</sub> isoform GS<sub>1</sub>β1, GS<sub>1</sub>β12, GS<sub>1</sub>γ1, and GS<sub>1</sub>γ2, transcripts were analyzed along with the *Glycine max* CDPK-related protein kinase (*GmCRK*) gene as an internal reference for standardization as described in (Libault et al. 2008). All the primers used for Q-PCR analysis are shown in table 2.2. For Q-PCR, 500 nM of each primer was mixed with cDNA samples in SYBR green Premix ExTaq II (Takara). Q-PCR was performed using the following parameters: 1 cycle of 5 minutes at 50°C, 1 cycle of 10 minutes at 95°C, and 55 cycles of 30 seconds at 95°C, 45 seconds at 48°C and 45 seconds at 72°C in a 96-well optical PCR plate (ABgene). Specific amplification of target genes was confirmed by melting curve analysis of PCR products. Data analysis was performed by using iQ5 Optical System software (Bio-Rad). The relative expression value of each gene was calculated by using the comparative threshold cycle (Ct) method as previously described (Pfaffl 2001; Schmittgen and Livak 2008). ΔCt was calculated using equation 2.1,

$$\Delta Ct = Ct_{(target)} - Ct_{(reference)} \quad (\text{Eq. 2.1})$$

where Ct<sub>(target)</sub> is the Ct value of gene of interest, and Ct<sub>(reference)</sub> is the Ct value of the reference. Relative expression was calculated by using following equation;

$$\text{Normalized expression} = 2^{-\Delta Ct} \quad (\text{Eq. 2.2})$$

**Table 2.2: - Oligonucleotide primers used for Q-PCR analysis.**

Primer Name	Comment	Sequence (5'-3')
<b>GS<sub>1</sub>β<sup>a</sup></b>	Forward	GAAGGGATATTTTGAGGACAGA
<b>GS<sub>1</sub>γ<sup>b</sup></b>	Forward	TTCCATGATTGCTGAGACAA
<b>GS<sub>1</sub>β1</b>	Reverse	AGGCACCAACCATAGTACCA
<b>GS<sub>1</sub>β2</b>	Reverse	CCTTGTTCCCTTGTTCCCTTGT
<b>GS<sub>1</sub>γ1</b>	Reverse	AAGGCATGTGTGATTATTTTGT
<b>GS<sub>1</sub>γ2</b>	Reverse	TGACCATCTAAACAACAATGC
<b>GmCRK<sup>c</sup></b>	Forward	GAGCACCATGCCTATC
<b>GmCRK<sup>c</sup></b>	Reverse	TGGTTATGTGAGCAGATG

<sup>a</sup> Forward primer was common for both GS<sub>1</sub>β1 and GS<sub>1</sub>β2 isoforms.

<sup>b</sup> Forward primer was common for both GS<sub>1</sub>γ1 and GS<sub>1</sub>γ2 isoforms.

<sup>c</sup> putative CDPK-related protein kinases cDNA (Libault et al. 2008).

## 2.4. Site directed mutagenesis of GS

Site directed mutagenesis of GS<sub>1</sub> was done by a PCR-based strategy as shown in figure 2.2. This technique requires four primers (A, B, C, and D from figure 2.2) where A and D primers are the gene specific primers at the 5' and 3' end of the ORF respectively, and the B and C primers are designed to engineer the mutation in the cDNA. The B and C sequence are complementary to each other containing ~20 base pairs on either side of the mutagenesis site. PCR 1 (primers A and B) and 2 (primer C and D) were performed using primer concentrations of 0.5  $\mu$ M of each, 1 mM dNTP and the Phusion Hot Start II High Fidelity DNA polymerase in Phusion-HS buffer (Thermo Scientific) with the following amplification parameters in Mastercycler (Eppendorf): 94°C for 30 seconds; followed by 33 cycles of: 94°C for 15 seconds, 55°C for 20 seconds, 72°C for 45 seconds; and a final elongation cycle of 72°C for 5 minutes. Primer annealing temperature and elongation time used in PCR were varied according to melting temperature ( $T_m$ ) of the primers and length of the template amplified. The products from PCR 1 and 2 were mixed in equimolar concentrations, and the mixture was used as a template for a third PCR reaction with gene specific primers A and B using the same conditions as in PCR 1 and 2. The PCR product was purified by electrophoresis on 1% [w/v] low melting agarose in TAE buffer followed by extraction using the Qiaquick gel purification kit (Qiagen). The purified product was cloned in pET28a vector as described above for the molecular cloning of GS. PCR-based site directed mutagenesis using the

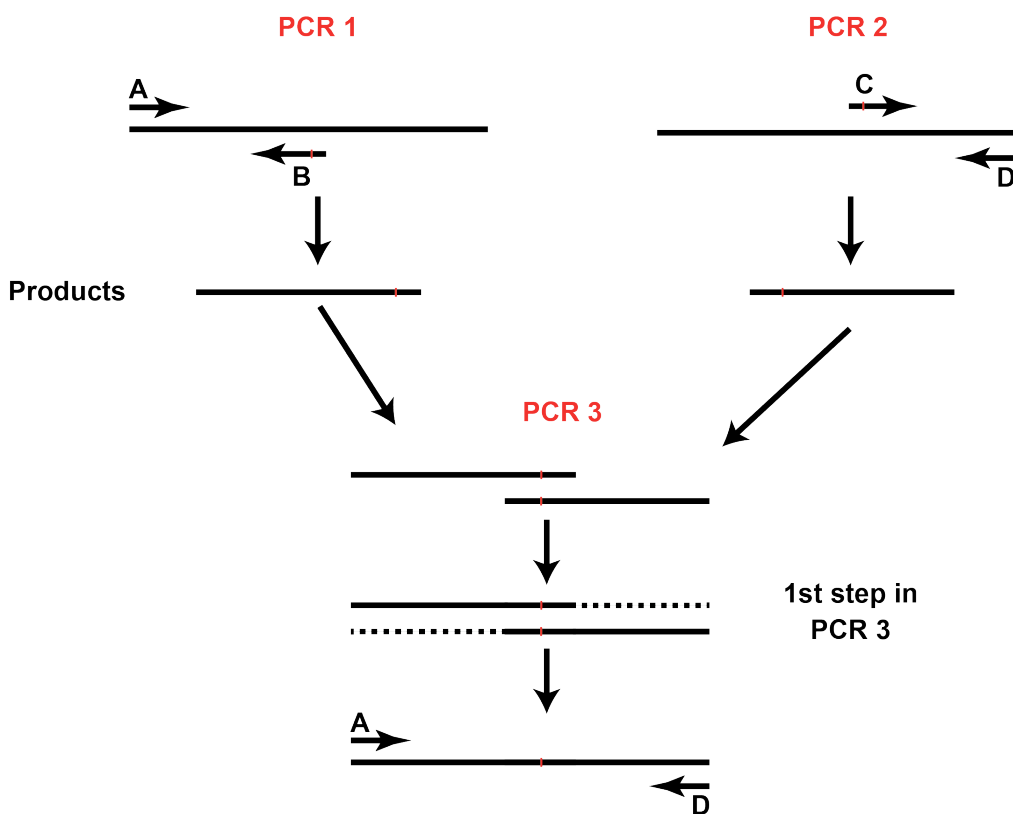


**Figure 2.2: Strategy for PCR-based site-directed mutagenesis.** Mutagenesis

primers (primer B and C) are shown with a red line representing the site of mutation.

Both the primers were complementary to each other overlapping ~ 20 base pairs. PCR 1 with primer A & B and PCR 2 with primer C & D where A & D are the gene specific primers were performed using the WT ORF as a template. The products from PCR 1 and 2 have complementary regions which will anneal with each other and act as priming sites for 1<sup>st</sup> step in PCR reaction 3 where DNA polymerase extend the strands it to produce the full length ORF with the desired mutation. Gene specific primers used in PCR 3 will amplify the product, which can be cloned in pET28a.

**Table 2.3: - Oligonucleotide primers used for generating site-directed GS<sub>1</sub> mutants.**

Primer Name <sup>a</sup>	Comment <sup>c</sup>	Sequence <sup>b</sup>
GS <sub>1</sub> γ1C92S Rev	Primer B	AGGAGTGTAAAGCATCAG <u><b>A</b></u> GACATAACCAGGATATT
GS <sub>1</sub> γ1C92S Ror	Primer C	AATATCCTGGTTATGT <u><b>C</b></u> TGATGCTTACACTCCT
GS <sub>1</sub> γ1C159S Rev	Primer B	GTTAGCACCAGTACC <u><b>AGA</b></u> AATAATATGGTCCTTGT
GS <sub>1</sub> γ1C159S For	Primer C	ACAAGGACCATATTAT <u><b>TCT</b></u> TGGTACTGGTGCTAAC
GS <sub>1</sub> γ1 NheI-For	Primer A	CGAG <u><b>CTAGCAT</b></u> GTTCGTTGCTCTCCGAT
GS <sub>1</sub> γ1 NotI-Rev	Primer D	CGAG <u><b>CGGCCGCT</b></u> TATGGTTTCCAAAGAATGGT

<sup>a</sup> For-Forward, Rev- Reverse. Primers are labeled with the gene name with the restriction site present on it. The amino acid residue and their positions along with the substituted residue are shown.

<sup>b</sup> Underlined regions represent sequences coding for restriction sites. Underlined and bold regions represent the sites of base substitutions.

<sup>c</sup> Primers used for site-directed mutagenesis are labeled from primer A to D.

primers shown in table 2.3 was performed to substitute serines for cysteine 92 and cysteine 159 residues in GS<sub>1</sub>γ1.

Chimeric proteins of GS<sub>1</sub> isoforms were generated using the PCR-based site-directed mutagenesis method shown in figure 2.3 which shows the generation of one of the chimeras (GS<sub>1</sub>β1γ1) used in this work. In this example, the 5' half was from the GS<sub>1</sub>β1 isoform and the 3' half was from the GS<sub>1</sub>γ1 isoform. The 5' half of the chimera was amplified (PCR 1) from the GS<sub>1</sub>β1 ORF using a 5' GS<sub>1</sub>β1-specific forward primer (primer A) and a reverse primer (primer B) complementary to the 3' end of the GS<sub>1</sub>β1 half of chimera with a 10 base pair overhang from the 5' end of the GS<sub>1</sub>γ1 half in chimera. The 3' half of the chimera was amplified (PCR 2) from the GS<sub>1</sub>γ1 ORF using a 3' GS<sub>1</sub>γ1-specific reverse primer (primer D) and a forward primer (primer C) complementary to the 5' end of the half of chimera with a 10 base pair overhang from the 3' end of the GS<sub>1</sub>β1 half in chimera. In the final PCR (PCR 3), products from first two PCRs where the 3' end of the product from PCR 1 and the 5' end of the product from PCR 2 have a complementarity region of 20 base pair were mixed in equimolar concentration to use as a template. Complementary regions from primers anneal to each other and were extended in first step in PCR 3. Primers A and D amplify the full-length chimeric product that was cloned in pET28a vector as described above. The sequences of the primers used to create chimeras are shown in the table 2.4.

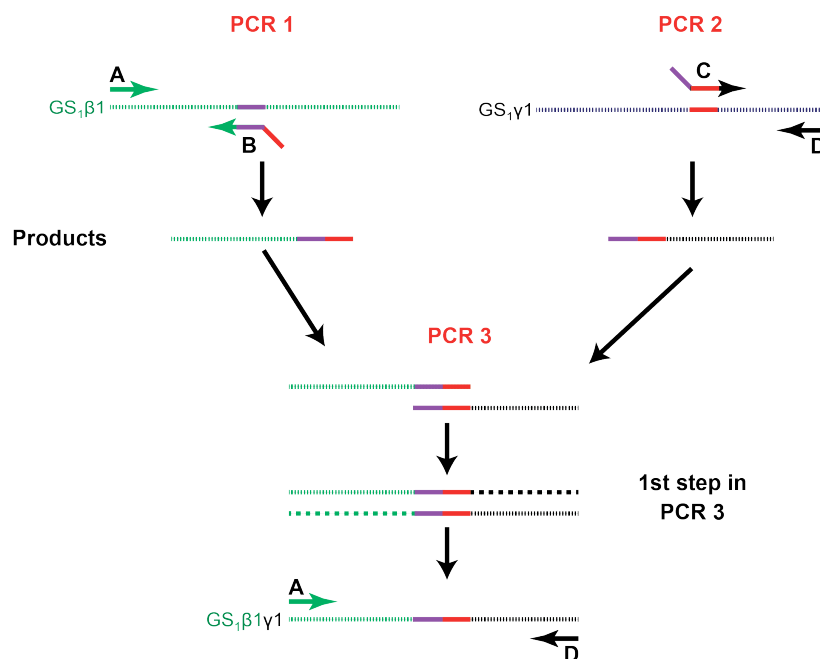


**Figure 2.3: Strategy for PCR based GS chimera synthesis.** Complementary chimeric primers containing overhanging sequences complementary to different isoforms were prepared (primers B and C, see table 2.4). The violate color shows regions of complementarity with the GS<sub>1</sub>β1 isoform and the red color shows regions of complementarity with the GS<sub>1</sub>γ1 isoforms. Both B and C primers were complementary to each other with an overlap of ~ 20 base pairs at their 5' ends. PCR 1 (with primers A and B) and PCR 2 (with primers C and D) were performed using GS<sub>1</sub>β1 and GS<sub>1</sub>γ1 ORFs as templates respectively. The 3' of product from PCR 1 and 5' end of product from PCR 2 share complementarity and will anneal with each other and act as priming site for PCR 3 where DNA polymerase will extend it to produce the full-length chimeric product. Gene specific primers used in PCR 3 will amplify the product, which can be cloned into pET28a. The final product is a chimera with N-terminal coding region of GS<sub>1</sub>β1 isoform and the C-terminal coding region of the GS<sub>1</sub>γ1 isoform.



**Table 2.4: - Oligonucleotide primers used for chimera cloning.**

Primer Name <sup>a</sup>	Comment <sup>c</sup>	Sequence (5' to 3')
Chimera 41 Rev	Primer B	CCGGTCCTGGGAGTGTCTTGCTTTGCT
Chimera 41 For	Primer C	AGGACACTCCCAGGACCGGTTAAAGACC
Chimera 66 Rev	Primer B	CACTATCTTCCCCAGGAGCTTGACCAGT
Chimera 66 For	Primer C	GCTCCTGGGGAAGATAGTGAAGTGATCT
Chimera 79 Rev	Primer B	TCCACTGATGTTGATGCCCGCATAAATACA
Chimera 79 For	Primer C	TGTATTTATGCGGGCATCAACATCAGTGGA
Chimera 250 Rev	Primer B	CCAGCACCATTCGAATCACCC
Chimera 250 For	Primer C	GGGTGATTGGAATGGTGCTGG

<sup>a</sup> Primers are labeled with amino acid residue at the junction of the two GS<sub>1</sub> isoforms in the chimeric protein.

<sup>b</sup> Primers are labeled as B and C for chimera synthesis reactions.

## **2.5. Purification of native nodule and recombinant soybean GS<sub>1</sub> isoforms from *E. coli* expression clones**

For the preparation of soybean nodule GS, 26 day old nodules were homogenized in 100 mM Tris-HCl, pH 8.4, 10 mM MgOAc, 10% [v/v] glycerol, 0.05% [v/v] triton X-100 (3 ml/g nodules) on ice. The extract was centrifuged at 35,000 X g at 4°C for 30 minutes, and the proteins from the supernatant fraction were precipitated by combining with an equal volume of chilled acetone with mixing. The precipitate was collected by centrifugation at 35,000 X g at 4°C for 30 minutes and was resuspended in 10 mM Tris-HCl, pH 7.5, 10 mM MgOAc, 10% [v/v] glycerol (Sephacryl Buffer) and was subjected to differential (NH<sub>4</sub>)<sub>2</sub>SO<sub>4</sub> precipitation. The pellet obtained from the 30 to 60% (NH<sub>4</sub>)<sub>2</sub>SO<sub>4</sub> saturation cut was resuspended in Sephacryl Buffer, and was chromatographed at 4°C on Sephacryl S300 (50 cm X 2 cm column) with flow rate of 0.5 ml/minute. Fractions (1.5 ml) were collected and GS activity was estimated as described below. Fractions with maximal GS activity were pooled and stored at -80°C.

For expression of recombinant GS<sub>1</sub>, expression constructs of soybean cytosolic GS<sub>1</sub> isoforms cloned into the bacterial expression plasmid pET28a were transformed into chemically competent *E. coli* Rosetta strain (Invitrogen) by the heat shock method (Sambrook et al. 2001). Transformants were cultured with shaking at 37°C in 0.5 liter of Luria Bertani (LB) broth media containing 50 µg/ml kanamycin. Cultures were grown to a cell density of A<sub>600</sub> 0.5, and were induced with 1 mM isopropyl β-D-1-thiogalactopyranoside (IPTG). Cultures were grown

for an additional 16 hr with shaking at room temperature. Cells were collected by centrifugation at 8000 X g for 15 minutes at 4<sup>0</sup>C and were resuspended in 20 ml of 20 mM Tris-HCl, pH 7.9, 300 mM NaCl, 25 mM imidazole, 10% [v/v] glycerol, 1 mM phenylmethylsulfonyl fluoride (PMSF), 1 µg/ml leupeptin, 0.1% (w/v) triton X-100, 100 µg/ml lysozyme. Resuspended cells were broken either in a French Press Pressure Cell (SIM-AMINCO Spectronic Instruments) or by 3 cycles of 30 second sonication and 30 second on ice using a Sonic Dismembrator (Artek Systems Corporation). The extract was centrifuged at 150,000 X g for 30 minutes at 4<sup>0</sup>C, and the supernatant fraction was applied to 1 ml of Ni<sup>2+</sup> - nitrilotriacetic acid agarose (Ni-NTA, Qiagen) pre-equilibrated in 20 mM Tris-HCl, pH 7.5, 300 mM NaCl, 30 mM imidazole (Wash Buffer). The column was washed with at least 0.5 liters of Wash Buffer and was eluted with 20 mM Tris-HCl, pH 7.5, 300 mM NaCl, 10% [v/v] glycerol, 0.5 M imidazole. Eluted fractions were analyzed by SDS-PAGE with the Laemmli buffer system of (Laemmli 1970) on 12.5% [w/v] polyacrylamide gels to determine protein purity. GS activity was determined as described below and the fractions containing GS activity were pooled, dialyzed against 20 mM Tris-HCl, pH 7.5, 150 mM NaCl, 5 mM MgCl<sub>2</sub>, 10% [v/v] glycerol and were stored at -80°C.

## **2.6. Glutamine synthetase (GS) activity assay**

GS activity was assayed by one of two methods: the hydroxylamine colorimetric method described in (Minet et al. 1997) or by the determination of the release of inorganic phosphate as described in (Gawronski and Benson

2004). The hydroxylamine colorimetric method was used for interaction assays and the inorganic phosphate estimation assay was used for kinetic studies. For the hydroxylamine-based method, assays were initiated by the addition of enzyme and were incubated at 37°C in 50 mM imidazole, 50 mM sodium glutamate, 20 mM MgCl<sub>2</sub>, 25 mM β-mercaptoethanol, 50 mM hydroxylamine, pH 7.3. Assays were terminated by the addition of 370 mM Fe(Cl)<sub>3</sub>, 300 mM trichloroacetic acid, 600 mM HCl. The concentration of the product (γ-glutamylhydroxamate) was determined spectrophotometrically by the absorbance at 492 nm by plotting standard graph of known γ-glutamylhydroxamate concentrations. For the inorganic phosphate-based method, assays were performed in 100 mM MOPS-NaOH, 50 mM sodium glutamate, 50 mM MgCl<sub>2</sub>, 10 mM ATP and 50 mM NH<sub>4</sub>Cl, pH 7.5. Assays were initiated by the addition of enzyme and the reaction was conducted for 5 minutes at 37°C. Assays were terminated by combining the reaction mix (50 µl) with 150 µl of 0.67% [w/v] ammonium molybdate tetrahydrate, 8% [w/v] L-ascorbic acid in 0.3N HCl. After incubation at room temperature for 5 minutes, 150 µl of 2% [w/v] sodium citrate, 2% [v/v] acetic acid was added and each sample was incubated for an additional 15 minutes before measuring the absorbance at 690 nm. The concentration of inorganic phosphate was determined from a standard curve generated with known inorganic phosphate concentrations.

GS kinetic studies were performed using the microtiter assay described in (Gawronski and Benson 2004). Kinetic studies were performed by varying concentrations of one of the substrate while concentration of other two substrates

was kept constant (50 mM glutamate, 50 mM NH<sub>4</sub>Cl and 10 mM ATP). Pseudo first order conditions were assumed and the  $V_{\max}$  and  $K_m$  values were calculated by data fitting to the Michaelis-Menten equation 2.3 in Graphpad Prism 5 (Graphpad software).

$$V_o = \frac{V_{\max} [S]}{K_m + [S]} \quad (\text{Eq. 2.3})$$

The turnover number of GS protein was determined using following equation 2.4

$$kcat = \frac{V_{\max}}{[E_t]} \quad (\text{Eq. 2.4})$$

where  $[E_t]$  is total enzyme concentration and  $V_{\max}$  is calculated from equation 2.3. Recombinant proteins were used therefore the molecular weight of recombinant protein (41.41 kDa for GS<sub>1</sub>β1 and 41.63 kDa for GS<sub>1</sub>γ1) were used to calculate  $[E_t]$

To determine the effect of nodulin 26 C-terminal peptides on GS activity, recombinantly purified GS<sub>1</sub>β1 was pre-incubated with 10 molar excess of soybean nodulin 26 peptide (CK-25 and CK-25(P)) at 37°C for 20 minutes in GS assay buffer before estimating the GS activity of the mixture by the inorganic phosphate estimation assay.

To determine the effect of reducing and oxidizing reagents on activity, recombinantly purified GS<sub>1</sub> isoforms were incubated either with reducing agent (25 mM β-mercaptoethanol) or oxidizing agent (3 mM H<sub>2</sub>O<sub>2</sub>) in 20 mM Tris-HCl, pH 7.5, 150 mM NaCl, 10% [v/v] glycerol for 30 minutes on ice. GS activity in all the samples was estimated using the inorganic phosphate estimation assay and

expressed as % GS activity standardized to the GS activity in reducing agent. To observe air oxidation, GS activity was determined in GS<sub>1</sub> proteins after 16 hr dialysis against 20 mM Tris-HCl, pH 7.5, 150 mM NaCl, 10% [v/v] glycerol at 4°C. To determine the reversibility of oxidation, 25 µg of dialyzed and air oxidized GS<sub>1</sub>γ1 was incubated with 4 mM DTT in 20 mM Tris-HCl, pH 7.5, 150 mM NaCl, 10% [v/v] glycerol for 30 minutes on ice. Half of the sample was further incubated with 40 mM oxidized glutathione (GSSG) for 30 minutes at room temperature and the activity of all the samples was determined by using phosphate estimation assay.

GS<sub>1</sub> proteins were analyzed using reducing and non-reducing SDS-PAGE to determine the effect of oxidation. Five µg of air oxidized GS<sub>1</sub> proteins were incubated with 10 mM DTT or 10 mM H<sub>2</sub>O<sub>2</sub> for 15 minutes. The samples along with untreated sample were mixed with 50 mM Tris-HCl, pH 6.8, 1.6% [w/v] SDS, 8% [v/v] glycerol, 60 µg/ml bromophenol blue and were separated by SDS-PAGE on 12.5% [w/v] SDS-polyacrylamide gels. Protein bands were visualized after staining with Coomassie stain.

## **2.7. Determination of free cysteinyl residues in reduced and oxidized GS<sub>1</sub>γ1**

For determination of the free cysteine concentration in oxidized and reduced GS<sub>1</sub>γ1, air oxidized recombinant GS<sub>1</sub>γ1 or air oxidized GS<sub>1</sub>γ1 treated with DTT was used without incubating with DTT. Recombinant GS<sub>1</sub>γ1 (100 µg) was reduced by incubating with 50 mM DTT in 20 mM Tris-HCl, pH 7.5, 150 mM

NaCl, 5 mM MgCl<sub>2</sub>, at 37°C for 1 hr. Reduced GS<sub>1</sub>γ1 was separated from DTT using Sephadex G-25 size exclusion resin (11cm X 0.5 cm) in 20 mM Tris-HCl, pH 7.5, 150 mM NaCl, 5 mM MgCl<sub>2</sub>. A BCA assay (Thermo Scientific) was performed to identify fractions containing GS<sub>1</sub>γ1, which were then pooled. The protein concentration in pooled fractions was estimated by BCA assay and free cysteine concentration was estimated by using Ellman's assay (Sedlak and Lindsay 1968). Free cysteine concentration was expressed as nmol of cysteine present per nmol of GS<sub>1</sub>γ1 monomer.

## **2.8. Affinity chromatography on peptide resins**

Synthetic peptides for preparing immobilized peptide resins were obtained from GenScript (Piscataway). Peptides were designed with an additional N-terminal cysteine which allows immobilization on resins or attachment of fluorescent labels (Table 2.5). Resins were prepared by immobilization of CK-25 (C-terminal peptide of soybean nodulin 26), CI-14 (C-terminal peptide of nodulin 26 from *Lotus japonicus*) and CG12(P) (phosphorylated C-terminal peptide of nodulin 26 from *Lotus japonicus*) (Table 2.5) to ω-aminohexyl agarose by the protocol of (Guenther et al. 2003). Prior to immobilization, peptides (2 mg) were reduced with 10 mM DTT in 10 mM Tris-HCl, pH 7.5 at room temperature for 30 minutes. Reduced peptides were purified by reverse phase chromatography on C18 Sep-pak (Waters) columns equilibrated with 10% [v/v] acetonitrile in 0.1% [v/v] trifluoroacetic acid (TFA). After washing with 10 ml 10% [v/v] acetonitrile in

**Table 2.5: - Sequences of nodulin 26 C-terminal peptides.**

Peptide Name <sup>a</sup>	Sequence <sup>b</sup>
CK-25	CRYTDKPLSEITKSASFLKGRAASK
CI-14	CREITKNVSFLKGI
CG12P	CEITKNVS <sub>(P)</sub> FLKG
CK-25(P)	CRYTDKPLSEITKSAS <sub>(P)</sub> FLKGRAASK

<sup>a</sup> Nodulin 26 peptides are labeled using first and last amino acid number representing the length of the peptide . In each case an additional N-cysteine which was not present in the parent sequence is included to serve as a site for attachment of fluorescent probes or immobilization on resins. C-terminal peptide of nodulin 26 from soybean and *L. japonicus* are labeled as CK-25 (phosphorylated form CK-25(P) and CI-14 (phosphorylated form CG12P) respectively.

<sup>b</sup> Phosphorylation is shown as (P) next to the phosphorylated amino acid residue.



0.1% [v/v] TFA, peptides were eluted with 60% [v/v] acetonitrile in 0.1% [v/v] TFA. Eluted peptides were dried under vacuum and were resuspended in 500  $\mu$ l water. The purified reduced peptides were cross-linked with  $\omega$ -aminohexyl agarose using the heterobifunctional cross-linker, m-maleimidobenzoyl N-hydroxysuccinimide (MBS) (Pierce).  $\omega$ -Aminohexyl agarose (1.5 ml) was washed and resuspended in 10 mM NaPO<sub>4</sub>, pH 7 followed by addition of 6.5 mg of MBS dissolved in 200  $\mu$ l DMSO (total volume of the mixture was 10 ml). After incubation at room temperature for 90 minutes, the resin was washed with 1 liter of 10 mM NaPO<sub>4</sub>, pH 7 and was resuspended in 10 ml of the same buffer. The resuspended resin was then combined with reduced peptide (2 mg/500  $\mu$ l) and was incubated at room temperature for 90 minutes. The resin was washed with 700 ml of 10 mM NaPO<sub>4</sub>, pH 7 and was resuspended in 10 ml of the same buffer. One mM  $\beta$ -mercaptoethanol was added to the resuspended resin to block unreacted MBS on the resin. The final resin was stored in 10 mM NaPO<sub>4</sub>, pH 7 at 4°C.

For chromatography on peptide resins, soybean nodule extracts were prepared as described above, and 5 ml (1 mg/ml protein) was applied to the resin (0.2 ml) equilibrated in 50 mM Tris-HCl, 150 mM NaCl, pH 7.5 (binding buffer). After washing with 10 ml of binding buffer, the resin was eluted with 50 mM Tris-HCl, 6 M urea, pH 7.5 and the eluent was analyzed by SDS-PAGE on 12.5% [w/v] SDS-polyacrylamide gels using the buffer system of Laemmli (Laemmli 1970).

For resin association assays, 50  $\mu$ l of peptide resin or underivatized  $\omega$ -aminoethyl agarose (negative control) were incubated with 50 units (1 U = 1 nmol  $\gamma$ -hydroxyglutamate/ minute at 37°C) of purified soybean GS in binding buffer for 30 minutes at 25°C with intermittent mixing. The resin was separated from the soluble fraction by centrifugation and was washed with 10 ml of binding buffer. The fraction of the GS activity bound to the resin or present in the unadsorbed supernatant fractions was determined.

## **2.9. Mass spectrometry**

Proteins were resolved by SDS-PAGE on 12.5% [w/v] polyacrylamide gels and protein bands were identified by Coomassie blue staining. Stained protein gel bands were excised and were washed with deionized water for 15 minutes, followed by 50% [v/v] acetonitrile for 15 minutes. The gel pieces were incubated in 100  $\mu$ l of 100 mM  $\text{NH}_4\text{HCO}_3$  for 5 minutes before adding 100  $\mu$ l of 100% acetonitrile. The gel pieces were washed in 100% acetonitrile and were dried under vacuum. The proteins were reduced in 100 mM  $\text{NH}_4\text{HCO}_3$  containing 10 mM DTT for 1 hr at 56°C, and were then alkylated by incubation with 100 mM  $\text{NH}_4\text{HCO}_3$ , 55 mM iodoacetamide for 45 minutes at 25°C. The gel pieces were washed with 100  $\mu$ l of 100 mM  $\text{NH}_4\text{HCO}_3$  for 5 minutes, and were dehydrated by addition of 100 % acetonitrile. This hydration/dehydration cycle was repeated and the gel pieces were dried. Four  $\mu$ l of 0.05  $\mu\text{g}/\mu\text{l}$  TPCK-treated trypsin (Thermo Scientific) was added, and the sample was incubated at 4°C for 1 hr. The residual trypsin solution was removed, and the gel pieces were incubated in

50 µl of 25 mM NH<sub>4</sub>HCO<sub>3</sub>, and 2 mM CaCl<sub>2</sub> at 37°C for 16 hr. Digested peptides were extracted in 60% [v/v] acetonitrile containing 0.1% [v/v] trifluoroacetic acid (TFA) and the extract was desalted and concentrated with a 10 µl ZipTip<sub>C18</sub> (Millipore, Bedford, MA), according to manufacturer's instructions. The digested peptides were eluted using 5 µl of saturated α-cyano-4-hydroxy-cinnamic acid in 60% [v/v] acetonitrile in 0.1% [v/v] TFA, and 1 µl of the eluent was deposited on the target plate for MALDI-TOF mass spectrometry. Peptide mass spectra were acquired on a Bruker microflex time-of-flight (TOF) mass spectrometer (Bruker Daltonics) with a nitrogen laser operating at 337 nm on a positive-ion mode. Calibration was performed using externally calculated masses of the peptide calibration standard II (Bruker Daltonics) which includes: bradykinin fragment 1-7, angiotensin II and I, substance P, bombesin, porcine renin substrate tetradecapeptide, ACTH clip fragments 1-17 and 18-39, and somatostatin 28. The acceleration voltage was set to 20 kV, and pressure in the TOF analyzer was set to 6 X 10<sup>-7</sup> bar.

## **2.10. Two-dimensional electrophoresis**

For two dimensional electrophoresis, protein samples (5 µg) were dissolved in a final volume of 150 µl of 8 M urea, 2% [w/v] octylglucoside, 4% [w/v] CHAPS, 1% [w/v] DTT, 0.16% [v/v] Biolytes 5-7, 0.04% [v/v] Biolytes 3-10. Separation of samples in the first dimension was done by isoelectric focusing (IEF) on 7 cm ReadyStrip IPG strips, (immobilized linear pH 5-8 gradient from Bio-Rad). Rehydration and IEF were performed in a PROTEAN IEF cell

apparatus (Bio-Rad) at 20°C. The strips were passively rehydrated for 12 hour, and were subsequently focused using the following five steps; 100 V for 200 Vhr, 500 V for 500 Vhr, 1000 V for 1000 Vhr, 1000 to 8000 V for 1 hr, and maintained at 8000 V for 8000 Vhr. After IEF, the IPG strips were equilibrated twice for 15 minutes with gentle shaking in 5 ml of 50 mM Tris-HCl, pH 6.8, 6 M urea, 20% [v/v] glycerol, and 2% [w/v] SDS. Two percent (2%, [w/v]) DTT was added to the first equilibration step followed by the addition of 2.5% [w/v] iodoacetamide in the second equilibration step. The IPG strips were placed on top of a 8.5% [w/v] SDS-polyacrylamide gel and were sealed with 0.7% [w/v] agarose in 25 mM Tris, 192 mM glycine, 0.1% [w/v] SDS before second-dimensional separation by standard SDS-PAGE.

## **2.11. Symbiosome membrane binding assays**

Symbiosome membranes were isolated from soybean (*Glycine max*) root nodules according to protocol of Udvardi and Day (1989) as described in (Weaver et al. 1991). Forty grams of 28 days old soybean root nodules were collected and were washed in 20 mM MOPS-NaOH, pH 7.0, 350 mM mannitol, 3 mM MgSO<sub>4</sub>, and were crushed gently in 25 mM MOPS-NaOH pH 7.0, 350 mM mannitol, 10 mM MgSO<sub>4</sub>, 15 mM ascorbate, 1% [w/v] PVP-40, 5 mM DTT, 10 mM EDTA, 1 µg/ml leupeptin, 0.7 µg/ml pepstatin A and 1 mM PMSF using a mortar and pestle. The extract was passed through one layer of Miracloth (Calbiochem) to remove cell debris. Eight ml of the filtered extract was layered on 15 ml discontinuous Percoll (Sigma) gradients (30%, 60% and 80% [v/v] in 20

mM MOPS-NaOH, pH 7, 3 mM MgSO<sub>4</sub>). Gradients were centrifuged in an HS-4 rotor at 5500 rpm for 15 minutes at 4°C. Symbiosomes were collected from the interface between the 60% and 80% [v/v] Percoll layers, were suspended in 100 ml of 20 mM MOPS-NaOH, pH 7, 350 mM mannitol, 3 mM MgSO<sub>4</sub>, and were centrifuged at 650xg for 4 minutes at 4°C. The supernatant fraction was discarded and the symbiosome pellet was resuspended in 10 ml 20 mM MOPS-NaOH, pH 7.0, 0.15 M KCl. Resuspended symbiosomes were broken either by vortex (Rivers et al., 1997) or by extrusion twice through 25-gauge ½ inch needle (Weaver and Roberts, 1994). Bacteroids were separated by centrifugation at 7700 rpm in an SS-34 rotor for 10 minutes at 4°C. The supernatant fraction was collected and was centrifuged at 100,000x g for 45 minutes at 4°C to pellet the purified symbiosome membrane fraction. Isolated symbiosome membranes were resuspended in 20 mM MOPS-NaOH, pH 7.0, 0.15 M KCl, 1 µg/ml leupeptin, 0.7 µg/ml peptstatin A and were stored at -80°C.

For binding experiments with native or recombinant GS<sub>1</sub>, symbiosome membranes (100 µg of protein) were incubated with 50 units (1 U=1 nmol γ-hydroxyglutamate/ min at 37°C) of GS in incubation buffer (50 mM Tris-HCl, pH 7.5, 150 mM NaCl, 5 mM MgCl<sub>2</sub>) for 1 hr at 4°C. Membranes were collected by centrifugation at 200,000 X g for 30 minutes at 4°C, and were washed with 2 ml of incubation buffer. The centrifugation/washing cycle was repeated three additional times, and the membranes were resuspended in 100 µl of the incubation buffer and assayed for GS activity. For peptide inhibition experiments, 10 µM peptide was pre-incubated with GS for 30 minutes at 4°C prior to

incubation with symbiosome membrane samples. To determine the effect of nodulin 26 phosphorylation on GS<sub>1</sub>β1 binding, symbiosome membranes were incubated with alkaline phosphatase enzyme to dephosphorylate nodulin 26 before performing symbiosome membrane binding experiments. The phosphorylation state of nodulin 26 was determined by Western blot using a nodulin 26 phosphorylation site-specific antibody (Guenther et al. 2003). One hundred µg of untreated and dephosphorylated symbiosome membranes were incubated with equal amount of GS<sub>1</sub>β1 and after washing with incubation buffer (1 ml buffer wash repeated 5 times), GS activity retained on the symbiosome membranes was determined by inorganic phosphate estimation assay.

## **2.12. Fluorescence binding assays**

Binding assays to determine the dissociation constants for the nodulin 26 C-terminal peptide and GS<sub>1</sub>β1 were performed using fluorescent analogs of CK-25 and CK-25(P) peptides. N,N'-dimethyl-N-(iodoacetyl)-N'-(7-nitrobenz-2-oxa-1,3-diazol-4-yl)ethylenediamine (IANBD amide, Molecular Probes) was used for labeling the N-terminal cysteine side chain of each peptide. Reduced peptides were dissolved in 75 µl of 50 mM Tris-HCl, pH 7.5 and were combined with a 10-fold molar excess of IANBD amide dissolved in DMSO (15 mg/ml), and the reaction mixture was incubated at 4°C for 16 hr. The NBD-labeled peptide was isolated from free excess IANBD amide reagent by chromatography on a Sephadex G-25 column (11 cm X 0.5 cm) in 50 mM Tris-HCl, pH 7.5. The labeled peptide concentration was calculated from the A<sub>497</sub> (NBD ε = 26,000 M<sup>-1</sup>

<sup>1</sup>cm<sup>-1</sup>) and residual unlabeled peptide was quantitated by using Ellman's assay (Sedlak and Lindsay 1968). Under these conditions labeling of the N-terminal cysteine was stoichiometric.

Fluorescence measurements were performed using a QuantaMaster UV VIS (Photon Technology International) spectrofluorometer at 22°C. Binding assays were done in 50 mM Tris-HCl, pH 7.5, 150 mM NaCl, 5 mM MgCl<sub>2</sub> with the fluorescent peptide kept constant and the concentration of GS varied. Binding reactions were incubated at room temperature for 5 minutes prior to fluorescence measurements (excitation λ= 480 nm, emission λ= 545 nm). The increase in fluorescence intensity as a function of added GS was fit to the following binding expression:

$$\Delta F = \frac{\Delta F_{\max} [GS]}{K_d + [GS]} \quad (\text{Eq. 2.5})$$

where ΔF is the change in fluorescence intensity, ΔF<sub>max</sub> is the maximal change in fluorescent intensity at saturation, [GS] is the concentration of GS, and K<sub>d</sub> is the dissociation constant.

### **2.13. *In vitro* kinase assay and effect of phosphorylation on GS activity**

*In vitro* kinase assays were performed in the presence of <sup>32</sup>P labeled ATP (MP Biomedicals). Reactions were initiated by adding recombinantly purified calcium dependent protein kinase (CDPK) to the reaction mixture of CK-25 peptide (100 μg), 25 mM MOPS-NaOH, pH 7.0, 7.5 mM β-mercaptoethanol, 10

mM  $\text{Mg}(\text{CH}_3\text{COO})_2$ , 0.2 mM ATP and 800 dpm/pmol of  $^{32}\text{P}$  labeled ATP and were incubated at 30°C for 60 minutes. The phosphorylated peptide was separated by using reverse phase chromatography on C18 Sep-pak columns as described above. Purified peptide was dried in speed-vac and the concentration of the peptide was estimated by Ellman's assay, and was used for crosslinking experiments.

## **2.14. Crosslinking methods**

To determine the binding site of nodulin 26 on  $\text{GS}_1\beta 1$ , CK-25 peptides were cross-linked with  $\text{GS}_1\beta 1$  using a sulfated form of m-maleimidobenzoyl-N-hydroxysuccinimide ester (sulfo-MBS, Pierce) as a cross-linker. Sulfo-MBS is a water-soluble, sulfhydryl and amino group specific cross-linker with a spacer arm length of 7.3 Å. The reduced CK-25 peptide was prepared as described above and was incubated with 10 molar excess of sulfo-MBS in PBS buffer (10 mM  $\text{Na}_2\text{HPO}_4$ , 1.8 mM  $\text{KH}_2\text{PO}_4$ , 137 mM NaCl, 2.7 mM KCl, pH 7.2) for 30 minutes. A ten-fold molar excess of  $\text{GS}_1\beta 1$  (dialyzed in PBS) was added to the solution, and incubation was continued at room temperature for 30 minutes. The sample was separated by SDS-PAGE on 10% [w/v] polyacrylamide gels and the cross-linked protein bands were identified by Coomassie blue staining. Stained protein gel bands were excised and were subjected to trypsin digestion and analyzed by MALDI-TOF by the approach in the mass spectrometry section above.



## 2.15. Bimolecular fluorescence complementation (BiFC) assay

BiFC was done by the general approach of (Li and Nebenfuhr 2007) with the constructs used in this study shown in figure 2.4. Prior to cloning into BiFC plasmids, the *Bam*HI restriction site in GS<sub>1</sub>β1 was removed by PCR-based site directed mutagenesis using a double stranded GS<sub>1</sub>β1 cDNA template and the mutagenesis primers shown in Table 2.6. This converted a T to a C at position 240 in the coding strand resulting in a silent mutation and the loss of the *Bam*HI restriction site. Constructs containing the soybean nodule GS<sub>1</sub>β1 or nodulin 26 ORFs as translational fusions with either the N-terminal 154 residues (YFP-N) or C-terminal 84 residues (YFP-C) of the yellow fluorescent protein were prepared in *pd35S-YFP-N* or *pd35S-YFP-C* vectors (a kind gift from Dr. Andreas Nebenführ, the University of Tennessee, Knoxville). For preparation of N-terminal fusions of GS<sub>1</sub>β1 and nodulin 26 (YFP-N-nod26 and YFP-C-GS<sub>1</sub>β1), ORFs were amplified using gene specific primers (Table 2.4) flanked by restriction sites for *Bam*HI on the forward primer and *Not*I on the reverse primer. The amplified ORFs of GS<sub>1</sub>β1 and nodulin 26 were cloned into *Bam*HI-*Not*I digested *pd35S-YFP-N* or *pd35S-YFP-C* vectors, respectively. For preparation of C-terminal fusions of nodulin 26 (nod26-YFP-N) the nodulin 26 ORF, lacking the stop codon, was amplified using primers (Table 2.6) flanked by *Xba*I and *Bam*HI sites to facilitate cloning into the *pd35S-YFP-N* vector. A linker region of ten-residues (GGHHHHHHGG) was introduced between the GS or nod26 sequences and the YFP sequences. All constructs were verified by automated

**Table 2.6: - Oligonucleotide primers used for generation of BiFC interaction plasmid constructs.**

Primer Name <sup>a</sup>	Comment <sup>b</sup>	Sequence (5'-3') <sup>c</sup>
GS <sub>1</sub> β1 T240C-Rev	Primer B	CAAGCCATTTTCAGGGACCCATTTCAGAAGGG GT
GS <sub>1</sub> β1 T240C-For	Primer C	ACCCCTTCTGAATGGGTCCCTGAAAATGGCTT G
GS <sub>1</sub> β1 BamHI-For	Primer A	CGAGGATCCGGTGGCCATCACCATCACCATC ACGGTGGCATGTCTCTGCTCTCAGATC
GS <sub>1</sub> β1NotI-Rev	Primer D	CGAGCGGCGCGCTCATGGCTTCCACAGAATGG
Nod26 BamHI-For	<i>BamHI</i> site	CGAGGATCCGGTGGCCATCACCATCACCATC ACGGTGGCATGGCTGATTATTCAGC
Nod26 NotI-Rev	<i>NotI</i> site	CGAGCGGCGCGCTTATTTGGAGGCAGCAC
Nod26 XbaI-For	<i>XbaI</i> site	GCGCTCTAGAATGGCTGATTATTCAGCAGG
Nod26 BamHI-Rev	<i>BamHI</i> site	CGAGGATCCGGTGGCCATCACCATCACCATC ACGGTGGCTTTGGAGGCAGCACAGCA

<sup>a</sup> For-Forward, Rev- Reverse. Primers are labeled with the gene name with the restriction site present on it. Site of mutation is shown flanked by the base substituted.

<sup>b</sup> Site-directed mutagenesis primers are labeled as primer A to D. Restriction sites present in the primer are labeled.

<sup>c</sup> Underlined and bold regions represent sequences coding for restriction sites. Linker regions used in BiFC constructs are shown in bold letters.

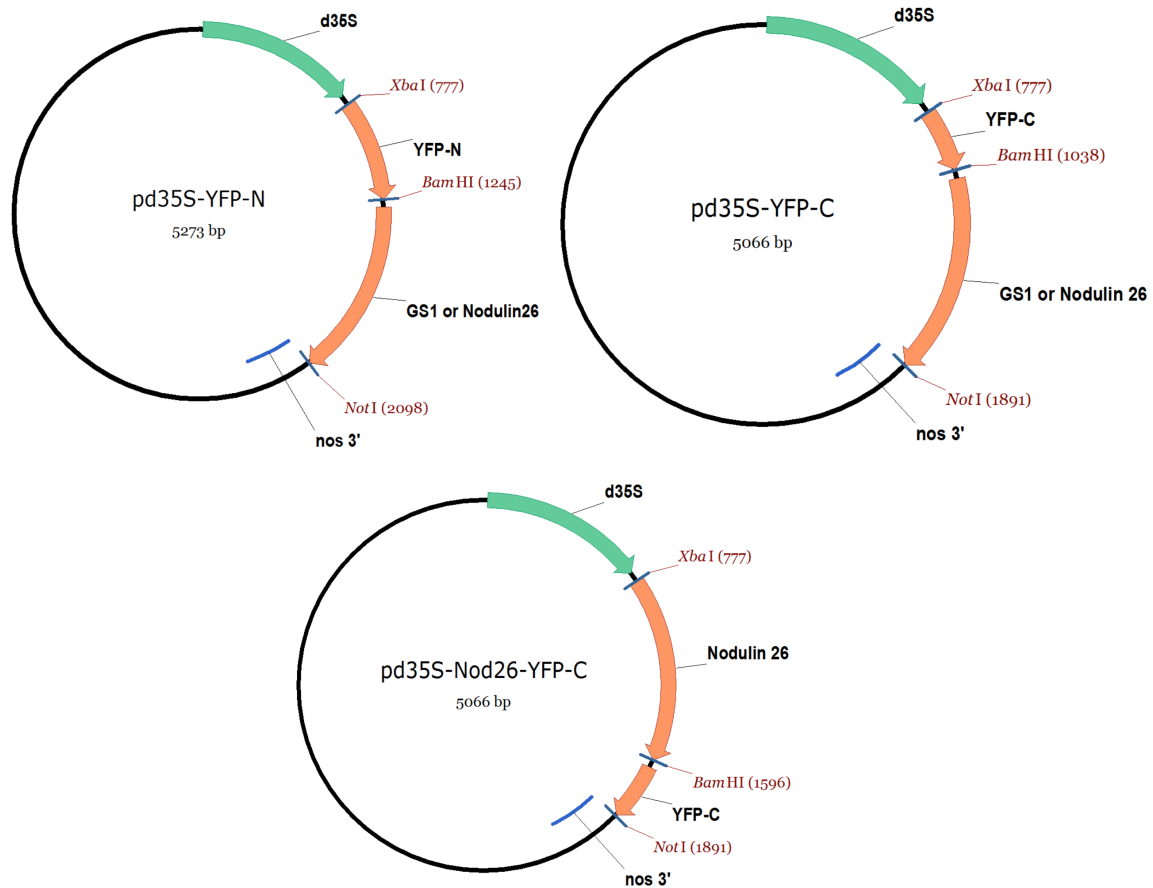


**Figure 2.4: Vector maps of BiFC constructs.** Open reading frames of either GS<sub>1</sub> or nodulin 26 were cloned using *Bam HI* and *Not I* restriction sites to produce N-terminal fusions with either C-terminal domain of YFP (YFP-C) or N-terminal domain of YFP (YFP-N). Nodulin 26 was cloned using *Xba I* and *Bam HI* sites to produce C-terminal fusions with YFP-C. All cloned fusions are under the control of double 35S tobacco mosaic virus promoter (d35S).

DNA sequencing in the Molecular Biology Resource Facility at The University of Tennessee, Knoxville.

Transient expression of fusion proteins and visualization of BiFC interactions was done by tungsten particle bombardment of onion bulb epidermal cells. Thirty mg of M17 (Bio-Rad) tungsten particles were suspended in 500  $\mu$ l of 70% [v/v] ethanol and were vortexed for 10 minutes. The particles were washed four times with 4 ml of sterile water before final resuspension in 500  $\mu$ l of 50% [v/v] sterile glycerol. YFP-N and YFP-C BiFC constructs (250 ng each in a total volume of 5-10  $\mu$ l) were mixed with 25  $\mu$ l of freshly prepared tungsten particles along with 25  $\mu$ l of 2.5 M  $\text{MgCl}_2$ , and 5  $\mu$ l of 200 mM spermidine. The mixture was vortexed for 5 minutes, and was allowed to settle for 1 min. The particles were washed with 100  $\mu$ l of 70% [v/v] ethanol, followed by 100% [v/v] ethanol and were resuspended in 25  $\mu$ l of 100% [v/v] ethanol. Eight  $\mu$ l of the resuspended particles were spread on the macrocarrier disks (Bio-Rad) and the disks were allowed to dry. Bombardment of onion epidermal cells placed on standard MS agar plates was done using a Biolistic Particle Delivery System with rupture disks of 1100-psi capacity (Bio-Rad). Onion cells were incubated for 24 hours at 28°C prior to microscopic examination with an Axiovert 200M microscope (Zeiss) equipped with filters for YFP fluorescence (Chroma, filter set 52017). Images were captured with a digital camera (Hamamatsu Orca-ER) controlled by the Openlab software (Improvision).

## 2.16. Protein analytical techniques

Protein concentrations were determined by using Bicinchoninic acid assay (BCA) (Walker 2009) or by the Bradford assay (Bradford 1976). Size exclusion chromatography was performed using pre-packed Superdex 200 10/300 GL (Tricorn) analytical column on an FPLC (AKTA) instrument. The chromatography was performed in 20 mM Tris-HCl, pH 7.5, 150 mM NaCl. The column was calibrated with a gel filtration standard (Cat # 151-1901, Bio-Rad) which included: bovine thyroglobulin (670 kDa), bovine gamma-globulin (158 kDa), chicken ovalbumin (44 kDa), horse myoglobin (17 kDa), vitamin B<sub>12</sub> (1.35 kDa). GS<sub>1</sub>Y1 and GS<sub>1</sub>Y1C159S proteins (200 µl) were injected on the size exclusion column and were chromatographed at a flow rate of 0.5 ml/min and 0.5 ml fractions were collected. Absorbance of the effluent was measured at 280 nm to monitor elution of protein peaks.

Analytical ultracentrifuge (AUC) experiments were performed using an Optima XL-I Beckman Coulter analytical ultracentrifuge equipped with an AN50Ti rotor. Sedimentation velocity experiments were performed on protein samples (400 µl of 0.5 mg/ml sample) dialyzed overnight in 20 mM Tris-HCl, pH 7.5, 20 mM imidazole, 10% [v/v] glycerol, 300 mM NaCl. Samples were loaded into the sample sector and dialysis buffer was loaded into the reference sector of double-sector epon centerpieces inside each centrifugation cell. Centrifugation cells were allowed to equilibrate at temperature inside the centrifuge under vacuum for 2 hr before centrifugation at 22°C and 30,000 rpm. Absorbance was measured

at 280 nm (200 scans at 1 minute intervals). Data were analyzed using continuous  $c(M)$  distribution model described by the Lamm equation (Eq. 2.6) with SEDFIT, freely available software (<http://www.AnalyticalUltracentrifugation.com>) (Dam and Schuck 2004; Schuck 2000).

$$\text{Min}_{c(M)} \left\{ \sum_{i,j} \left[ a(r_i, t_j) - \int c(M) L(M, r_i, t_j) dM \right]^2 \right\} \quad (\text{Eq. 2.6})$$

Here  $L(M, r, t)$  denotes the sedimentation profile of a monodisperse species of size  $M$  at radius  $r$  and time  $t$ ,  $a(r, t)$  denotes the experimentally observed signal. Continuous  $c(M)$  distribution gives differential molar mass distribution. In our analysis the covered molecular weights were from 0 to 2000 kDa with a resolution of 100 and a confidence level (F-ratio) of 0.95. Best fit was assumed when the run test Z values were below 40 with rmsd values below 0.01 absorbance units.

Sedimentation equilibrium experiments were performed using recombinantly purified samples dialyzed against 20 mM Tris-HCl, pH 7.5, 300 mM NaCl at 10°C. Centrifugation was conducted at 3,800, 6,000 and 7,500 rpm. Absorbance optics was collected at 6 hour intervals by averaging 20 scans at 280 nm until equilibrium was achieved at each speed. Absorbance data was collected for at least seven time points at each speed. Global analysis of the data collected was done using the discrete species model in SEDPHAT, a freely

available software (<http://www.AnalyticalUltracentrifugation.com>) (Dam and Schuck 2004; Schuck 2000) using equation 2.7 and mass was calculated using equation 2.8

$$a(r) = \sum_n c_{n,o} \varepsilon_n d \exp \left[ \frac{M_n (1 - v_n \rho) \omega^2}{2RT} (r^2 - r_0^2) \right] + \delta \quad (\text{Eq. 2.7})$$

$$M = \frac{2RT}{(1 - v_{\text{particle}} \rho_{\text{solvent}}) \omega^2} \times \frac{d(\ln \rho^*)}{dr^2} \quad (\text{Eq. 2.8})$$

where  $R$  is gas constant,  $T$  is temperature,  $v$  is partial specific volume,  $\omega$  is rotor angular velocity,  $\varepsilon$  is extinction coefficient,  $r$  is distance from the center of rotation,  $r_0$  is an arbitrary reference radius,  $d$  is optical pathlength,  $\rho$  is solvent density,  $\rho^*$  is mass concentration at particular radial distance. Bottom of the cell and molecular weights of the protein species were kept floating during analysis. The best fit was determined by achieving RMSD values below 0.007 absorbance units and chi-squared values near 1.

Sedimentation velocity experiments were performed on samples used for sedimentation equilibrium experiments. The buffer density, viscosity, and partial specific volume of all proteins were estimated using the program SEDNTERP 1.09 (<http://sednterp.unh.edu/>). Frictional coefficient used in our experiments was kept constant at 1.12. The density and viscosity of the buffer was 1.01331 g/ml and 0.01181 P respectively. The partial specific volume was 0.7334 ml/g.

## 2.17. Molecular modeling techniques

Homology models for soybean GS<sub>1</sub> were prepared by using the molecular operating environment (MOE) software package (Chemical Computing Group Inc) using the maize glutamine synthetase GS1a structure (PDB # 2d3a) as a template. Maize GS1a has 86% protein sequence identity with soybean GS<sub>1</sub>. Ten models were generated using the AMBER99 forcefield with medium model refinement. All the models have the root mean square deviation (RMSD) of less than 1 Å compared to maize GS1a. The quality of the models were also accessed by analysis for disallowed angles by Ramchandran plot analysis by using MOE software. The model with lowest RMSD and minimum disallowed angles was selected for further study. Monomeric models were superposed on the holoenzyme structure of maize GS1a to generate the holoenzyme models of each isoform.



## CHAPTER III RESULTS

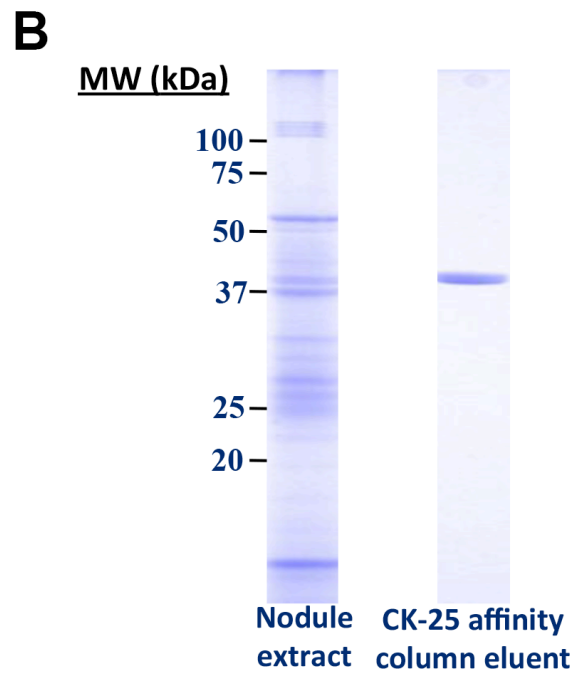
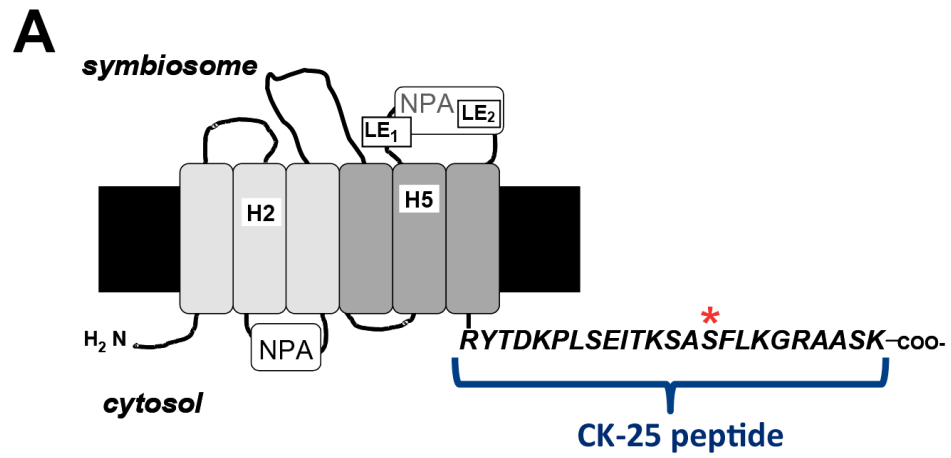
### 3.1. Interaction of glutamine synthetase with nodulin 26

*The work in this section was published as a first author manuscript (Masalkar P, Wallace IS, Hwang JH, Roberts DM. (2010) Interaction of cytosolic glutamine synthetase of soybean root nodules with the C-terminal domain of the symbiosome membrane nodulin 26 aquaglyceroporin. J Biol Chem. 285:23880-23888). Part of this work was done in collaboration with two other students, Jin Ha Hwang and Ian Wallace.*

#### ***I. Isolation of proteins interacting with the C-terminus of nodulin 26.***

As discussed in the introduction, nodulin 26 is a member of the major intrinsic protein/aquaporin superfamily (MIPs) of integral membrane channels, and is the major membrane protein of the soybean symbiosome membrane. The C-terminus of nodulin 26 is composed of a hydrophilic 24 amino acid extension (Figure 3.1.1A) which is exposed to the cytosolic side of the soybean symbiosome (Weaver et al. 1991). This C-terminal sequence is conserved among members of the group I nodulin 26-like intrinsic proteins (Wallace et al. 2006). MIP proteins are known to be the most concentrated proteins on their resident membrane and previous studies (Fan et al. 2005; Girsch and Perecchia 1991; Liu and Liang 2008; Noda et al. 2004a; Noda et al. 2004b; Noda and Sasaki 2005; Rose et al. 2008; Yu and Jiang 2004; Yu et al. 2005) suggest that the C-terminal domain of MIPs is a site for protein-protein interaction with various cytosolic proteins which regulate their function. To investigate the

**Figure 3.1.1: Isolation of soybean nodule proteins interacting with the C-terminus of nodulin 26.** (A) Diagram showing the topology of soybean nodulin 26 on the symbiosome membrane based on the conserved MIP fold and homology modeling (Wallace and Roberts 2004). Nodulin 26 has six trans-membrane  $\alpha$ -helical domains with hydrophilic C and N terminal regions on the cytosolic side. The C-terminal cytosolic sequence used to design the CK-25 peptide is shown. The unique site of CDPK phosphorylation is indicated by an asterisk. (B) Affinity chromatography with CK-25 peptide resin. Affinity chromatography of a soluble soybean nodule extract was performed on an affinity resin consisting of an immobilized peptide (CK-25) containing the C-terminal sequence of nodulin 26. Lane 1 shows a nodule extract prior to chromatography on CK-25 agarose. Lane 2 represents the bound fraction of the chromatography after elution with 6 M urea.



possibility that the nodulin 26 cytosolic C-terminal extension serves as a protein interaction site for nodule proteins, a synthetic peptide consisting of the 25 amino acids of the nodulin 26 C-terminus (CK-25) was immobilized on agarose to generate a peptide resin. The resulting CK-25 resin was used in an affinity chromatography with an extract of soluble soybean nodule protein. This chromatography resulted in the adsorption and purification of a major 40 kDa protein which bound tightly to the resin. Attempts to elute the protein by varying the pH and salt concentration of elution buffer were unsuccessful, and a high concentration of chaotrope (6 M urea) was required for elution. This was the only protein detectable by SDS-PAGE from the urea eluent (Figure 3.1.1B).

## ***II. Identification of the 40 kDa protein interacting with nodulin 26.***

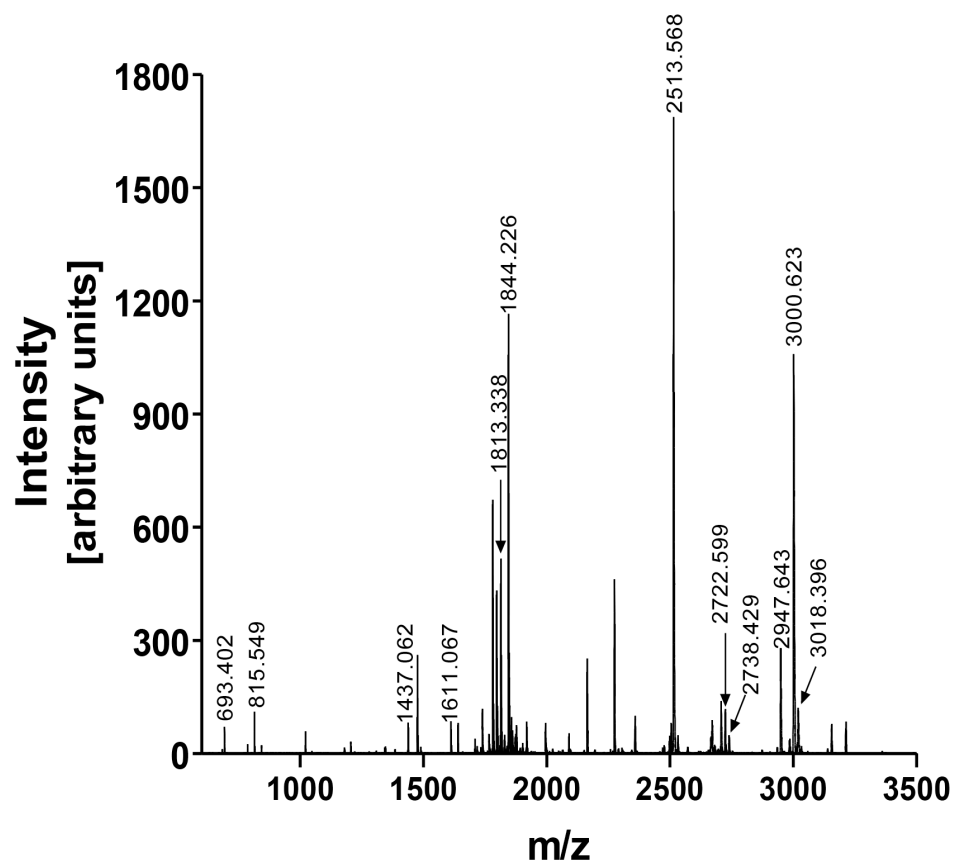
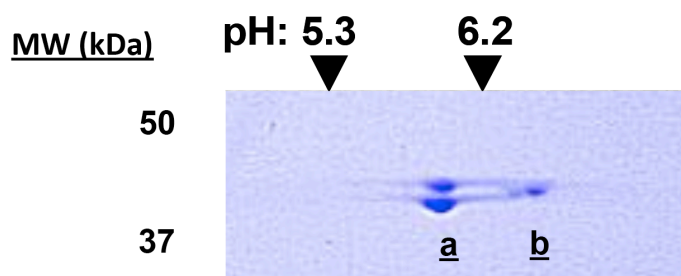
Identification of the 40kDa protein interacting with nodulin 26 was done using mass spectrometry. The 40 kDa protein band was excised from an SDS-PAGE gel, digested with trypsin, and was subjected to MALDI-TOF mass spectrometric analysis. Figure 3.1.2A shows the peptide mass spectra obtained from the 40kDa protein. Analysis of the masses of the peptides using PROWL identified soybean cytosolic glutamine synthetase GS<sub>1</sub>β1 as the most likely candidate protein (E value =  $6.1 \times 10^{-5}$ , 56 % sequence coverage). The peptides identified are listed in table 3.1.1. Confirmation of this assignment was obtained by MS-MS analysis of a 1610.022 Da tryptic peptide that yielded a sequence (277-HKEHIAAYGEGNER-290) characteristic of soybean GS<sub>1</sub>β1. In addition, the predicted molecular weight of soybean GS<sub>1</sub>β1 ( $M_r = 38,759$ ) is in agreement with

the observed 40 kDa molecular weight of the protein on an SDS-PAGE gel (Figure 3.1.1B).

To verify that glutamine synthetase is the protein that binds to the resin, interaction assays were performed using purified native glutamine synthetase (NGS) purified from soybean nodule extract as described in the Materials and Methods. Resins with immobilized C-terminal peptides of nodulin 26 from soybean (CK-25) or *Lotus japonicus* (CI-14) or the unconjugated solid support ( $\omega$ -aminohexyl agarose, a negative control) were incubated with purified NGS and after thorough washing, GS activity retained on the resin was measured. Nodule GS binds quantitatively to nodulin 26 peptide resins, but not to a negative control resin ( $\omega$ -aminohexyl agarose) (Figure 3.1.3). Overall, these experiments show that cytosolic GS is the major 40 kDa protein from soybean nodule extract that interacts with the nodulin 26 C-terminal 25 amino acid domain.

Previous studies have shown that the 4 isoforms of cytosolic glutamine synthetase are expressed in soybean root nodules which can be separated by two-dimensional gel electrophoresis (Morey et al. 2002). The four isoforms belong to two subclasses of cytosolic GS  $\beta$  and  $\gamma$  and are designated, GS $_1\beta$ 1, GS $_1\beta$ 2, GS $_1\gamma$ 1, GS $_1\gamma$ 2. A sequence comparison of the four isoforms is shown in figure 1.3.3. In order to achieve insight into which glutamine synthetase isoforms interact with the nodulin 26 C-terminal peptide, two-dimensional electrophoresis was performed on the proteins eluted from the CK-25 peptide resin. All four isoforms of glutamine synthetase could be resolved and identified on the

**Figure 3.1.2: Identification of the 40 kDa CK-25 interacting protein as cytosolic glutamine synthetase (GS).** (A) MALDI-TOF spectra of CK-25-interacting 40 kDa protein. MALDI-TOF spectrometric analysis was performed on protonated tryptic peptides ( $MH^+$ ) of the 40 kDa protein isolated by affinity chromatography on CK-25 agarose was performed. The 40 kDa protein was resolved by electrophoresis as in figure 3.1.1B and was subjected to in gel tryptic digestion and mass spectroscopic analysis. The Y-axis shows the intensity as arbitrary units. The mass to charge ratio is plotted on the X-axis. A summary of the peptides and proposed assignments is shown in Table 3.1.1. (B) 2D electrophoresis. Three  $\mu\text{g}$  of the purified CK-25 interacting protein was separated by 2D electrophoresis. The position of pH markers in the first dimension and the molecular weight standards in the second dimension are shown. The letters a and b show the position of migration of soybean glutamine synthetase  $GS_1\beta$  and  $\gamma$  isoforms respectively based on the work of Morey et al. (2002)

**A****B**

**Table 3.1.1: - Mass of 40 kDa protein tryptic peptides determined by MALDI-TOF.**

Measured mass <sup>a</sup>	Predicted mass	Residue indices <sup>c</sup>	Sequence <sup>d</sup>
692.392	692.385	(.007) <sup>b</sup>	219-223 YILER
785.382	785.334	(.048)	327-332 GYFEDR
814.532	814.491	(.041)	268-275 AAIDKLGK
1436.042	1435.755	(.287)	39-52 TLPGPVSDPSELPK
1610.022	1609.759	(.263)	277-290 HKEHIAAYGEGNER <sup>e</sup>
1737.602	1737.854	(-.252)	276-290 KHKEHIAAYGEGNER
1779.212	1778.902	(.310)	19-34 VIAEYIWIGGSGMMMDLR
1812.332	1812.039	(.293)	224-240 ITEIAGGGVVVSFDPKIPK
1843.212	1842.901	(.312)	296-311 HETADINTFLWGVANR
2356.362	2356.172	(.190)	85-106 GNNILVICDAYTPAGEIPTNK
2512.562	2512.273	(.289)	85-107 GNNILVICDAYTPAGEIPTNKR
2512.562	2512.273	(.289)	84-106 RGNNILVICDAYTPAGEIPTNK
2668.442	2668.374	(.068)	84-107 RGNNILVICDAYTPAGEIPTNKR
2946.632	2946.479	(.153)	113-137 VFSHPDVVAEVPWYGIEQEEYTLQK
2999.612	2999.392	(.220)	53-79 WNYDGSSTGQAPGEDSEVILYPQAIFR
3017.392	3017.416	(-.023)	138-165 DIQWPLGWPVGGFPGPQGPYYCGVGADK

<sup>a</sup> The experimental mass of each peptide from the MALDI-TOF experimental spectrum is shown along with the theoretical mass of the corresponding tryptic digest peptide from soybean GS<sub>1</sub>β1. Each mass is reported in Daltons.

<sup>b</sup> The error between the experimental and theoretical masses of each peptide is shown parenthetically.

<sup>c</sup> The amino acids of soybean GS<sub>1</sub>β1 corresponding to each peptide are shown

<sup>d</sup> The derived primary sequence of each soybean GS<sub>1</sub>β1 peptide is shown.

<sup>e</sup> The peptide sequence that was confirmed by MS/MS analysis.



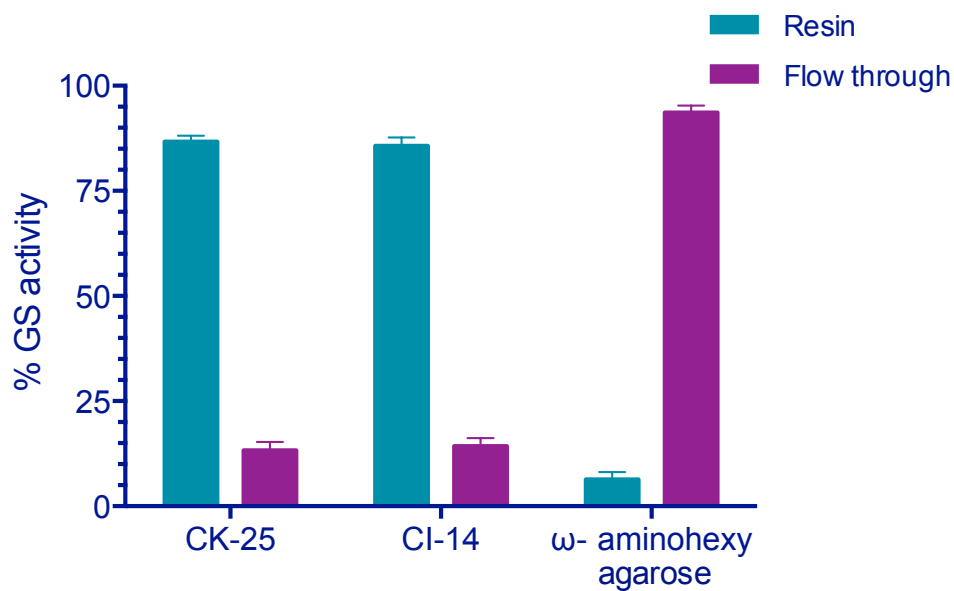


**Figure 3.1.3: Interaction of purified NGS with the C-terminal domain of nodulin 26.** CK-25 and CI-14 peptides were immobilized on  $\omega$ -aminohexyl agarose and were incubated with 50 units of NGS. An equivalent amount of GS was incubated with underivatized  $\omega$ -aminohexyl agarose, which served as a negative control. The resin was separated from the sample by centrifugation, and the fraction of the GS activity bound to the resins (Solid bars) as well as in the unadsorbed (flow through) fractions (open bars) was measured. Error bars show the SEM (n=6).

resulting 2D gel, each with a distinct pI and slightly different molecular weights (Figure 3.1.2B). The observed pattern of separation was identical to the pattern observed previously (Morey et al. 2002).

### ***III. Determination of the $K_d$ for the interaction of glutamine synthetase with the C-terminal peptide of nodulin 26.***

To quantify the interaction of the C-terminal nodulin 26 domain with cytosolic GS<sub>1</sub>β1, a fluorescence spectroscopy approach was used (Figure 3.1.4). The open reading frame corresponding to GS<sub>1</sub>β1 was obtained by RT-PCR of total soybean nodule RNA and was expressed with an amino terminal His-tag in the Rosetta 2 *E. coli* strain and purified by Ni<sup>2+</sup>-chelate chromatography (Figure 3.1.4A). The fluorescent label nitrobenzoxadiazole (NBD) was linked to the amino-terminal cysteine of the CK-25 peptide. The fluorescence properties of NBD are sensitive to the environment and can be used to assess binding of ligands to proteins (Shi et al. 2005; Sloan and Hellinga 1998). To test whether this is a useful property to investigate the CK-25 and GS<sub>1</sub> interaction, the fluorescence spectrum of NBD-CK-25 (0.64 μM) was determined in the presence of purified GS<sub>1</sub>β1 (1.36 μM of GS<sub>1</sub>β1 monomers) (Figure 3.1.4). In the presence of an equal molar or higher concentration of purified GS<sub>1</sub>β1 monomers, the labeled CK-25 peptide shows an increase in fluorescence intensity at its emission maximum of 545 nm (Figure 3.1.4B). This change in fluorescence was used as an index for peptide-enzyme interaction and the determination of binding

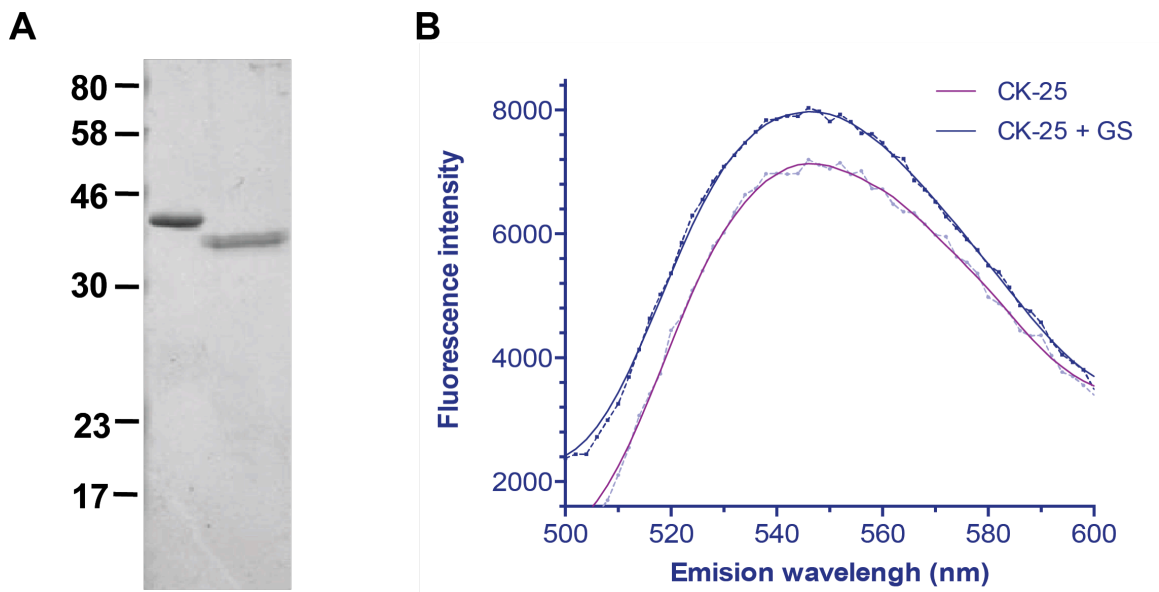


**Figure 3.1.4: Binding of fluorescent NBD-labeled CK-25 with purified GS.**

**(A)** SDS-PAGE profile of purified GS. **Lane 1**, purified recombinant soybean GS<sub>1</sub>  $\beta$ 1; **Lane 2**, purified native soybean nodule GS. Each lane contains 0.5  $\mu$ g of purified protein. **(B)** Fluorescence emission spectra of 0.64  $\mu$ M NBD-labeled CK-25 in the presence (blue line) or absence (purple line) of 1.36  $\mu$ M recombinant soybean GS<sub>1</sub>  $\beta$ 1.  $\lambda_{\text{ex}}$ =480 nm.

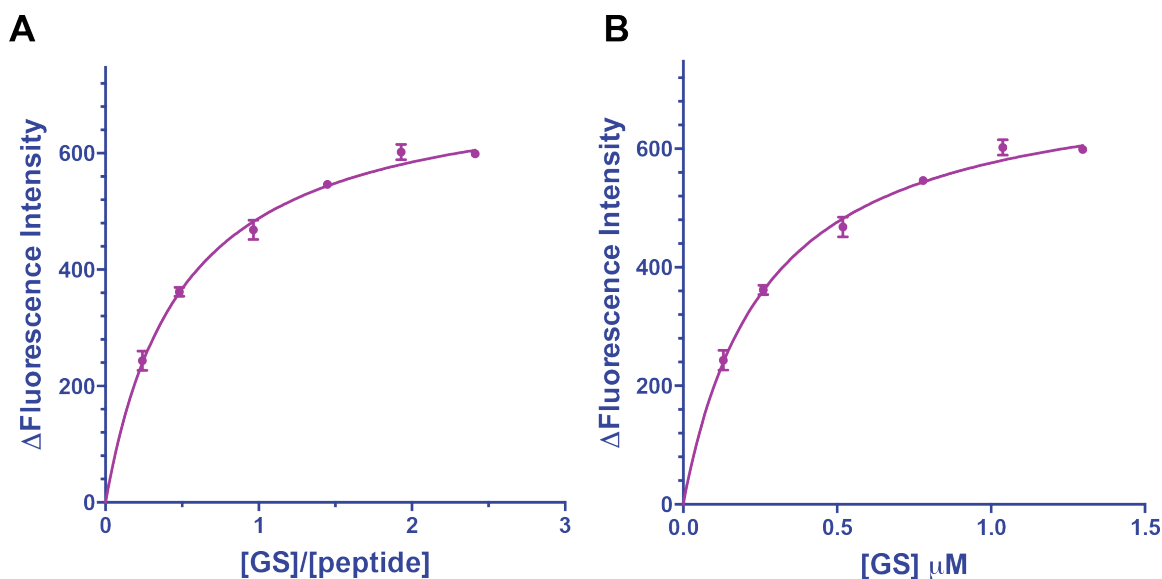


**Figure 3.1.5: Quantitation of the interaction between GS<sub>1</sub> and the C-terminal peptide of soybean nodulin 26 (CK-25).** (A) Binding curve of NBD-labeled CK-25 and recombinant soybean GS<sub>1</sub>β1. The peptide was kept constant at 0.67  $\mu M$ , and the change in the intensity of fluorescence emission at 545 nm was monitored in response to an increase in the concentration of GS<sub>1</sub>β1. Graph shows the response as a function of the molar ratio of GS/peptide. (B) shows fit to the quadratic binding equation for the determination of  $K_d$  (described in Materials and Methods) assuming a binding stoichiometry of 1:1.

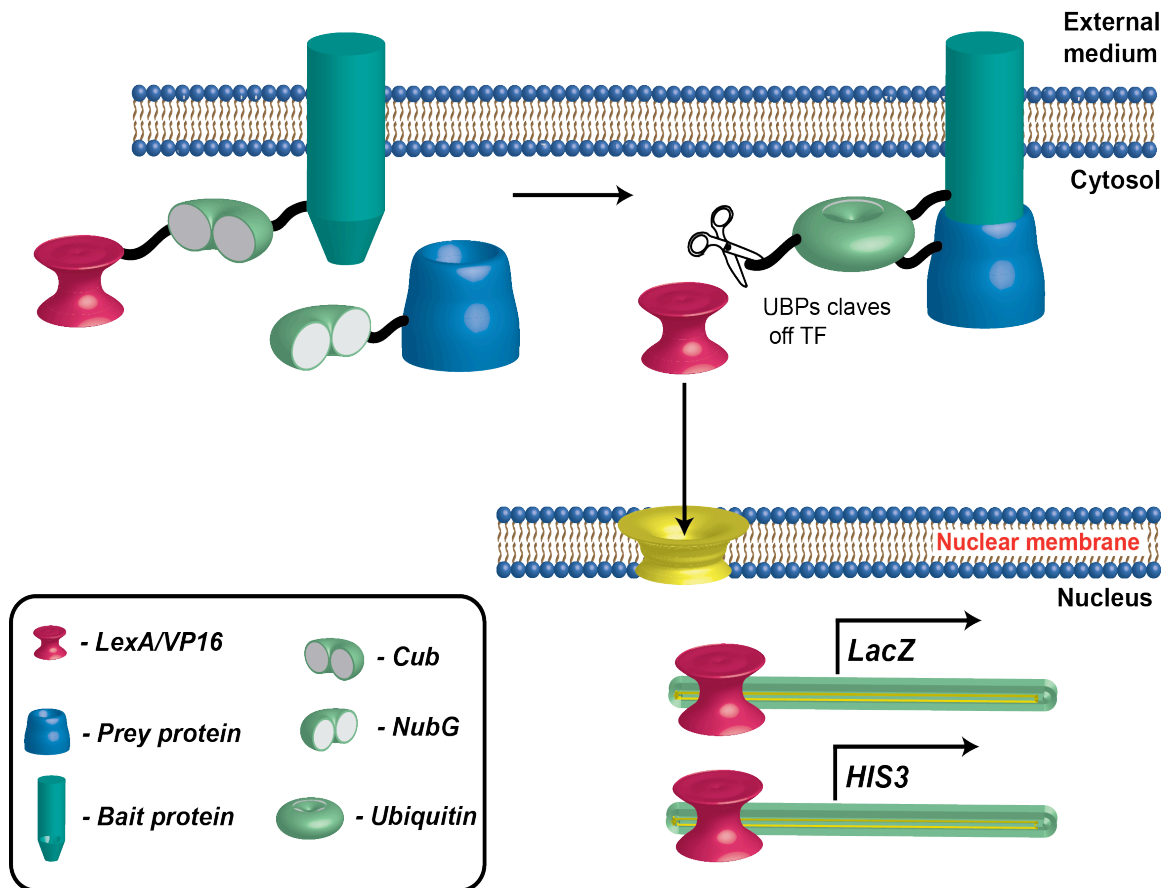
affinity and stoichiometry. The peptide shows saturable binding with half-saturation occurring at a [GS]/[NBD-CK-25] ratio of 0.51, suggesting a binding stoichiometry of 1 peptide:1 GS monomer (Figure 3.1.5A). Assuming a 1:1 binding stoichiometry, a fit of the binding data yields a  $K_d$  of 266 nM (SEM=18nM) for peptide binding to GS<sub>1</sub>β1. Based on the predicted concentrations of nodulin 26 and GS in nodules, these results strongly suggest that cytosolic GS binds to the nodulin 26 C-terminus at biologically relevant concentrations.

#### ***IV. Interaction of glutamine synthetase with full-length nodulin 26.***

Analysis of the 2D electrophoretic profile in this study (Figure 3.1.2B) suggests that both β and γ isoforms are represented in the nodule GS fraction that binds to the C-terminal nodulin 26 peptide. To determine: 1. If GS interacts with full-length nodulin 26 and 2. Which isoforms interact with nodulin 26, interaction of glutamine synthetase isoforms with full-length nodulin 26 was investigated by using the split ubiquitin yeast two hybrid (split Ub) assay of (Obrdlik et al. 2004) which is designed for the interaction of membrane proteins with binding partners.

A diagrammatic representation of the split Ub assay is shown in figure 3.1.6. In this assay, one of the possible interacting partners was expressed as a fusion to a modified N-terminal fragment of ubiquitin (NubG) and another as the C-terminal (Cub) fragment of ubiquitin along with the VP-16/LexA transcription factor which is susceptible to ubiquitin-activated lyase. Interaction between the two possible interacting partners brings the NubG and Cub fragments of ubiquitin

**Figure 3.1.6: Split-ubiquitin yeast two-hybrid methodology.** Bait protein was translationally fused to the C-terminal fragment of ubiquitin (Cub) followed by a synthetic VP16-LexA transcription factor. The prey protein was translationally fused to NubG, the N-terminal fragment of ubiquitin with an Ile to Gly mutation. The reduced affinity of NubG and Cub due to this mutation allow them to reconstitute ubiquitin only when the bait and prey proteins are interacting with each other. Interaction of the bait and prey proteins will allow NubG and Cub to form a functional ubiquitin which is cleaved by ubiquitin specific proteinases (UBPs) leading to release of LexA/VP16LexA/VP16. LexA/VP16 then diffuses into the nucleus to activate the transcription of *HIS3* and *LacZ* ( $\beta$ -galactosidase) reporter genes. Positive interaction can be assayed by using *HIS3* gene expression which is assayed by the ability of yeast strain to grow on media lacking histidine and the activity of  $\beta$ -galactosidase can be assayed colorimetrically in presence of X-gal.



in close proximity resulting in reconstitution of a functional ubiquitin which activates the ubiquitin-specific protease. Cleavage by this proteinase releases the VP-16/LexA transcription factor which diffuses into the nucleus and transcribes the reporter genes controlled by the LexA promoter ( $\beta$ -galactosidase and HIS3). Full-length cDNAs corresponding to GS<sub>1</sub> $\beta$ 1, GS<sub>1</sub> $\beta$ 2, GS<sub>1</sub> $\gamma$ 1, and GS<sub>1</sub> $\gamma$ 2 “preys” were cloned as translational fusions to NubG, and nodulin 26 (“bait”) was translationally fused to Cub followed by a synthetic VP-16/ LexA transcription factor.

Nodulin 26 was used as positive control since it forms homotetramers like other MIPs (Fu et al. 2000; Harries et al. 2004; Sui et al. 2001a; Törnroth-Horsefield et al. 2006). In addition the multimeric *Arabidopsis* potassium channel AtKAT1 was also used as positive control (Obrdlik et al. 2004). The subunit-subunit interactions between monomers of these proteins show the most robust interactions in this screen (Figure 3.1.7B). The homooligomerization results also suggest that both of these proteins are properly expressed and folded in the yeast heterologous system. Additionally, the wild-type N-terminal fragment of ubiquitin (NubWT) serves as a system control because it constitutively interacts with Cub and activates both reporter genes without prey protein attached (Figure 3.1.7B).

Mating of yeast strains containing the four soybean GS isoform prey constructs with strains containing the nodulin 26 bait construct results in a positive interaction as indicated by  $\beta$ -gal expression and growth on histidine

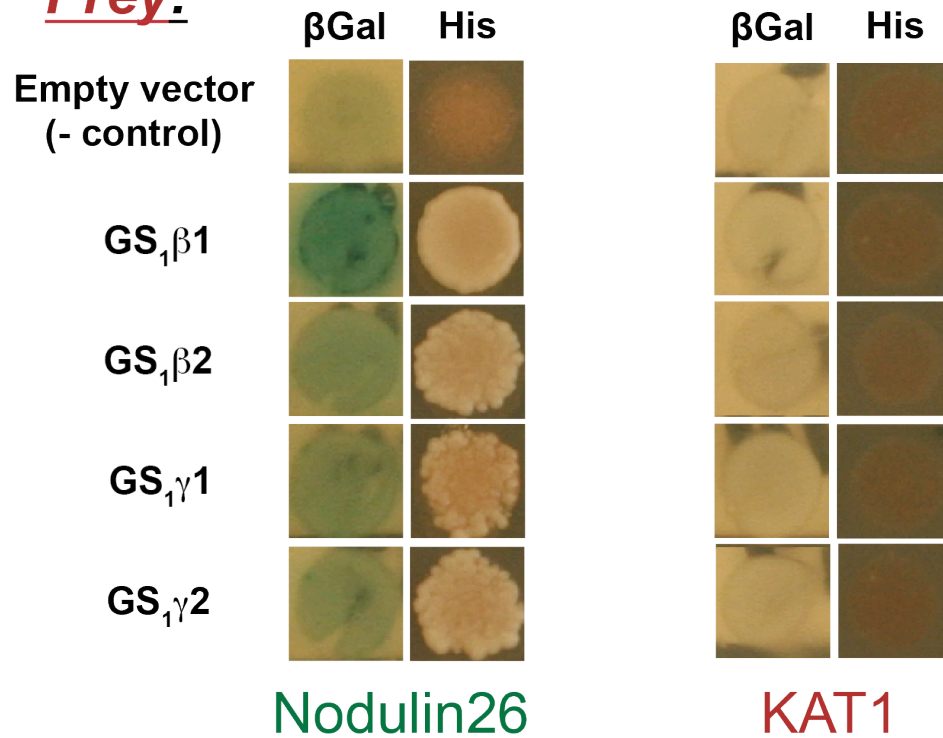


**Figure 3.1.7: Analysis of interactions between soybean glutamine synthetase isoforms and nodulin 26 *in vivo* using the yeast split-ubiquitin system.**

**system.** (A) Yeast strains (THY.AP4) containing bait constructs consisting of the nod26 cDNA or the Arabidopsis KAT potassium channel cloned as a translational fusions to the C-terminal fragment of ubiquitin (CuB) fused to a synthetic VP-16/ LexA transcription factor were mated with THY.AP5 strains containing prey constructs consisting of the cDNAs of GS<sub>1</sub> isoforms. Interaction of bait and prey proteins was tested by activation of two reporter genes:  $\beta$ gal (left panel), shows the results of a  $\beta$ -galactosidase overlay assay; and his (right panel) shows growth on selection media lacking histidine. The empty vector control shows the results of mating of the indicated bait vectors to the empty vector. (B) The result of positive control matings are shown. In the case of nod26 and mating of homologous bait and prey constructs resulting in homo-oligomerization was performed. Similar matings resulting in the dimerization of AtKAT1 (Obrdlik et al., 2004) were performed. Ub shows the results of using wild-type ubiquitin, which constitutively interacts with Cub fragments, and has been used previously as positive control in this system (Obrdlik et al., 2004).

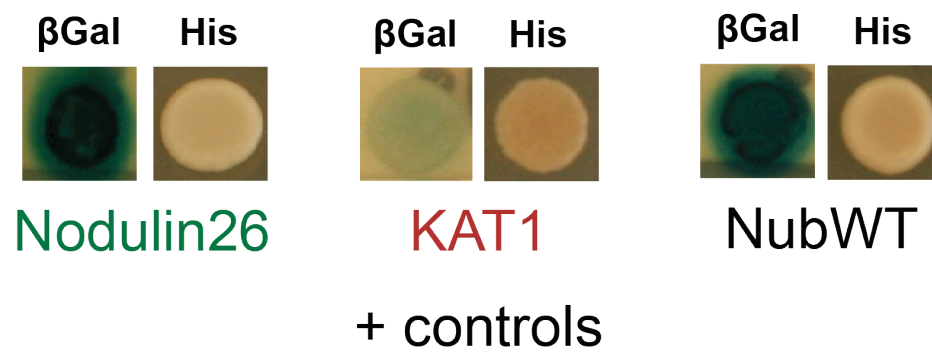
**A**

**Prey:**



**Bait proteins**

**B**



selection media (Figure 3.1.7A). As a negative control, an AtKAT1 potassium channel bait construct was used (Obrdlik et al. 2004) in mating experiments with the GS<sub>1</sub> prey constructs. These mating showed no apparent interaction based on expression of  $\beta$ -gal or growth on histidine selection media (Figure 3.1.7A). Overall, the data suggest that all four cytosolic soybean nodule GS isoforms form a complex with soybean nodulin 26.

To determine whether nodulin 26 interacts with GS *in planta*, bimolecular fluorescence complementation (BiFC) experiments were performed (Kerppola 2008). BiFC is a protein interaction technique in which two putative interacting proteins are translationally fused to either an N or C-terminal fragment of yellow fluorescent protein (YFP-N and YFP-C) and are transiently expressed in *planta*. Upon interaction of test binding partners, the N and C terminal fragments of YFP are brought together leading to reconstitution of functional YFP, which can be visualized by fluorescence microscopy (Figure 3.1.8). To perform BiFC, nodulin 26 was translationally fused to the YFP-N fragment at either its amino (YFP-N:nod26) or carboxyl (nod26:YFP-N) terminal end. The YFP-C terminal fragment was translationally fused to the amino terminal end of GS<sub>1</sub> $\beta$ 1 (YFP-C:GS<sub>1</sub> $\beta$ 1). The *Arabidopsis* transcription factor HY5 has been previously demonstrated to dimerize in BiFC experiments (Li and Nebenfuhr 2007) and was used as a positive control for this assay. Transient expression of the various constructs in onion epidermal cells was done by particle bombardment as explained in the Materials and Methods. Individual transformation of the each nodulin 26 and GS

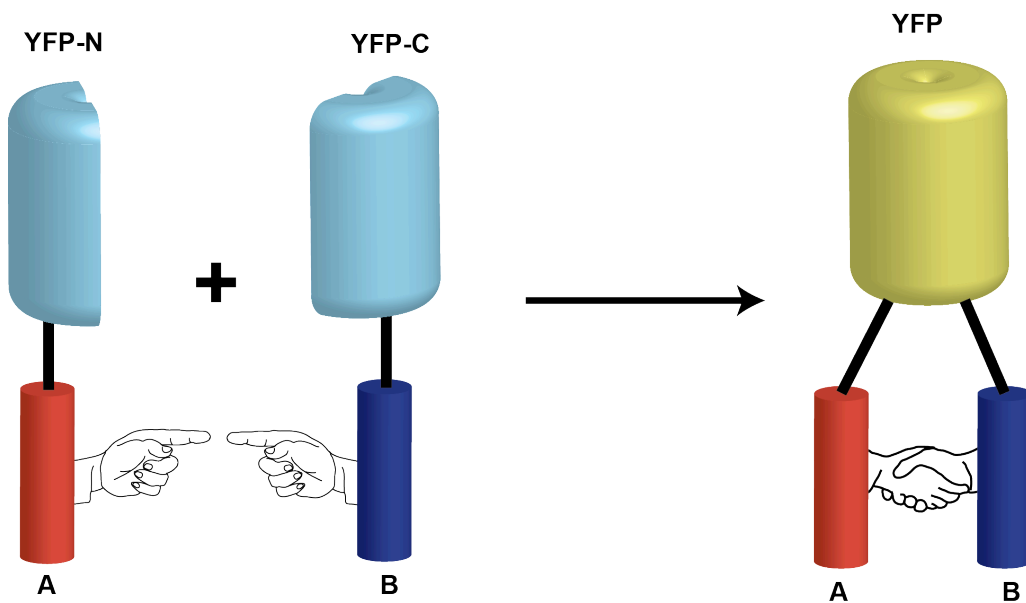
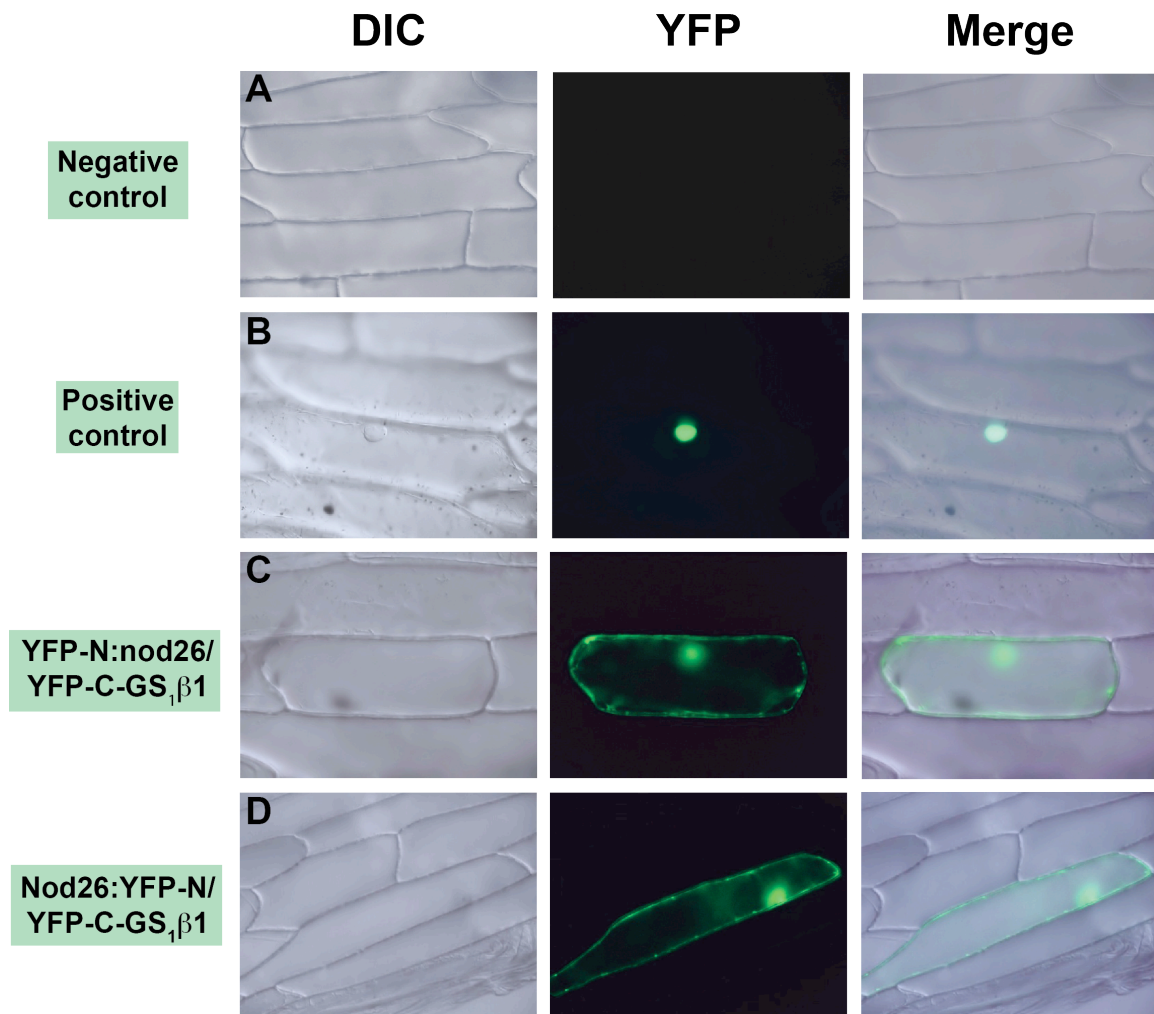


**Figure 3.1.8: Bimolecular fluorescence complementation assay**

**methodology.** ORFs of potential interaction partners (A and B) are translationally fused with N-terminal (YFP-N) and C terminal (YFP-C) domains of yellow fluorescence protein as described in Materials and Methods. YFP-N and YFP-C have low affinity towards each other and do not form the functional YFP when expressed alone. When the potential interacting partners linked to YFP-N and YFP-C interact with each other, the N and C terminal domains of YFP are brought in close proximity leading to reconstitution of fully functional YFP. Therefore, the fluorescence of YFP is considered as the positive interaction between potential interacting partners.

**Figure 3.1.9: Visualization of the interaction of nodulin 26 with soybean**

**nodule GS<sub>1</sub>  $\beta$ 1 by BiFC in onion cells.** Onion epidermal cells were transiently co-transformed with the BiFC constructs containing ORFs of gene of interest translationally fused to YFP-N and YFP-C. Transformed onion epidermal cells were analyzed for YFP fluorescence after 24 hr incubation. YFP and differential interference contrast (DIC) images of the same area on the onion epidermal cells are taken and were merged together to analyze the location of fluorescence on the cell. BiFC pairs used in co-transformation are shown on the left. A negative control construct consisting YFP-N:HY5/YFP-C:GS<sub>1</sub> $\beta$ 1 (A), a positive control construct consisting of the pair N:HY5/YFP-C:HY5 (B) were used in the experiment. An amino terminal fusion of YFP-N:nod26 with an amino-terminal fusion of YFP-C:GS<sub>1</sub> $\beta$ 1 (C), and a carboxyl terminal fusion of nod26:YFP-N with YFP-C:GS<sub>1</sub>  $\beta$ 1 (D) were used to test the interaction between GS<sub>1</sub> $\beta$ 1 and nodulin 26. DIC, Differential interference contrast optics, YFP, fluorescent images using the Yellow Fluorescent Protein filter set, and Merge, the superimposition of both images.



construct yielded negative results. Co-transformation of YFP-N:HY5 and YFP-C:GS<sub>1</sub>β1 also yielded negative results suggesting that reconstitution of YFP did not happen due to lack of interaction between HY5 and GS<sub>1</sub>β1. However, co-transformation of YFP-C:GS<sub>1</sub>β1 with either the nod26:YFP-N or YFP-N:nod26 constructs reconstituted the YFP signal (Figure 3.1.9) suggesting an interaction between both nodulin 26 constructs and GS<sub>1</sub> β1. Overall, the findings show that cytosolic soybean GS interacts with soybean nodulin 26 with the site(s) of interaction likely to include the C-terminal cytosolic domain.

#### ***V. Interaction of glutamine synthetase with native nodulin 26 on symbiosome membrane.***

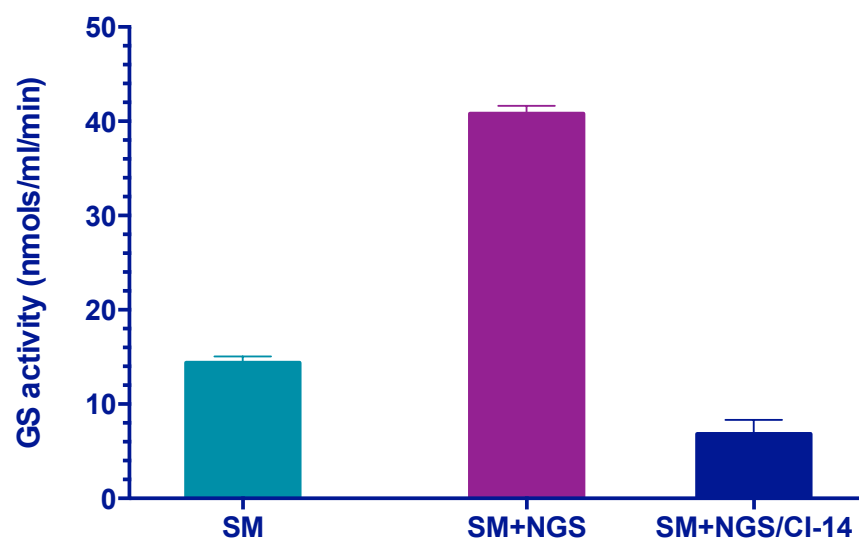
Split Ub and BiFC assays show that full-length nodulin 26 interacts with GS<sub>1</sub>β and GS<sub>1</sub>γ isoforms. The ability of native nodulin 26 to interact with glutamine synthetase was determined by the ability of GS to interact with nodulin 26 on the symbiosome membrane. For this assay, symbiosome membranes were isolated from soybean nodules by the Percoll step gradient method, which produces vesicles with the hydrophilic nodulin 26 C-terminus exposed on the outer surface of the vesicle (Weaver et al. 1991). GS activity assays performed on purified symbiosome membranes shows that a small but significant amount of GS is associated with them (Figure 3.1.10A). This is consistent with previous proteomic analyses that show that symbiosome membranes possess peripherally associated GS (Catalano et al. 2004). Further incubation of purified symbiosome membranes with purified native soybean nodule GS (NGS) shows

**Figure 3.1.10: Interaction of GS with isolated soybean symbiosome**

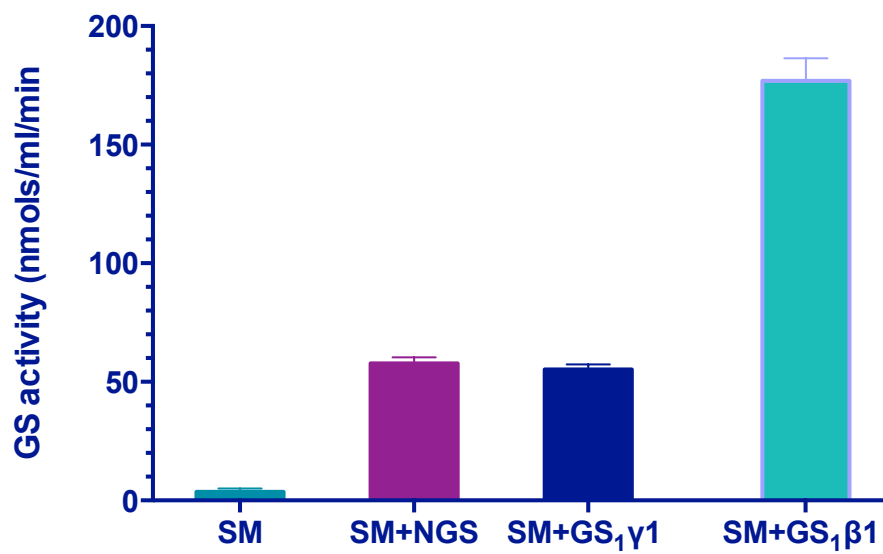
**membranes.** (A) Symbiosome membranes were isolated from soybean root nodules by on Percoll gradients and were incubated with soybean nodule GS (SM+GS) as well as soybean nodule GS pre-incubated with C-terminal peptide of nod26 (SM+GS/peptide). As a control, symbiosome membranes were incubated with an equivalent volume of binding buffer without added GS (SM). Membranes were washed and the GS activity bound was assayed. Error bars show the SEM (n=6). (B) Purified SM were incubated with equal enzyme units of soybean nodule GS (native GS) as well as the recombinantly purified GS<sub>1</sub> isoforms from soybean root nodules (GS<sub>1</sub>β1 and GS<sub>1</sub>γ1). As a control, symbiosome membranes were incubated with an equivalent volume of binding buffer without added GS. Membranes were washed and the GS activity bound was assayed. Error bars show the SEM (n=3).



**A**



**B**



an additional membrane adsorption of GS which can be competitively inhibited by pre-incubating the NGS with 10  $\mu$ M of nodulin 26 C-terminal peptide (Figure 3.1.10), suggesting that the nodulin 26 C-terminus is responsible for symbiosome membrane binding of GS. Consistent with the results of the split Ub assays, both GS<sub>1</sub> $\beta$  and GS<sub>1</sub> $\gamma$  isoforms showed interaction with isolated symbiosome membranes (Figure 3.1.10B). These results show that both cytosolic GS isoforms from soybean interact with nodulin 26 on symbiosome membrane.

#### ***VI. Effect of phosphorylation of nodulin 26 on interaction with glutamine synthetase.***

The C-terminus of nodulin 26 is phosphorylated specifically on ser 262 by calcium-dependent protein kinase (CDPK) (Weaver et al. 1991; Weaver and Roberts 1992) (Figure 3.1.1), and since this is the region of the CK-25 sequence, the effect of phosphorylation of the C-terminus of nodulin 26 on its interaction with cytosolic GS<sub>1</sub> $\beta$ 1 was investigated by fluorescence spectroscopy (Figure 3.1.11). A CK-25 peptide was synthesized with the serine (ser 16 in the CK-25 sequence corresponding to ser 262 in nodulin 26) of the CDPK site phosphorylated (CK-25P) and binding studies were conducted as described above. In the presence of purified GS<sub>1</sub>  $\beta$ 1, the NBD-labeled CK-25P peptide shows an increase in fluorescence intensity at its emission maximum of 545 nm (Figure 3.1.11A). Using the same approach for assay of the binding of GS to unphosphorylated CK-25, the binding affinity of CK-25P was evaluated (Figure 3.1.11B). Assuming 1:1 binding stoichiometry, a fit of the binding data yields a

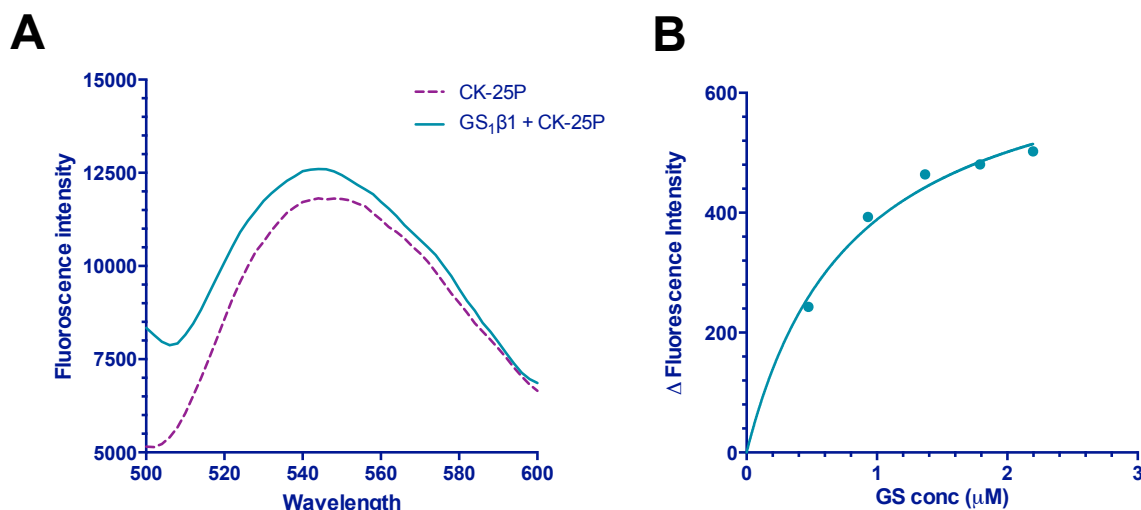


**Figure 3.1.11: Quantitation of the interaction between GS<sub>1</sub> and the phosphorylated C-terminal peptide of soybean nodulin 26 (CK-25P).** (A)

Fluorescence emission spectra of 0.64 μM NBD-labeled CK-25P in the presence (solid line) or absence (dotted line) of 1.36 μM recombinant soybean GS<sub>1</sub>β<sub>1</sub>.  $\lambda_{\text{ex}}$ =480 nm. (B)

Binding curve of NBD-labeled CK-25P and recombinant soybean GS<sub>1</sub>β<sub>1</sub>. The peptide was kept constant at 0.67 μM, and the change in the intensity of fluorescence emission at 545 nm was monitored in response to an increase in the concentration of GS<sub>1</sub>β<sub>1</sub>.

Graph shows fit to the quadratic binding equation for the determination of  $K_d$  assuming a binding stoichiometry of 1:1.

$K_d$  of 818 nM (SEM = 54 nM) for peptide binding to recombinant GS<sub>1</sub>β1.

Although this is 3.5-fold higher than the  $K_d$  for unphosphorylated peptide (CK-25), the results suggest that GS still retains the ability to bind to the nodulin 26 C-terminal sequence regardless of its phosphorylation state.

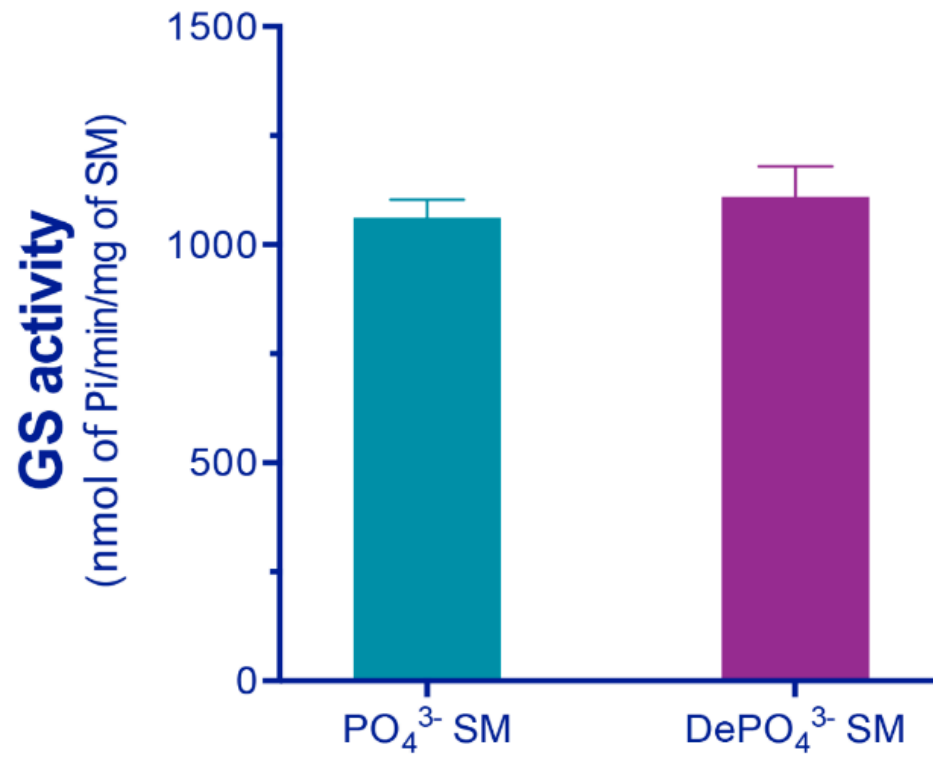
To determine the effect of phosphorylation of symbiosome membrane nodulin 26 on GS interaction, symbiosome membranes containing phosphorylated and dephosphorylated nodulin 26 were prepared as described by Guenther et al. (2003). The phosphorylation state was determined by performing western blot (Figure 3.1.12B) using anti-phospho nodulin 26 antibodies (Guenther et al. 2003). Symbiosome membranes with phospho or dephospho nodulin 26 were incubated with purified GS<sub>1</sub>β1. GS activity associated with symbiosome membranes showed that there is no difference in the GS activity associated with either phosphorylated or dephosphorylated symbiosome membranes (Figure 3.1.12A). Overall, the results suggest that phosphorylation of ser262 does not drastically affect the ability of GS to associate with the C terminal domain of nodulin 26.

## ***VII. Determination of the interaction site for nodulin 26 on glutamine synthetase.***

The interaction site for nodulin 26 on glutamine synthetase was examined by using an *in vitro* crosslinking approach. The CK-25 peptide was cross-linked with recombinant GS<sub>1</sub>β1 using the hydrophilic heterobifunctional cross-linker, sulfo-MBS. Sulfo-MBS contains functional groups that target both cysteine

**Figure 3.1.12: Effect of nodulin 26 phosphorylation on its interaction with**

**GS<sub>1</sub>β1**. (A) Symbiosome membranes were isolated from soybean root nodules on percoll gradients and were treated with shrimp alkaline phosphatase. Untreated symbiosome membranes ( $\text{PO}_4^{3-}$ ) and alkaline phosphatase-treated symbiosome membranes (De  $\text{PO}_4^{3-}$ ) were incubated with soybean GS<sub>1</sub>β1. Membranes were washed and the GS activity bound was assayed and expressed as nmol of Pi/min/mg of symbiosome membrane. Error bars show the SEM (n=3). (B) Phosphorylation state of the nodulin 26 on the symbiosome membranes from (A) were analyzed by western blotting using anti-nodulin 26 specific and anti-phosphorylated nodulin 26 antibody. Phosphorylation state and the concentration nodulin 26 on membranes from  $\text{PO}_4^{3-}$  (1) and membranes from De  $\text{PO}_4^{3-}$  (2) are shown.

**A****B**

sulfhydryl groups and primary amines. To test the crosslinking,  $^{32}\text{P}$ -CK-25 was incubated with sulfo-MBS and GS<sub>1</sub>β1 and was separated by SDS-PAGE. An autoradiogram showed a radioactive band migrating at 43 kDa, which suggests a covalent complex of  $^{32}\text{P}$ -CK-25 and GS<sub>1</sub>β1 was formed (Figure 3.1.13). To map the potential site of interaction, CK-25 cross-linked GS<sub>1</sub>β1 was prepared and resolved by SDS-PAGE. The GS band was excised and subjected to trypsin digestion followed by peptide fingerprinting by MALDI-TOF analysis (Figure 3.1.14). To determine the masses of the peptide from GS<sub>1</sub>β1 cross-linked with CK-25, the masses of the CK-25 peptide and the cross-linker were subtracted from the total mass of the peptides obtained from the spectra, and the remaining mass was compared with the virtual peptides from GS<sub>1</sub>β1 generated using the online software MS-Digest (<http://prospector.ucsf.edu/prospector/cgi-bin/msform.cgi?form=msdigest>). The list of the GS<sub>1</sub>β1 peptides identified as cross-linked targets by this approach is shown in table 3.1.2. A total of seven lysine residues within these peptide regions were identified as potential targets for crosslinking, and are highlighted in table 3.1.2. All lysine residues lie between amino acid residue 259- 301, and five of the seven are between amino acid residues 289-300. This suggests that the CK-25 interaction site on GS<sub>1</sub>β1 is located near these lysine residues. To determine the location of these lysine residues on the GS<sub>1</sub>β1 structure, a homology model was developed using maize glutamine synthetase (PDB ID: 2D3A\_A) as a template. This enzyme shows 86% identity with the soybean GS<sub>1</sub>. The homology model with lowest RMSD was

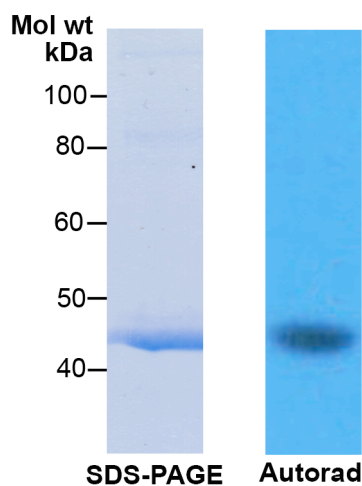


**Figure 3.1.13: Crosslinking of  $^{32}\text{P}$ -CK-25 with  $\text{GS}_1\beta 1$ .**  $^{32}\text{P}$ -CK-25 preincubated with sulfo-MBS and then with  $\text{GS}_1\beta 1$  and was separated by SDS-PAGE. Proteins were visualized by Coomassie staining and dried gel was exposed to X-ray film.



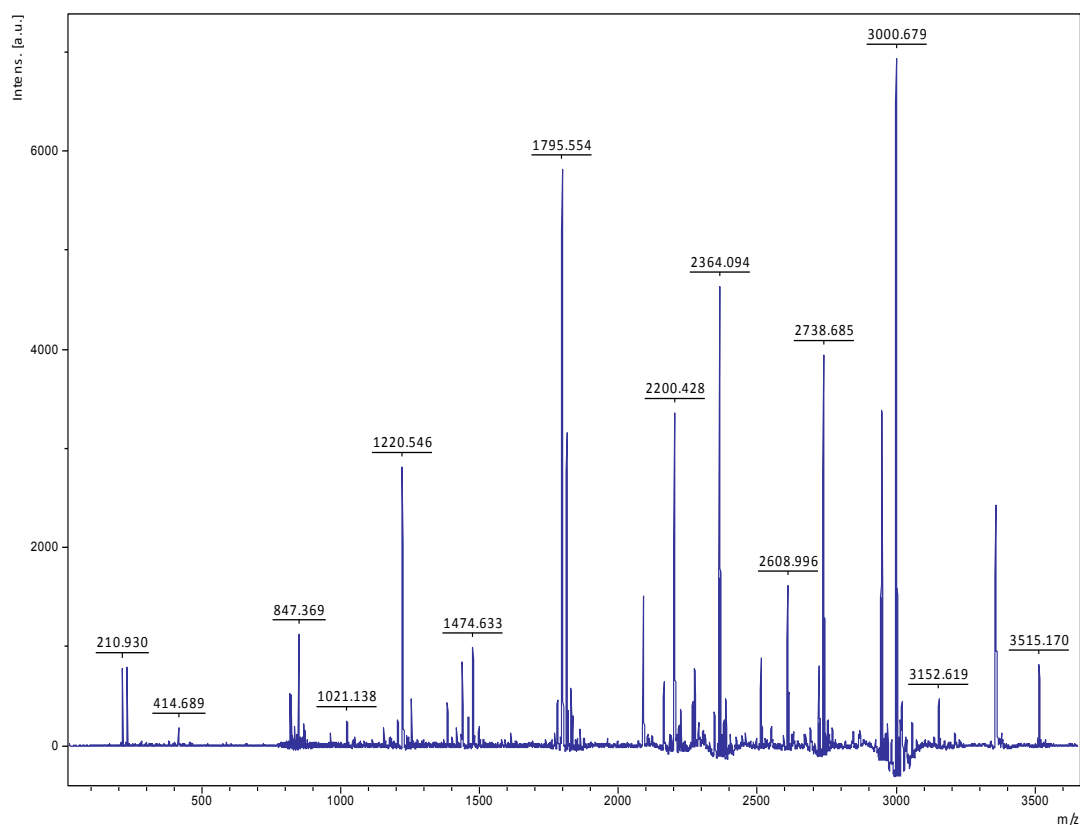


**Figure 3.1.14: MALDI-TOF spectra of tryptic digest of CK-25 cross-linked with GS<sub>1</sub>β1.** GS<sub>1</sub>β1 was cross-linked with CK-25 and was resolved by SDS-PAGE.

The cross-linked product was subjected to in-gel tryptic digestion and the purified peptides were analyzed by mass spectroscopic analysis. The MALDI-TOF spectra of protonated tryptic peptides (MH<sup>+</sup>) of the cross-linked product is shown. The Y-axis shows the intensity as arbitrary units. The mass to charge ratio is plotted on the X-axis.

**Table 3.1.2: - List of GS tryptic peptides involved in crosslinking with CK-**

**25.**

Cross-linked peptide <sup>a</sup>	GS peptide in cross-linking <sup>b</sup>	Position <sup>c</sup>	#MC <sup>d</sup>	Peptide sequence <sup>e, f</sup>
3152.619	2693.0403	290-313	5	AAID <b>K</b> LG <b>KKHKE</b> HIAAYGEG NERR
3056.315	2536.8528	290-312	4	AAID <b>K</b> LG <b>KKHKE</b> HIAAYGE GNER
2947.681	2488.9728	241-262	1	YILERITEIAGVVVSFD <b>P</b> <b>KPIK</b>
2273.182	1814.175	246-262	1	ITEIAGVVVSFD <b>P</b> <b>KPIK</b>
2265.701	1807.0533	281-297	2	EDGGYEVI <b>K</b> AAID <b>K</b> LG <b>K</b>
2738.685	944.1619	290-298	2	AAID <b>K</b> LG <b>KK</b>

<sup>a</sup> The experimental mass of each peptide from the MALDI-TOF experimental spectrum is shown.

<sup>b</sup> GS<sub>1</sub>β1 peptide mass in the cross-linked peptide is shown after subtracting the mass of the linker and CK-25 peptide.

<sup>c</sup> The amino acids of soybean GS<sub>1</sub>β1 corresponding to each peptide are shown.

<sup>d</sup> Number of missed cleavage (MC) in the sequence are shown.

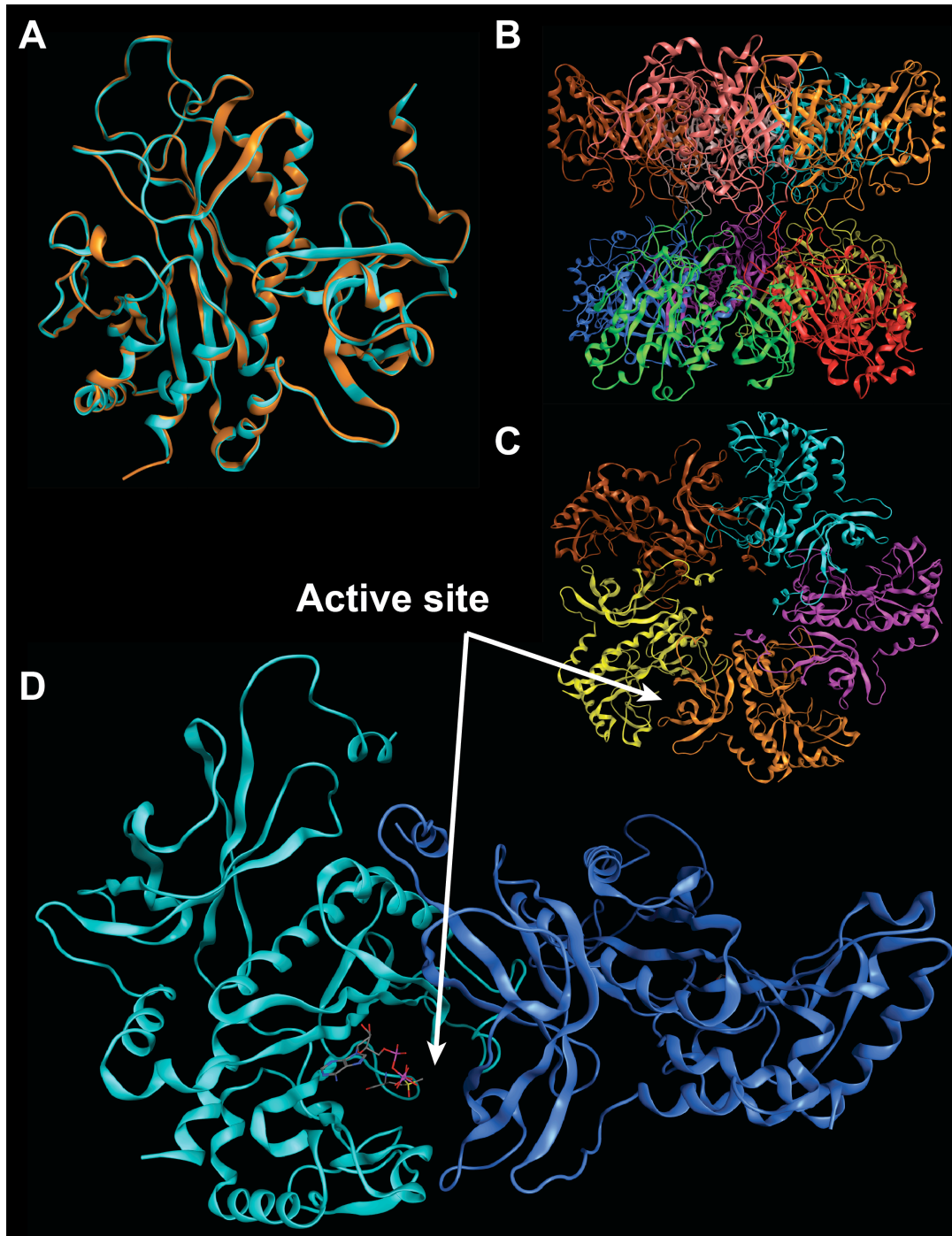
<sup>e</sup> The derived primary sequence of each soybean GS<sub>1</sub>β1 peptide is shown.

<sup>f</sup> Potential K residues involved in crosslinking are shown as red bold letters.

selected for further structural analysis. Figure 3.1.15A shows the superposition of GS<sub>1</sub>β1 on maize GS1a. The maize GS and resulting soybean GS<sub>1</sub>β1 homology model holoenzyme are decameric, consisting of two pentameric rings that stack together (Figure 3.1.15B&C). The active site is formed at the monomer-monomer interface within each pentameric ring (Figure 3.1.15C&D). Lysine residues proposed to be involved in crosslinking are represented in a space filling format on one monomer of a GS<sub>1</sub>β1 dimer in figure 3.1.16. The predicted location of the GS binding site is a linear sequence adjacent to the active site opening exposed on the surface of the enzyme. To determine the potential effect of CK-25 binding to the region on GS activity, kinetic analysis of GS<sub>1</sub>β1 was performed in presence of CK-25 or CK-25P. The results show that GS exhibits similar kinetics for the critical substrate NH<sub>4</sub><sup>+</sup> in the presence and absence of peptide (Figure 3.1.17 and Table 3.1.3).

In summary, the results suggest that the C-terminus of nodulin 26 interacts with a linear sequence adjacent to the active site of soybean GS<sub>1</sub> in a manner that does not appear to affect GS enzyme activity. However, this nodulin 26 region is necessary for association of GS with the surface of the symbiosome. Given the proposed location of the binding sites on nodulin 26 and GS, this association could position the GS<sub>1</sub> active site near the nodulin 26, channel vestibule. Since nodulin 26 is an ammonia channel, and GS<sub>1</sub> is the first step in ammonia assimilation in nodule cytosol, this interaction might be important for efficient ammonia assimilation and prevention of ammonia toxicity in nodules. The significance of this interaction is discussed in the discussion section.

**Figure 3.1.15: Homology model of GS<sub>1</sub>β1.** Homology model of soybean GS<sub>1</sub>β1 is prepared using maize GS1a (PDB ID: 2d3b) as a template. (A) Superimposition of GS<sub>1</sub>β1 with maize GS1a (PDB ID: 2d3b) is shown with GS<sub>1</sub>β1 modeled in brown and the maize GS1a in cyan. Superimposition was excellent with root mean square deviation (RMSD) < 1Å for the peptide backbone. (B) Side view of the holoenzyme structure of the GS<sub>1</sub>β1 homology model is shown illustrating the stacking of two pentameric rings. Each subunit is shown in a different color. (C) Top view of the pentameric ring in the holoenzyme is shown. The active sites are present each monomer-monomer interface. (D) A close up of the active site formed at the interface of two monomers is shown. AMPPNP (an ATP substrate analog) bound in the active site is shown as a ball and stick model.



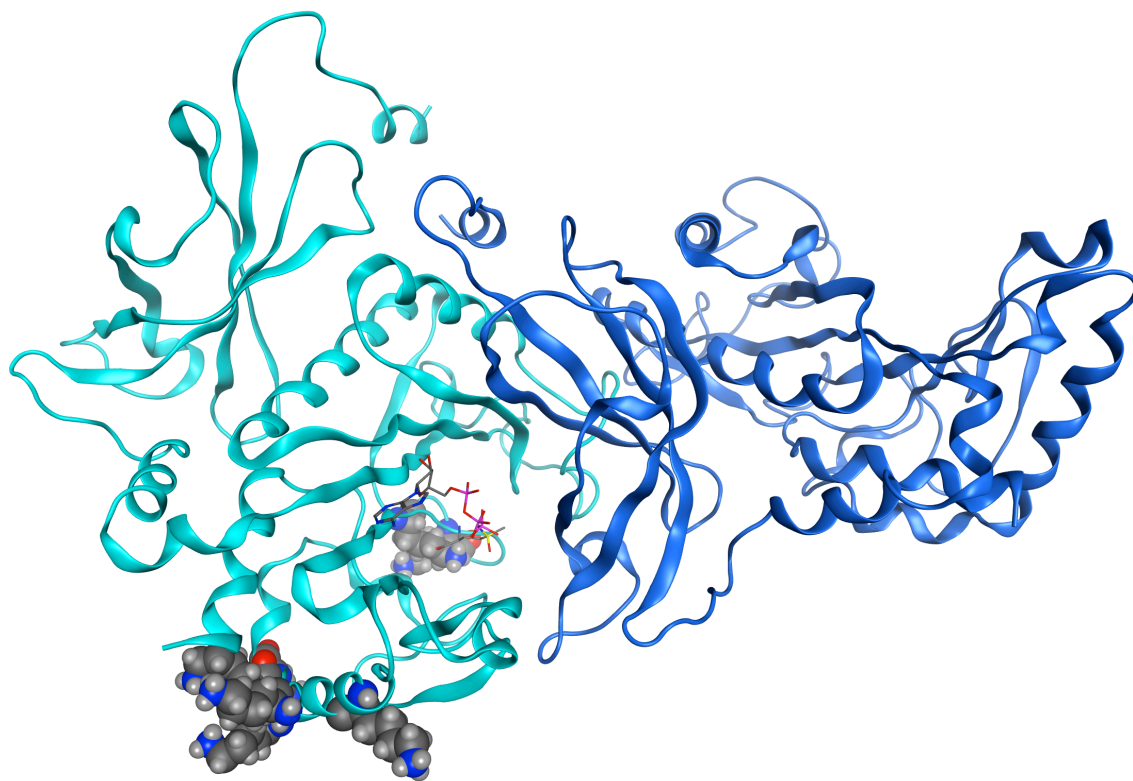


**Figure 3.1.16: Predicted interaction site of CK-25 on the GS.** GS<sub>1</sub>β1 dimer model was prepared using MOE on Maize GS1a (PDB ID: 2d3b) template. Predicted lysine (K) residues involved in the crosslinking are shown as space filling structures along with AMPPNP in the active site.

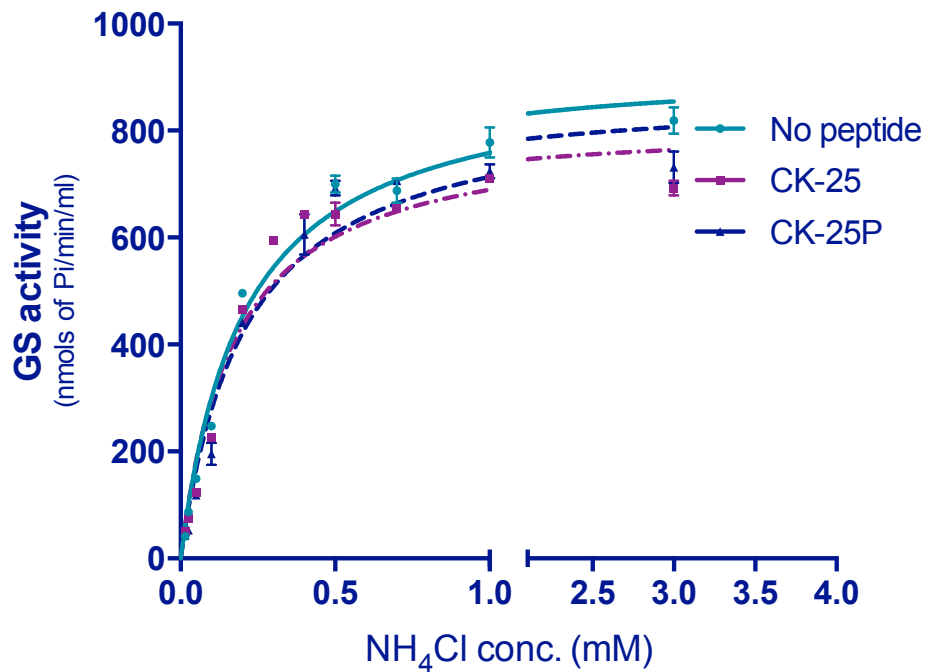


**Figure 3.1.17: Effect of C-terminal nodulin 26 peptide on recombinant GS**

**activity.** The effect of the C-terminal CK-25 peptide of nod26 on GS<sub>1</sub>β1 activity was analyzed. Comparison of the activity of GS<sub>1</sub>β1 in the presence as well as in absence of a 10-fold molar excess of CK-25 and CK-25P as a function of NH<sub>4</sub><sup>+</sup> concentration was determined by phosphate estimation assay. Activity is expressed in nmol of Pi/min/ml. Error bars represent SEM (n=3).

**Table 3.1.3: - Effect of interaction of peptide on kinetic properties of GS<sub>1</sub>β1.**

$K_m$  and  $V_{max}$  values are determined using inorganic phosphate estimation method as described in materials and methods. Peptide concentrations were kept constant at 10  $\mu$ M. All values are mean + SD (n=3)

	$K_m$ ( $\mu$ M)	$V_{max}$ (nmol of Pi/min/ml)
No peptide	203 $\pm$ 22	912 $\pm$ 28
CK-25	171 $\pm$ 22	807 $\pm$ 30
CK-25(P)	209 $\pm$ 29	863 $\pm$ 37



### **3.2. Differential regulation of cytosolic glutamine synthetase isoforms from soybean root nodules by reversible oxidation**

As mentioned earlier, four isoforms of GS<sub>1</sub> are expressed (GS<sub>1</sub>β1, GS<sub>1</sub>β2, GS<sub>1</sub>γ1, and GS<sub>1</sub>γ2) in mature soybean nodules that have greater than 86% amino acid sequence identity (Figure 1.3.3). To analyze the expression profile of these GS<sub>1</sub> isoforms, Q-PCR analysis was performed using RNA samples from soybean roots and nodules. It was observed that both GS<sub>1</sub>γ isoforms are expressed in a nodule-specific manner, whereas GS<sub>1</sub>β isoforms were expressed in roots and nodules. The expression levels of GS<sub>1</sub>β1 isoform are significantly higher in nodules compared to the other three isoforms (Figure 3.2.1). A question can be raised regarding the need for various isoforms in nitrogen fixation and nodule metabolism, and whether they have distinct metabolic roles in nodules. It has been previously observed from the investigation of *Arabidopsis* cytosolic glutamine synthetases that minor differences in amino acid sequence can cause large changes (>250 fold change in K<sub>m</sub>) in the kinetic properties with respect to the critical substrate ammonia (Ishiyama et al. 2004b). The kinetic properties of representatives from the GS<sub>1</sub>β and GS<sub>1</sub>γ groups show that they are not drastically different with respect to their kinetic properties (Table 3.2.1). However, during the course of my research on the soybean GS isoforms, evidence for differential regulation of GS<sub>1</sub>γ isoforms by oxidation was obtained. This work is summarized below.

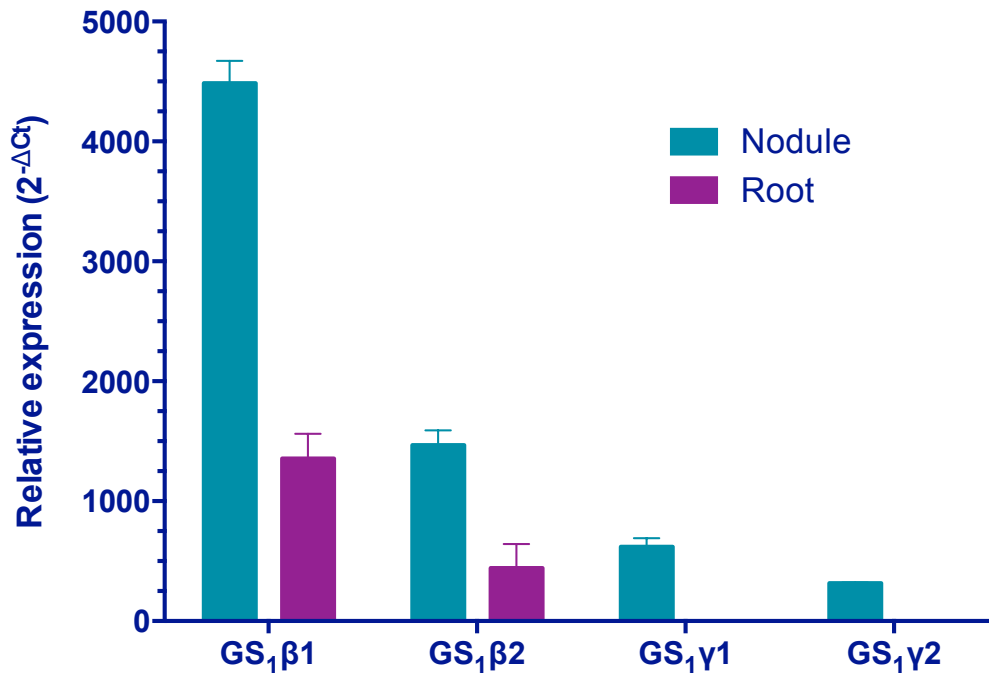


**Figure 3.2.1: Q-PCR analysis of GS<sub>1</sub> isoforms from soybean root and root**

**nodules.** Total RNA was extracted from root and nodules of 26 day old soybean plants and expression of all the GS<sub>1</sub> isoforms was analyzed by Q-RT-PCR. Relative expression of all the genes is shown with CDPK related gene (*GmCRK*) used as the internal reference as described by (Libault et al. 2008).

**Table 3.2.1: Kinetic properties of GS<sub>1</sub> isoforms for each substrate.**

K<sub>m</sub> and k<sub>cat</sub> values are determined using inorganic phosphate estimation method described in the Materials and Methods section. All values are mean + SD (n=3)

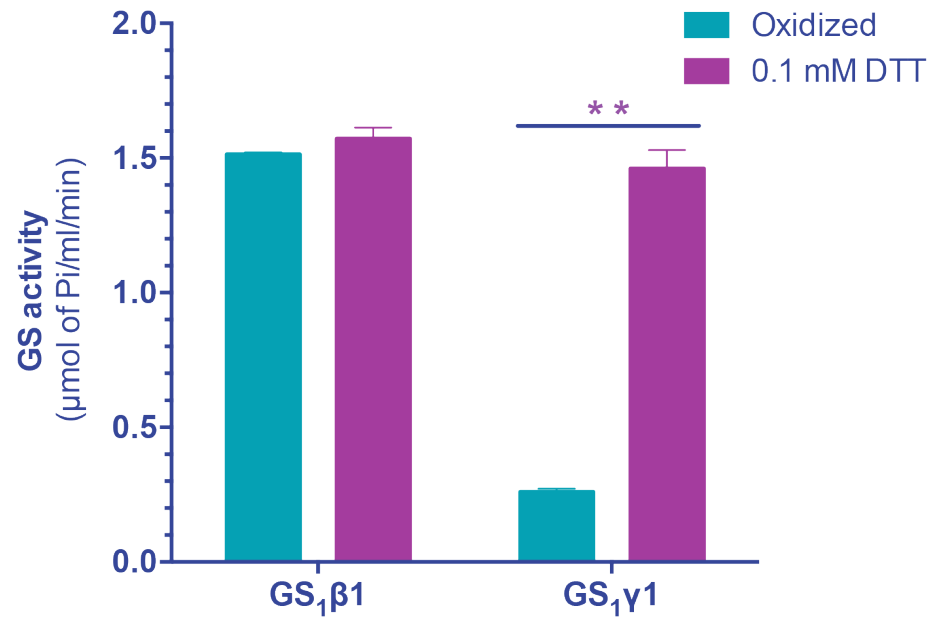
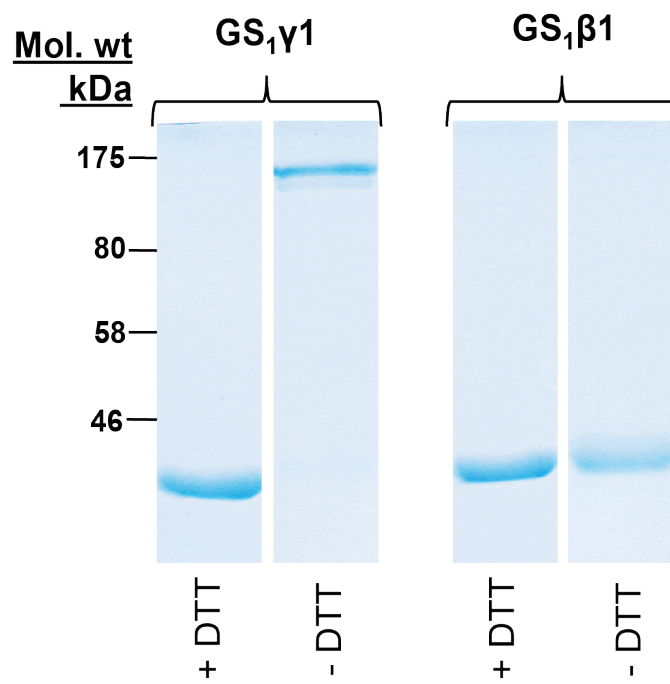
GS <sub>1</sub> isoform	K <sub>m</sub>			k <sub>cat</sub> (sec <sup>-1</sup> )
	Glu (mM)	NH <sub>4</sub> <sup>+</sup> (μM)	ATP (μM)	
GS <sub>1</sub> β1	5.2 ± 0.6	282 ± 54	209 ± 26	2.55 ± 0.14
GS <sub>1</sub> γ1	12.4 ± 0.9	205 ± 18	901 ± 84	2.15 ± 0.12

***I. Selective inhibition of cytosolic glutamine synthetase isoforms from soybean root nodules by oxidation.***

It was consistently observed that purified GS<sub>1</sub>γ1 has an enhanced tendency to lose activity due to air oxidation compared to GS<sub>1</sub>β1. For example, when incubated for 16 hrs at 4°C, GS<sub>1</sub>γ1 becomes inactivated, and it was observed that this loss of activity can be reversed by incubation with reducing agent (DTT) (Fig. 3.2.2A). In contrast, there was no difference in the activity of GS<sub>1</sub>β1 treated in the same fashion. Upon subsequent analysis on non-reducing SDS-PAGE, air oxidized GS<sub>1</sub>γ1 undergoes a transition to a higher apparent molecular weight suggesting possible oligomerization (Figure 3.2.2B). In contrast, the GS<sub>1</sub>β1 isoform shows only a single major band at 40 kDa, corresponding to the expected monomeric subunit size of the enzyme. It was hypothesized that the loss of activity and oligomerization might be the result of selective air oxidation of the GS<sub>1</sub>γ1 isoform.

To investigate whether GS<sub>1</sub>β and GS<sub>1</sub>γ have different susceptibility to oxidation, freshly purified and active GS<sub>1</sub>β1 and GS<sub>1</sub>γ1 were incubated with oxidizing (H<sub>2</sub>O<sub>2</sub>) or reducing (β-mercaptoethanol) agents or with wash buffer for 30 minutes. Incubation with H<sub>2</sub>O<sub>2</sub> resulted in 90% loss of GS<sub>1</sub>γ1 activity whereas loss of GS<sub>1</sub>β1 activity was more modest (Figure 3.2.3A). Incubation with reducing agent has a slight stimulatory effect on GS<sub>1</sub>γ1 but was not statistically different for GS<sub>1</sub>β1. Comparison of H<sub>2</sub>O<sub>2</sub> treated GS<sub>1</sub>γ1 and GS<sub>1</sub>β1 on non-reducing SDS-PAGE shows oligomerization of GS<sub>1</sub>γ1 where as GS<sub>1</sub>β1 shows

**Figure 3.2.2: Sensitivity of GS<sub>1</sub> isoforms to oxidation.** (A) GS activity of recombinant GS<sub>1</sub>β1 and GS<sub>1</sub>γ1 isoforms was determined after incubation at 4°C for 16 hrs in the presence or absence of reducing agent (DTT). Activity is expressed in μmol of Pi/ml/min. Error bars show SEM (n=3). (\*\* p < 0.01). (B) SDS-PAGE profile of recombinant GS<sub>1</sub>β1 and GS<sub>1</sub>γ1 from (A) on 12.5% SDS-polyacrylamide gels in the presence (+DTT) or absence (-DTT) of DTT. Coomassie stained gels are shown with the electrophoretic positions of molecular weight markers on the left.

**A****B**

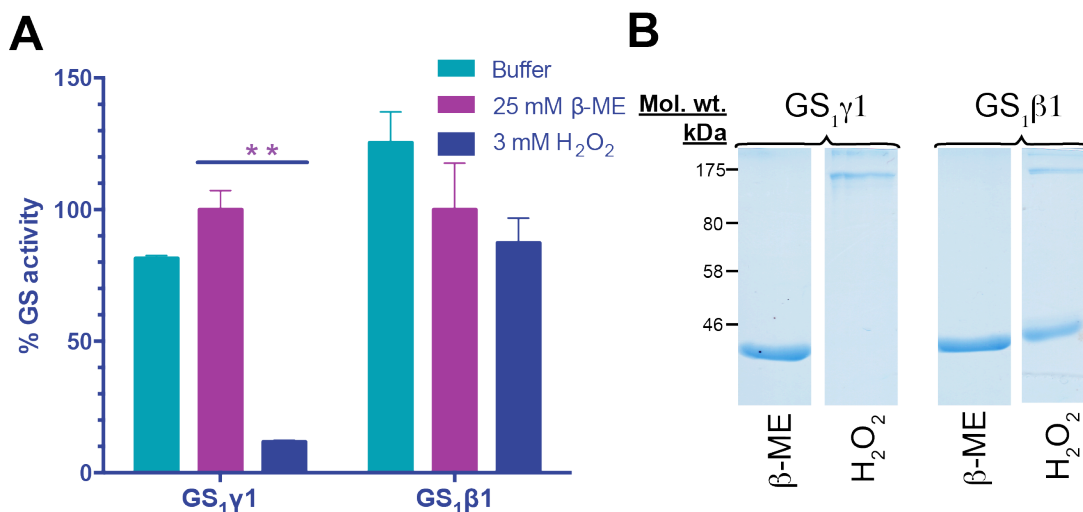


**Figure 3.2.3: Effect of oxidizing and reducing agents on the activity of  $GS_1$**

**isoforms.** (A) Immediately after purification, recombinant  $GS_1\beta_1$  and  $GS_1\gamma_1$  isoforms were treated with reducing agent ( $\beta$ -mercaptoethanol ( $\beta$ -ME)) or an oxidizing agent ( $H_2O_2$ ) for 30 minutes before determination of their GS activity. GS activity is expressed in percentage with GS activity with  $\beta$ -ME set as 100%. Error bars represent SEM (n=3). (\*\*  $p < 0.01$ ) (B) SDS-PAGE profile recombinant  $GS_1\beta_1$  and  $GS_1\gamma_1$  on non-reducing SDS-PAGE on 12.5% [w/v] polyacrylamide gels in presence or reducing ( $\beta$ -ME) or oxidizing agent ( $H_2O_2$ ). Coomassie stained gels are shown with molecular weight markers on the left. Each lane is labeled with name of the isoform on the top and at the bottom with the reagent with which the sample was incubated.

mild oligomerization with most of the protein separated as monomer (Figure 3.2.3B). This supports the proposal that the GS<sub>1</sub>γ1 undergoes oxidative inhibition.

## ***II. Reversibility of cysteine-specific oxidation of GS<sub>1</sub>γ1.***

Incubation with DTT reactivates the oxidized GS<sub>1</sub>γ1 (Figure 3.2.4). One of the possible means of oxidation that leads to oligomerization is the formation of intersubunit disulfide bonds. To investigate whether cysteine disulfide formation is involved, GS<sub>1</sub>γ1 was further incubated with oxidized glutathione (GSSG), which catalyzes disulfide exchange with free cysteines. The treatment with GSSG leads to inactivation of the enzyme (Figure 3.2.4). Although not shown in the figure, GS<sub>1</sub>γ1 oxidized by GSSG can be reactivated again by incubation with DTT illustrating reversibility of oxidation.

Each subunit of GS<sub>1</sub>γ1 has three cysteine residues at position 92, 159 and 179 (Figure 3.2.5). To determine whether the oxidized GS<sub>1</sub>γ1 forms disulfide bonds, free cysteine estimation was performed on the oxidized and the reduced forms of GS<sub>1</sub>γ1. It was observed that the reduced GS<sub>1</sub>γ1 has an average of 2.9 free cysteine residues per monomer, whereas the oxidized and inactive GS<sub>1</sub>γ1 had only 1.4 (Figure 3.2.6A). This suggests that some of the cysteine residues are involved in disulfide bond formation in the oxidized GS<sub>1</sub>γ1. Consistently, the activity of the air oxidized GS<sub>1</sub>γ1 used for cysteine determination is negligible as compared to the reduced form (Figure 3.2.6B). Taken together, the results



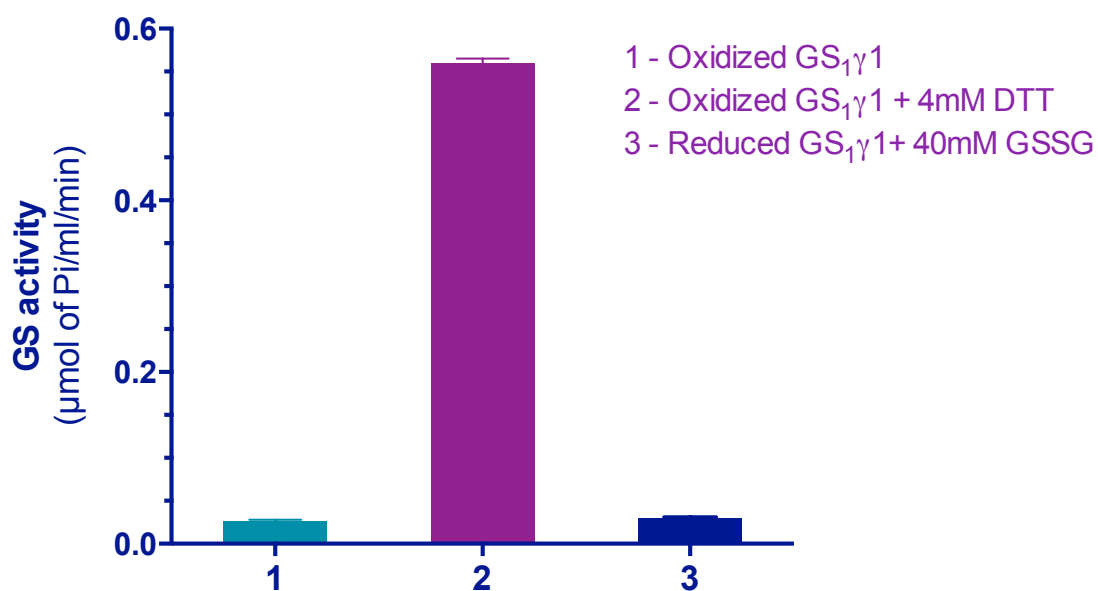


**Figure 3.2.4: Cysteine specific reversible oxidation of GS<sub>1</sub>γ1.** Air oxidized GS<sub>1</sub>γ1 was treated with a reducing agent (4 mM DTT) and further treated with a disulfide bond promoting agent GSSG (oxidized glutathione) to determine the reversibility of oxidative inhibition of GS<sub>1</sub>γ1. Activity of oxidized GS<sub>1</sub>γ1 is shown in column 1. Column 2 shows the activity of oxidized GS<sub>1</sub>γ1 following incubation with 4 mM DTT and column 3 shows the activity of reduced GS<sub>1</sub>γ1 after oxidation by 40 mM GSSG. Error bars represent SEM (n=4).

GS1beta1	1	MSLLSDLINLNLSDTTEKVIAEYIWIGGSGMDLRSKARTL	I
GS1gamma1	1	.....I.D.....V.....M.....	
GS1beta1	41	PGPVSDPSELPKWNYDGSSTGQAPGEDSEVILYPQAIFRD	
GS1gamma1	41	S...K...K.....Q.....K..	
GS1beta1	81	PFRRGNNILVICDAYTPAGEPIPTNKRHAAAKVFSHPDVV	
GS1gamma1	81	.....S.....M.....NN...I.G....A	
GS1beta1	121	AEVPWYGIEQEYTLQKDIQWPLGWPFVGGFPGPQGPYYCG	II
GS1gamma1	121	..E....L.....V.....L.....	
GS1beta1	161	VGADKAFGRDIVDAHYKACIYAGINISGINGEVMPGQWEF	
GS1gamma1	161	T..N.....S.....	
GS1beta1	201	QVGPSVGISAGDEIWAARYILERITEIAGVVVSFDPKPIK	
GS1gamma1	201	.....I....A..L.V.....L.....Q	
GS1beta1	241	GDWNGAGAHTNYSTKSMEDGGYEVIKAAIDKLGKKHKEH	
GS1gamma1	241	.....N.....K..A..E.R....	
GS1beta1	281	IAAYGEGNERRLTGRHETADINTFLWGVANRGASVRVGRD	III
GS1gamma1	281	.....M...V.....I.....	
GS1beta1	321	TEKAGKGYFEDRRPASNMDPYVVTSMIADTTILWKP	
GS1gamma1	321	.....E.....	

**Figure 3.2.5: Sequence alignment of soybean GS<sub>1</sub> isoforms.** The sequences of *Glycine max* (soybean) GS<sub>1</sub>β1 (Glyma11g33560.1), and GS<sub>1</sub>γ1 (Glyma14g39420.1) were aligned using the Clustal W alignment algorithm and the BioEdit software version 5.0.6 ([www.mbio.ncsu.edu/BioEdit/BioEdit.html](http://www.mbio.ncsu.edu/BioEdit/BioEdit.html)). Cysteine residues are indicated by (★). Regions of amino acid sequence that were used to generate chimeric constructs in figure 3.2.10 are highlighted and boxed: red, region I; green, region II; blue, region III.

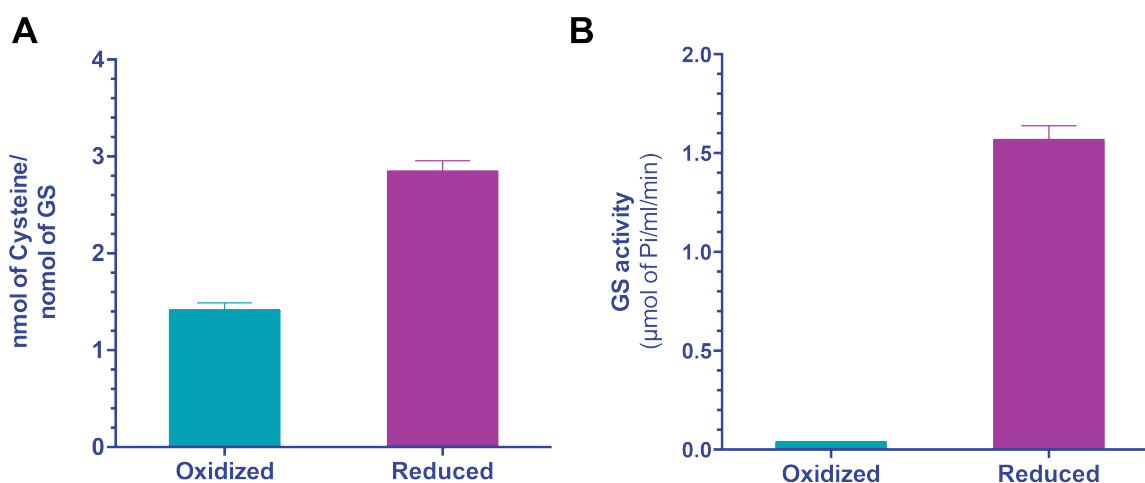


**Figure 3.2.6: Determination of free cysteine in oxidized and reduced**

**GS<sub>1</sub>γ1.** (A) The concentration of free cysteine residues in air-oxidized and DTT reduced GS<sub>1</sub>γ1 was determined by using Ellman's assay. The concentration of free cysteine residues is expressed as nmol of cysteine/nmol GS<sub>1</sub> monomer. Error bars represent SEM (n=8). (B) GS activity was determined for oxidized as well as reduced forms of GS<sub>1</sub>γ1 from (A). GS activity is expressed in nmol of Pi/min/ml and error bars represent SEM (n=3).

suggest that the GS<sub>1</sub>Y1 undergoes inactivation by reversible disulfide bond formation.

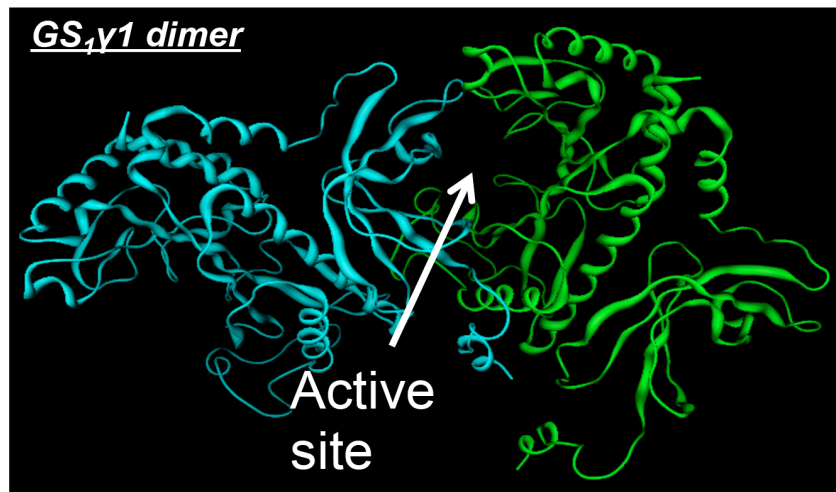
### ***III. Intersubunit disulfide bond formation in GS monomers results in inhibition of GS<sub>1</sub>Y1.***

Based on non-reducing SDS-PAGE (Figure 3.2.2B), it appears that oxidation results in covalently-linked oligomers, likely by intersubunit disulfide bond formation. As described above, based on the structure of the maize cytosolic glutamine synthetase, GS<sub>1</sub> forms a homodecameric structure with two stacked pentameric rings (Unno et al. 2006). A shared active site is formed between the N-terminal domain of one subunit and the C-terminal domain of the adjacent subunit (Figure 3.2.7A). To investigate the potential for cross-subunit disulfide bond formation, which may lead to oligomerization and inactivation of the enzyme, the position of the three cysteine residues was investigated in the GS<sub>1</sub>Y1 model. The model showed the proximity of two residues, cys92 from one monomer and cys159 from an adjacent monomer present at the shared active site, which could potentially form a disulfide bond (Figure 3.2.7B). Formation of an intersubunit disulfide bond between these residues would span and potentially block the active site, which could explain the observed inhibition of the enzyme in response to oxidation.

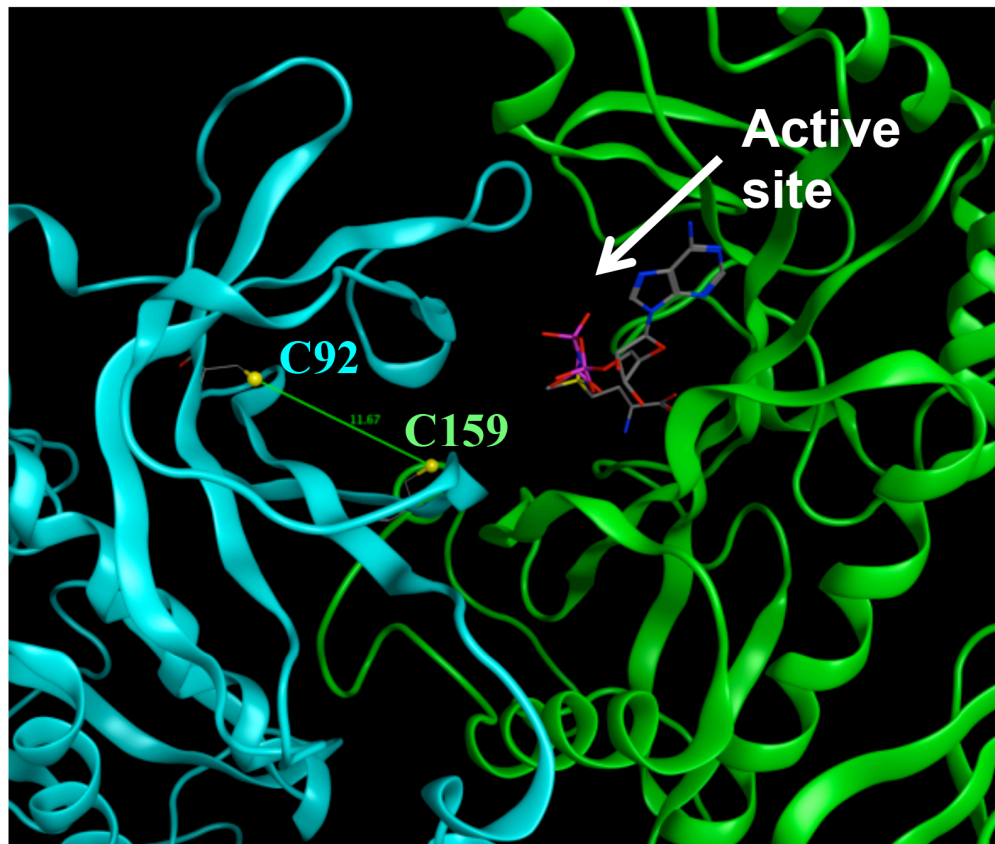
The possibility that oligomerization was the result of an intersubunit disulfide between cys92 and cys159, was investigated by site-directed mutagenesis in which each cysteine residue was replaced by serine

**Figure 3.2.7: Location of cysteine residues on GS<sub>1</sub>γ1.** A homology model of GS<sub>1</sub>γ1 generated by using maize GS1a (PDB ID: 2D3A\_A) as a template. The holoenzyme structure is shown in figure 3.1.13B. (A) The active site of GS is formed at the subunit interfaces. (B) Close-up of the active site is shown highlighting C92 and C159 amino acid residues. The ATP analog, AMPPNP, is shown bound to the active site.

A



B

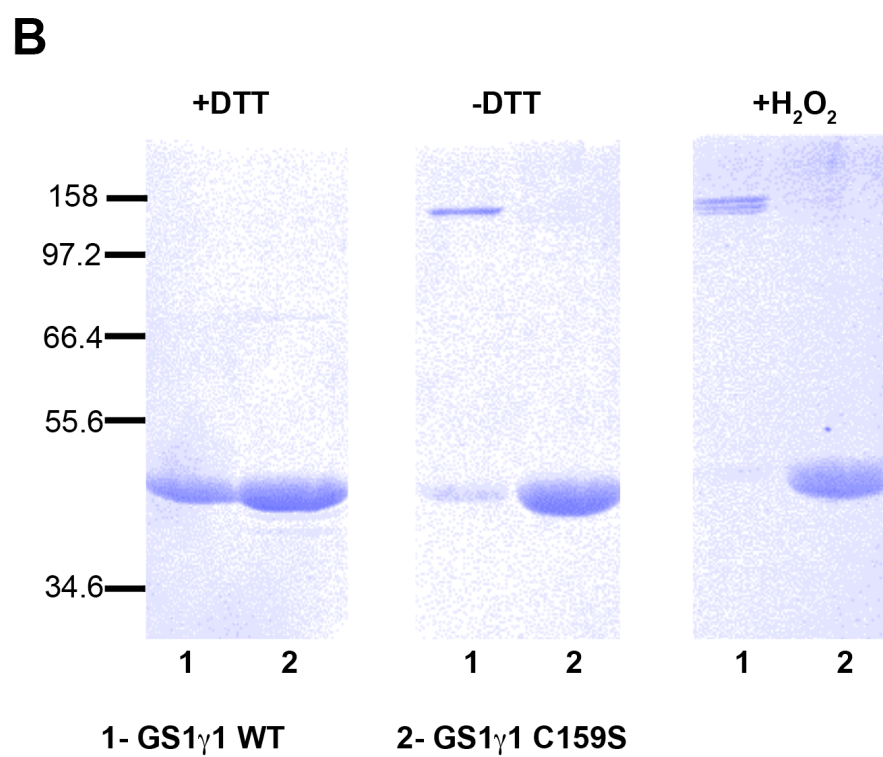
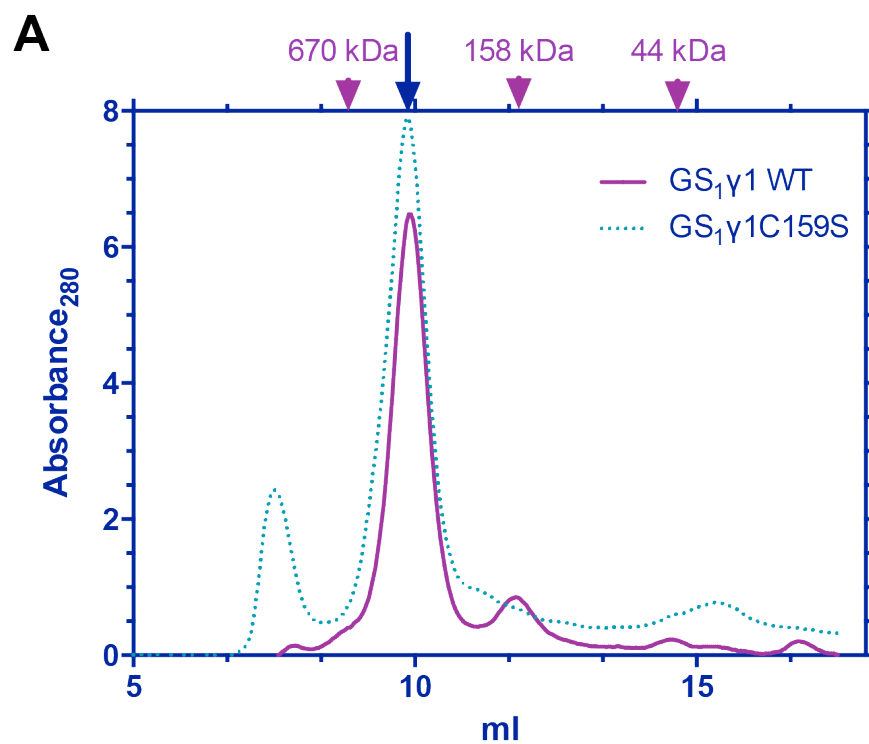


(GS<sub>1</sub>Y1C92S and GS<sub>1</sub>Y1C159S). Of these two mutants, only GS<sub>1</sub>Y1C159S produced enzymatically active protein. Both wild type as well as the GS<sub>1</sub>Y1C159S mutant produced major peaks with an apparent molecular weight of 401 kDa based on size exclusion chromatography (Figure 3.2.8A). After exposure to oxidizing conditions (air oxidation or H<sub>2</sub>O<sub>2</sub> incubation), purified GS<sub>1</sub>Y1C159S and GS<sub>1</sub>Y1 were analyzed by non-reducing SDS-PAGE to determine the effect of oxidation on oligomerization. In contrast to wild type GS<sub>1</sub>Y1, high molecular weight oligomeric species were not observed in the GS<sub>1</sub>Y1C159S mutant (Figure 3.2.8B). Even incubation with a strong oxidizing agent (H<sub>2</sub>O<sub>2</sub>) failed to show any oligomerization of GS<sub>1</sub>Y1C159S on non-reducing SDS-PAGE gels. Overall, it is proposed that cys159 is involved in oligomerization of GS<sub>1</sub>Y1 monomers through disulfide bond formation. Based on molecular modeling, this is likely through the formation of an intersubunit disulfide pair with cys92.

Comparison of the amino acid sequences of GS<sub>1</sub>β1 and GS<sub>1</sub>Y1 shows 38 substitutions, with most in non-catalytic regions (Figure 3.2.5). Analysis of homology models showed that two residues at position 41 and 65 are present at the interface of the two monomers in the holoenzyme structure and show significant differences between the two isoforms (pro41, glu65 in GS<sub>1</sub>β1 and ser41 and gln65 in GS<sub>1</sub>Y1). To determine whether these residues affect subunit-subunit interactions in a manner that affects disulfide bond formation, ser41 and gln65 residues in GS<sub>1</sub>Y1 were mutated to pro and glu respectively to create a

**Figure 3.2.8: Identification of a cysteine residue in GS<sub>1</sub>γ1 that is involved in disulfide bond formation.** (A) Recombinantly purified GS<sub>1</sub>γ1 WT and GS<sub>1</sub>γ1C159S were separated on a Superdex 200 10/300 GL column by using an FPLC instrument. The elution profile from the column is shown where the Y-axis shows the absorbance at 280 nm and the X-axis shows the elution volume. Elution positions of molecular marker proteins are indicated with violet arrows on the top. The blue arrow indicates the elution position of the oligomeric protein GS<sub>1</sub> protein. (B) Recombinant GS<sub>1</sub>γ1 WT (lane 1) and GS<sub>1</sub>γ1C159S (lane 2) separated on non-reducing SDS-PAGE gels under reducing (+DTT) and oxidizing (+H<sub>2</sub>O<sub>2</sub>) conditions.





double mutant GS<sub>1</sub>γ1SQ-PE. GS activity analysis of GS<sub>1</sub>γ1SQ-PE shows that it behaves similar to WT GS<sub>1</sub>γ1 with respect to sensitivity to oxidation (Figure 3.2.9). This suggests that substitutions of these two residues at the subunit-subunit interface are not sufficient to confer β-like properties on the γ subunit.

In addition to these two residues, GS<sub>1</sub> isoforms show significant substitutions in regions from 41-79 and 259-279 and these regions lie at the monomer-monomer interfaces (Figure 3.2.5). To take a more global approach to identify the contribution of these regions to sensitivity to oxidizing conditions, chimeric combinations of GS<sub>1</sub>β1 and GS<sub>1</sub>γ1 were created (Figure 3.2.10). GS activity of each chimeric protein was determined under oxidizing and reducing conditions (Figure 3.2.11). Comparison of the activities of the various chimeras show substitution of region II (79-250) in GS<sub>1</sub>γ1 with the corresponding region from GS<sub>1</sub>β1 results in loss of sensitivity to oxidizing conditions. This suggests that substitutions within this region might be responsible for the structural change that affects cysteine/disulfide bond formation.

#### ***IV. GS<sub>1</sub>γ1 and GS<sub>1</sub>β1 form distinct oligomeric structures.***

Comparison of the amino acid sequences of GS<sub>1</sub>β1 and GS<sub>1</sub>γ1 isoforms shows high sequence identity, including the conservation of the three cysteine residues and similar subunit molecular weights (Figure 3.2.5). Homology models of both isoforms were created using the maize GS1a structure as template using MOE. Homology models showed that both GS<sub>1</sub>β1 and GS<sub>1</sub>γ1 isoforms have inter-subunit cys159 and cys92 residues at comparable distances (11Å -12Å).

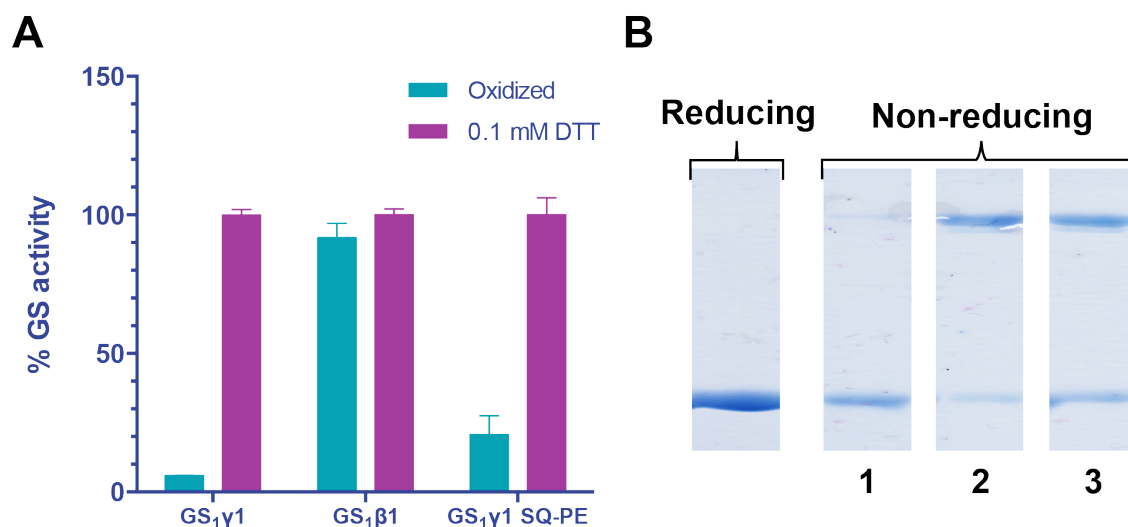


**Figure 3.2.9: Activity analysis of GS<sub>1</sub>γ1SQ-PE mutant.** A double substitution mutant of GS<sub>1</sub>γ1 (GS<sub>1</sub>γ1SQ-PE) was created where amino acid residues ser41 and gln65 were substituted for pro and glu respectively. (A) GS activity of both GS<sub>1</sub> isoforms and GS<sub>1</sub>γ1SQ-PE was estimated on the dialyzed protein samples before and after incubation with 0.1 mM DTT. % GS activity is shown with the activity of protein sample incubated with DTT represents 100%. (B) Oxidation induced oligomerization was also analyzed by reducing and non-reducing SDS-PAGE on 12.4% [w/v] polyacrylamide gels. GS<sub>1</sub>β1 (1), GS<sub>1</sub>γ1 (2) and GS<sub>1</sub>γ1SQ-PE (3) samples separated under non-reducing conditions are shown along with representative sample separated under reducing conditions.

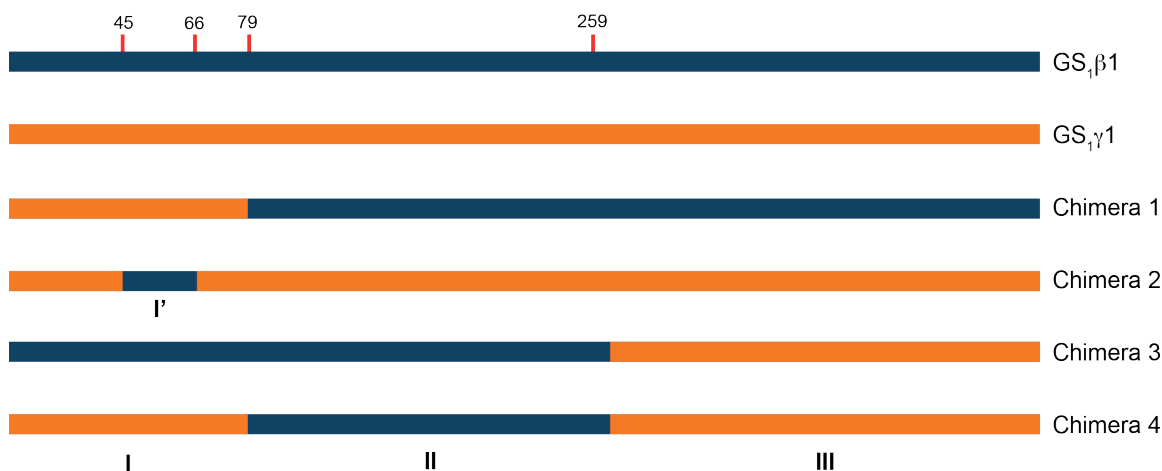


**Figure 3.2.10: Chimeric constructs of GS<sub>1</sub>β<sub>1</sub> and GS<sub>1</sub>γ<sub>1</sub>.** Full-length GS<sub>1</sub>β<sub>1</sub> and GS<sub>1</sub>γ<sub>1</sub> isoforms are shown in blue and orange respectively. Length of GS<sub>1</sub> isoforms as well as chimera proteins is 356 amino acids. The positions of amino acid residues at the interface of different proteins in chimera are highlighted at the top and the names of the chimera proteins are shown on the right side. Regions (I, II, III and I') of GS<sub>1</sub>β<sub>1</sub> and GS<sub>1</sub>γ<sub>1</sub> isoforms in chimera proteins are shown by blue and orange respectively.

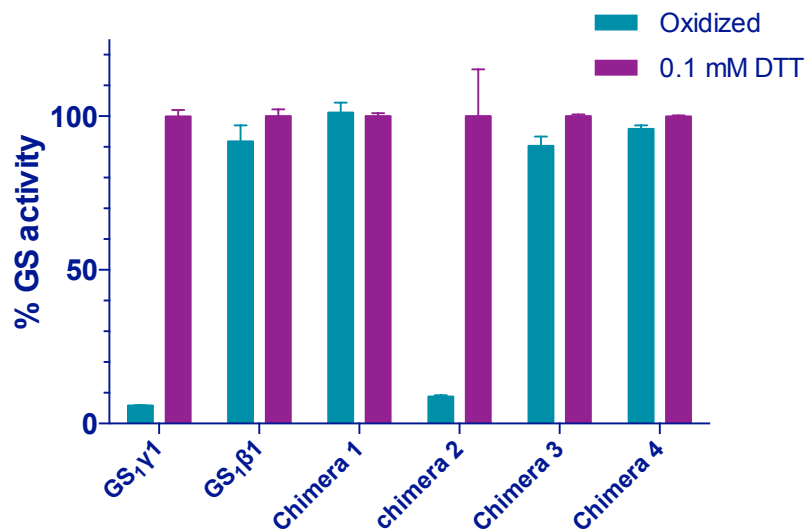


**Figure 3.2.11: Effect of oxidation on the activity of GS<sub>1</sub> chimeric proteins.**

Chimeric proteins of GS<sub>1</sub>β1 and GS<sub>1</sub>Y1 were created as shown in figure 3.2.10. Purified proteins were air oxidized and their activities were measured before and after incubation with 0.1 mM DTT. Activity of each chimeric protein is standardized with the activity of samples incubated with DTT set as 100%. Error bars represent SEM (n=3).

Given this observation, and the high degree of sequence similarity between the two isoforms, it is not clear why one isoform would be more susceptible to disulfide oxidation.

Comparison of the two GS<sub>1</sub> isoforms by native PAGE showed that GS<sub>1</sub>γ1 has a reduced electrophoretic mobility compared to GS<sub>1</sub>β1 (Figure 3.2.12). Given the similarity of the monomeric molecular weight and amino acid compositions of the two isoforms, this difference in electrophoretic mobility may be the result of difference in holoenzyme molecular weight, and a difference in subunit stoichiometry. This was further tested by using sedimentation velocity analytical ultracentrifugation (AUC). A good fit was obtained using the c(M) distribution model in SEDFIT with rmsd values below 0.01 (Figure 3.2.13). The molecular weight distribution shows that there is a difference in the calculated molecular weight of each isoform with GS<sub>1</sub>γ1 (492 kDa) exhibiting higher molecular weight compared to GS<sub>1</sub>β1 (405 kDa) (Figure 3.2.14).

To elucidate the native molecular weight and subunit composition of each GS<sub>1</sub> isoform more precisely, equilibrium AUC was performed using recombinant GS<sub>1</sub>γ1 and GS<sub>1</sub>β1 proteins (Figure 3.2.15). A good fit was obtained using the discrete species model in SEDPHAT with rmsd values below 0.007 absorbance units and chi-squared values near 1. The molecular weight calculated from equilibrium AUC for GS<sub>1</sub>γ1 is 499.28 kDa whereas GS<sub>1</sub>β1 is 409.55 kDa (Figure 3.2.15), supporting the results of velocity AUC. Considering the monomeric molecular weight of both isoforms, the 499.28 kDa GS<sub>1</sub>γ1 would represent an

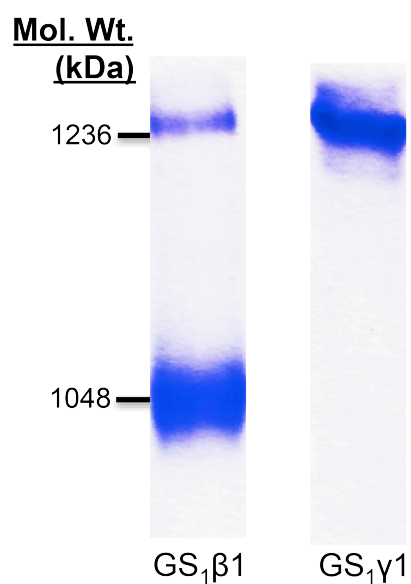


**Figure 3.2.12: Native PAGE analysis of  $GS_1\beta 1$  and  $GS_1\gamma 1$  isoforms.**

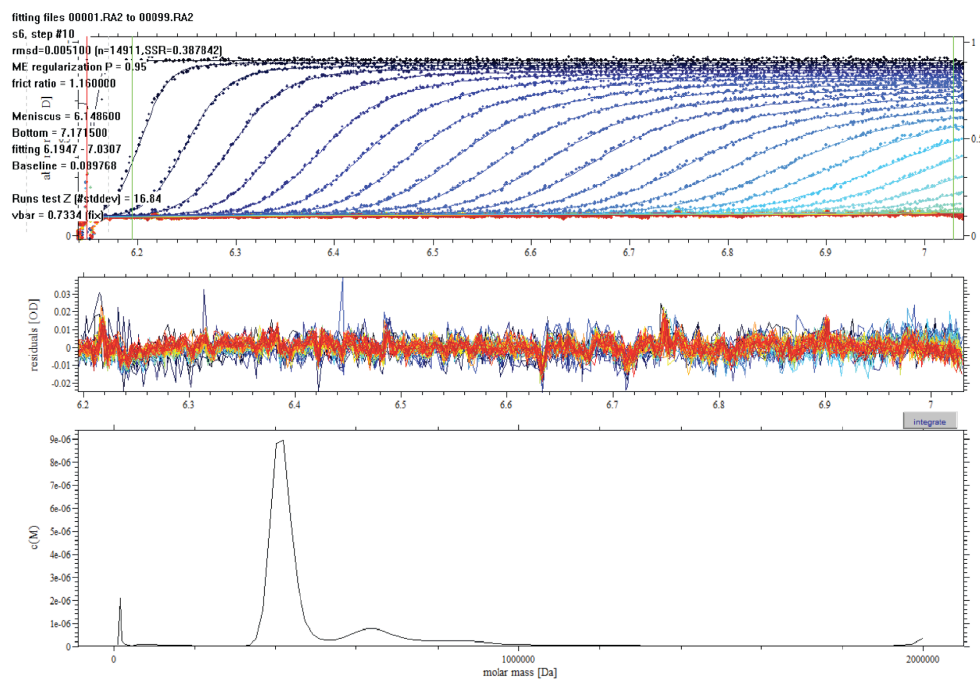
Five  $\mu\text{g}$  of recombinant  $GS_1\beta 1$  and  $GS_1\gamma 1$  proteins were separated by native PAGE on 6% [w/v] Tris Glycine gels. Each lane is labeled with respective protein sample and the mobility of a native PAGE protein marker is noted on the left.

**Figure 3.2.13: Sedimentation velocity AUC studies of GS<sub>1</sub> isoforms.**

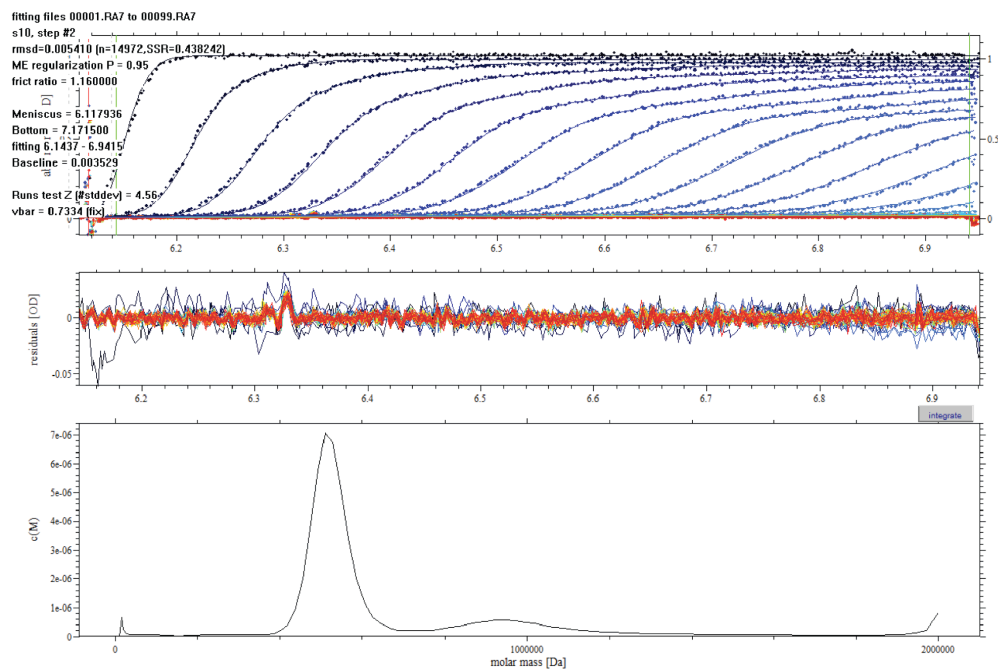
Absorbance data of sedimenting protein samples were collected at 30000 rpm at 20°C and fitted to the c(M) distribution model as described in the Materials and Methods. Fitted data for GS<sub>1</sub>β1 (A) and GS<sub>1</sub>γ1 (B) is shown. The top panel shows the absorbance scans with the fitted parameters indicated. The X-axis shown the radius position and the Y-axis shows the absorbance at 280 nm. The middle panel shows the residuals of the fit and the bottom panel shows the distribution plot of different sedimenting species c(M) vs molecular weight in daltons.

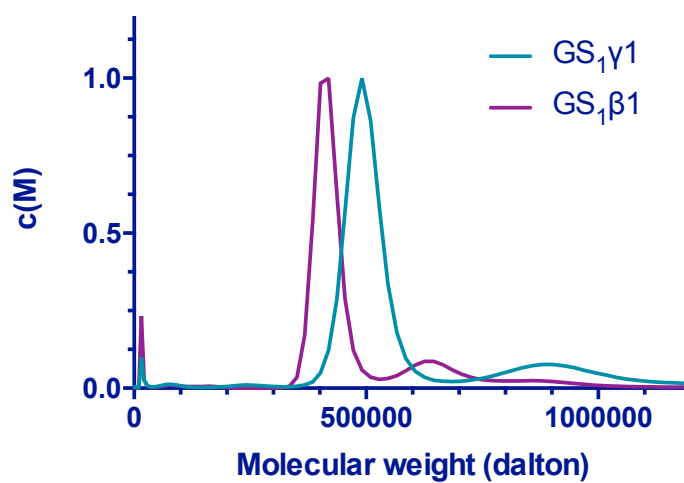


**A**



**B**

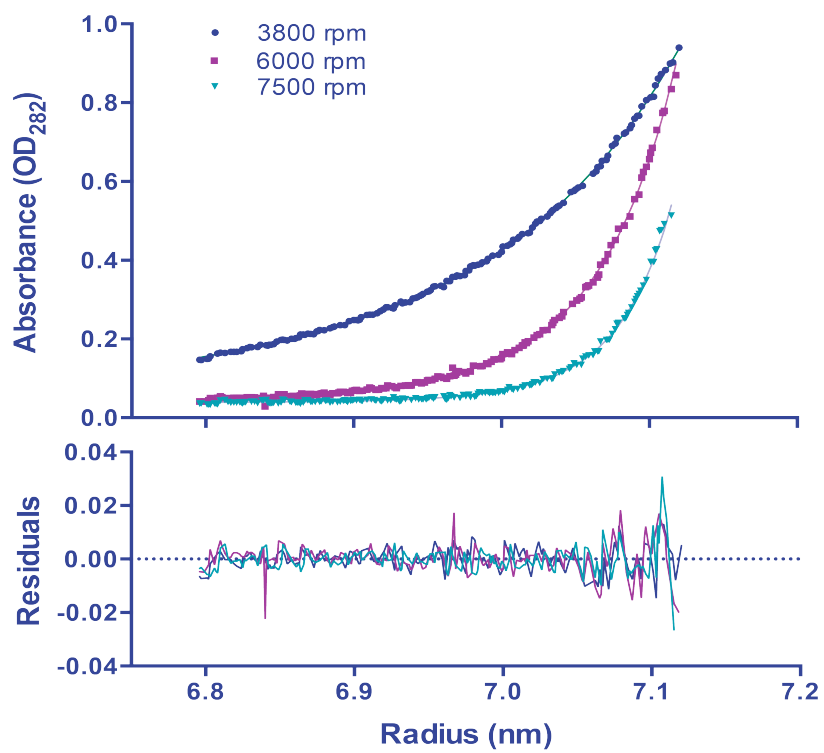
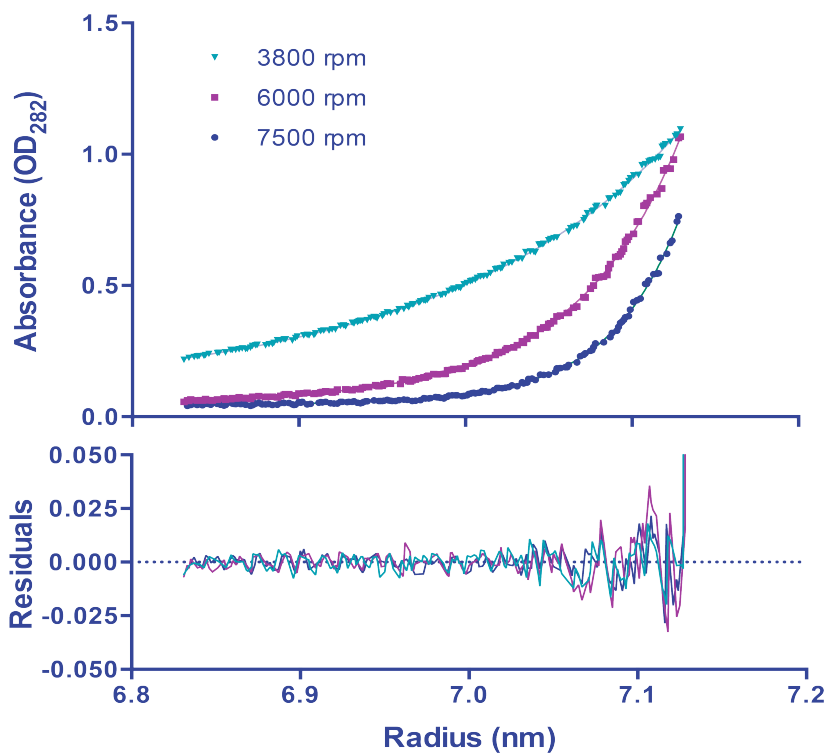




**Figure 3.2.14: Sedimentation velocity analysis of GS<sub>1</sub> isoforms.** GS<sub>1</sub> protein samples (0.5 mg/ml) were analyzed by sedimentation velocity AUC at 30000 rpm and 20°C. 200 scans at 280 nm were taken at 1 min interval and were analyzed using the SEDFIT using c(M) distribution model.

**Figure 3.2.15: Recombinant GS<sub>1</sub> protein analysis using sedimentation**

**equilibrium AUC.** Protein samples were centrifuged at 10°C in 20 mM Tris-HCl, pH 7.0, 300 mM NaCl, for at least 30 hrs at 3,800 (circle), 6,000 (square) and 7,500 (triangle). The solid lines represent the global nonlinear least squares best-fit of all the data to a discrete molecular species with a molecular mass of 499.28 kDa (for GS<sub>1</sub>γ1) and 409.55 kDa (for GS<sub>1</sub>β1). Residuals of the fit at all rotor speeds are also shown and the rmsd is 0.0068 (GS<sub>1</sub>γ1) and 0.0050 (for GS<sub>1</sub>β1) absorbance units. Examples of absorbance scans at 280 nm at equilibrium for are plotted versus the distance from the axis of rotation for GS<sub>1</sub>β1 (A) and GS<sub>1</sub>γ1 (B) protein are shown. All data analysis was performed with the SEDFIT and SEDPHAT software.

**A****B**

oligomer of 12 subunits, which is distinct from the 409.55 kDa GS<sub>1</sub>β1 which would represent a decameric enzyme similar to maize GS1a enzyme (Unno et al. 2006). It is proposed that this dodecameric arrangement of the GS<sub>1</sub>γ1 may be responsible for its greater sensitivity to disulfide bond formation, perhaps by decreasing the distance between adjacent cysteine residues at the monomer-monomer interface.

## CHAPTER IV DISCUSSION

### 4.1. Interaction of glutamine synthetase with nodulin 26

Under limiting conditions of nitrogen, a number of plants from the *Leguminosae* family enter in a symbiotic relationship with diazotrophic rhizobia bacteria to fulfill their nitrogen demand. In this association, the plant host provides a carbon source and microaerobic conditions for bacteria to enable fixation of nitrogen to ammonia which is provided to the plant for assimilation. The symbiosomes are the specialized organelle structures which host the nitrogen-fixing form of the bacteria. The plant symbiosome membrane is a unique symbiotic interface between the legume host and endosymbiotic rhizobia bacteria. Biogenesis of the symbiosome membrane occurs early in the rhizobia infection process and is accompanied by the biosynthesis of a variety of nodulin proteins (Fortin et al. 1985). Many of these proteins become integral components of the mature symbiosome membrane and mediate transport and regulatory processes associated with metabolite exchange between the symbiotic partners (Day et al. 2001; Udvardi and Poole 2013; Udvardi and Day 1997; White et al. 2007). Among these proteins is nodulin 26 which is a major component of the mature symbiosome (Fortin et al. 1987; Rivers et al. 1997; Weaver et al. 1991). Nodulin 26 confers a high intrinsic water permeability (Rivers et al. 1997; Wallace et al. 2006) to the symbiosome membrane, and fulfills other functions as a channel that facilitates transport of neutral metabolites

such as glycerol and  $\text{NH}_3$  (Dean et al. 1999; Hwang et al. 2010; Niemietz and Tyerman 2000; Rivers et al. 1997).

Glutamine synthetase (EC 6.3.1.2) is the critical and major enzyme for assimilation of environmental ammonia and reassimilation of ammonia produced metabolically in plants (Forde and Lea 2007; Tabuchi et al. 2007; Teixeira et al. 2005). In root nodules,  $\text{GS}_1$  constitutes 2% of the total protein content in nodules (Streeter 1989). Plant glutamine synthetases are divided into two isoform classes that are distinguished by their subcellular location, with  $\text{GS}_1$  found in the cytosol, while  $\text{GS}_2$  resides in plastids (Bernard and Habash 2009; Forde et al. 1989; Marquez et al. 2005; Mifflin and Habash 2002). Plant  $\text{GS}_1$  is encoded by a small, highly conserved gene family (Bernard et al. 2008; Goodall et al. 2013; Ishiyama et al. 2004a; Ishiyama et al. 2004c; Lara et al. 1983; Li et al. 1993; Martin et al. 2006; Morey et al. 2002; Nogueira et al. 2005; Stanford et al. 1993; Swarbreck et al. 2011; Teixeira et al. 2005; Tingey et al. 1987) with three  $\text{GS}_1$  isoform classes (designated  $\alpha$ ,  $\beta$  and  $\gamma$ ) typically present in legumes (Forde et al. 1989; Gebhardt et al. 1986; Morey et al. 2002).  $\text{GS}\alpha$ ,  $\beta$  and  $\gamma$  show differential expression during development and in response to environmental and metabolic cues (Morey et al. 2002). In mature  $\text{N}_2$ -fixing soybean nodules 4  $\text{GS}_1$  isoforms ( $\beta 1$ ,  $\beta 2$ ,  $\gamma 1$ ,  $\gamma 2$ ) exhibit high expression (Morey et al. 2002). The  $\beta$  isoforms are characterized as the “constitutive”  $\text{GS}_1$  subclass that exhibit a broad expression pattern in soybean tissues, but show particularly high expression in nodules and are inducible by high levels of ammonia (Morey et al. 2002; Temple et al. 1995).

The  $\gamma$  isoforms are selectively expressed as nodulin proteins in a developmentally regulated fashion in soybean nodules (Morey et al. 2002; Temple et al. 1996) and other legumes (Forde et al. 1989; Stanford et al. 1993; Temple et al. 1995). The expression of the four GS<sub>1</sub> isoforms during soybean nodule development coincides with the onset of nitrogen fixation (Morey et al. 2002), consistent with their role as the major enzyme responsible for the ATP-dependent assimilation of fixed ammonia transported from the symbiosome to the cytosolic compartment of the plant host. The expression of GS<sub>1</sub> (occurring at approximately day ten in nodule development, (Morey et al. 2002)) also parallels the appearance of nodulin 26 protein in developing nodules (Guenther et al. 2003).

A major finding of the present work is that soybean nodule GS<sub>1</sub> forms a molecular complex with symbiosome membrane nodulin 26. This association is mediated by the binding of GS<sub>1</sub> to the exposed hydrophilic C-terminal domain of nodulin 26 on the surface of the symbiosome, and is essential for the association of GS with the symbiosome. The four soybean GS<sub>1</sub> isoforms expressed in nodules share more than 88% amino acid sequence identity (Figure 1.3.3), and the observation that all interact with nodulin 26 suggests that these proteins contain a conserved interaction site for the nodulin 26 C-terminal domain with any isoform conceivably capable of forming a complex with nodulin 26 *in vivo*. X-ray crystallography of plant cytosolic GS<sub>1</sub> (Unno et al. 2006) shows a homodecameric structure of two stacked pentameric subunit rings with catalytic



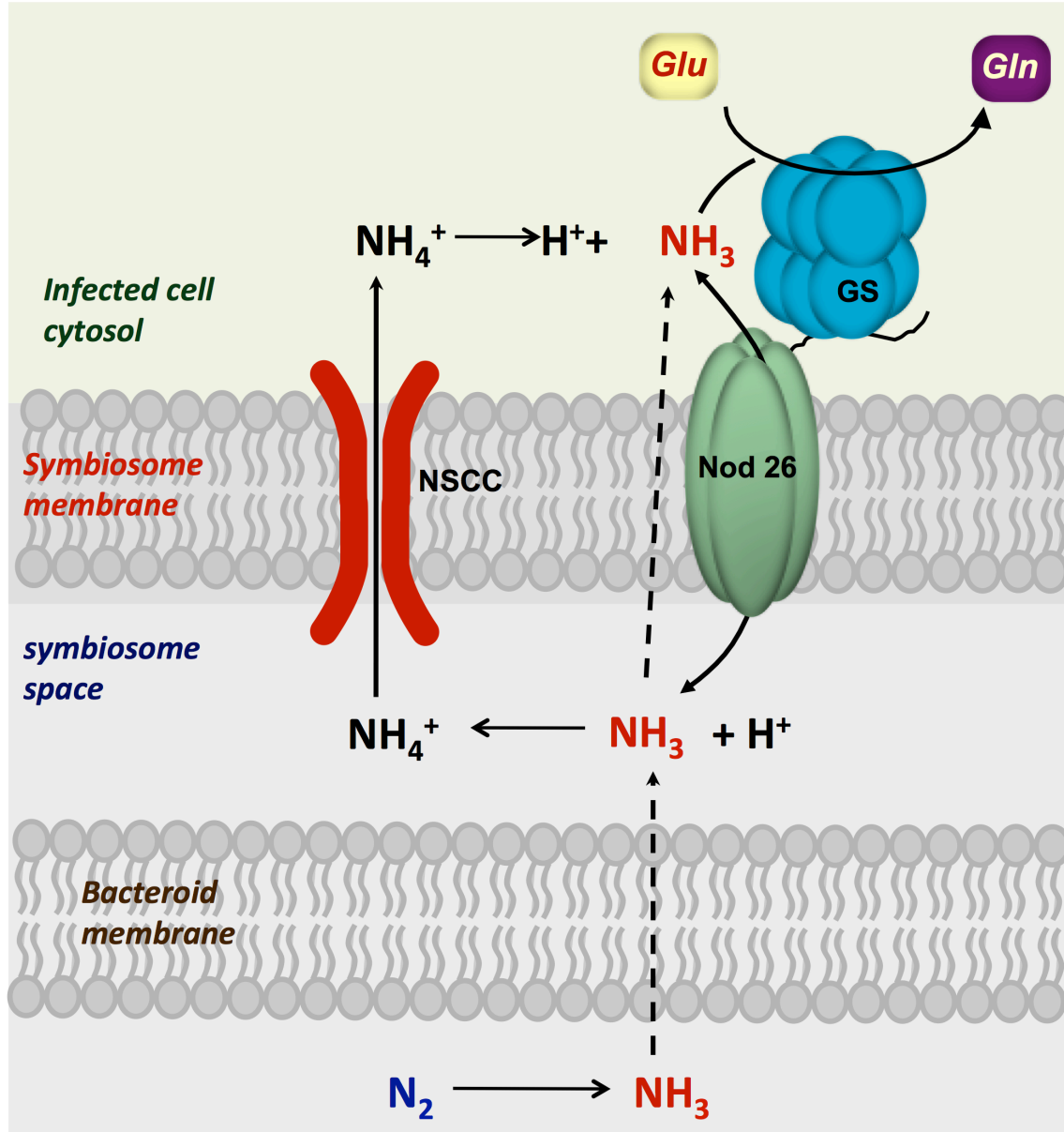
sites shared between adjacent monomeric subunits. The finding of a one to one binding stoichiometry suggests that each GS<sub>1</sub> monomer possess a binding site for the nodulin 26 C-terminal domain. Crosslinking experiments showed that the potential interaction site of nodulin 26 on GS<sub>1</sub> is present on a linear sequence between 260-300 on the surface of GS<sub>1</sub> adjacent to the opening of the shared active site. The binding of CK-25 peptides does not affect the GS activity, and it is suggested that the interaction with nodulin 26 could serve principally to localize GS to the surface of the symbiosome membrane, at the site of ammonia efflux through the nodulin 26 channel. From holoprotein perspective, question remains regarding the stoichiometry of the interaction *in vivo*. In *in vivo* conditions, nodulin 26 forms a tetramer were as GS<sub>1</sub> forms a decamer (in case of GS<sub>1</sub>β1). Oligomeric structures of both the proteins will not allow 1:1 stoichiometry observed in interaction of C-terminal peptide of nodulin 26 and GS<sub>1</sub> monomer. The structural arrangement of the decameric GS<sub>1</sub> on the nodulin 26 tetramer and the position of the GS active site relative to the nodulin 26 channel requires further structural analysis.

The potential symbiotic significance of nodulin 26 interaction with GS<sub>1</sub> can be understood from the perspective of the known transporters and pumps on the symbiosome membrane (Day et al. 2001; Niemietz and Tyerman 2000; Obermeyer and Tyerman 2005; Roberts and Tyerman 2002; Tyerman et al. 1995; reviewed in Udvardi and Poole 2013; Udvardi and Day 1989; 1990; Udvardi and Day 1997), and the inherent toxicity of ammonia/ammonium

transport across energized membranes (Britto et al. 2001), and is summarized in figure 3.4.1.  $\text{N}_2$ -fixation by rhizobium bacteroids results in the production of  $\text{NH}_3$  which diffuses across the bacteroid membrane into the symbiosome space. Efflux of  $\text{NH}_3/\text{NH}_4^+$  from the symbiosome space to the cytosol can occur by: 1. Directional transport of  $\text{NH}_4^+$  cation to the cytosol by an inwardly rectified, voltage-activated cation channel (Obermeyer and Tyerman 2005; Roberts and Tyerman 2002; Tyerman et al. 1995); or 2. passive diffusion of uncharged  $\text{NH}_3$  through the symbiosome membrane (Udvardi and Day 1990) with facilitated diffusion of  $\text{NH}_3$  through nodulin 26 potentially providing a low energy efflux pathway (Hwang et al. 2010; Niemietz and Tyerman 2000). The relative contributions of these pathways remains a subject of debate and depends upon the pH of the symbiosome space and the resting potential of the symbiosome membrane, both of which are primarily controlled by an putative energizing  $\text{H}^+$ -pumping ATPase on the symbiosome membrane (Udvardi and Day 1989). An interaction between nodulin 26 and  $\text{GS}_1$  as shown here in this study would localize this critical assimilatory enzyme to the surface of the symbiosome, the site of fixed  $\text{NH}_3/\text{NH}_4^+$  release into the infected cell cytosol. Direct interaction of  $\text{GS}_1$  with nodulin 26 could facilitate rapid assimilation of reduced nitrogen in the form of unprotonated  $\text{NH}_3$  transported through the nodulin 26 channel, potentially as a "metabolic funnel" (Figure 4.1.1). Additionally, since nodulin 26 is the most abundant symbiosome membrane protein, interaction with  $\text{GS}_1$  would increase the local concentration of the enzyme at the symbiosome surface which would

**Figure 4.1.1: Metabolic model for interaction of nodulin 26 and glutamine synthetase and its effect on nitrogen assimilation in nitrogen-fixing**

**nodules.** A model for efflux and assimilation of fixed nitrogen in symbiosomes is shown. Ammonia produced by the action of nitrogenase in the bacteroid moves into the symbiosome space by simple diffusion (Udvardi and Day 1990). Efflux of fixed nitrogen from the symbiosome space can occur as either  $\text{NH}_4^+$  or  $\text{NH}_3$ .  $\text{NH}_4^+$  is directionally transported to the cytosolic side of the symbiosome membrane by a non-selective cation channel (NSCC) which is voltage-activated and is inwardly rectified (Obermeyer and Tyerman 2005; Roberts and Tyerman 2002; Tyerman et al. 1995). A diffusive pathway for  $\text{NH}_3$  efflux also exists with nodulin 26 representing a low energy facilitated pathway for this gas (Hwang et al. 2010; Niemietz and Tyerman 2000). Binding of GS to the C-terminal domain of nodulin 26 increases the concentration of this assimilatory enzyme at the symbiosome surface and also serves as a potential site for rapid assimilation of ammonia traversing nodulin 26.



enhance the rate of assimilation of  $\text{NH}_3/\text{NH}_4^+$  that leaves the symbiosome through the other efflux pathways.

An additional advantage of the nodulin 26/GS<sub>1</sub> association may stem from the observation that high levels of ammonium are inherently toxic to plants, which is potentially the result of wasteful “ammonia futile cycling” (Britto et al. 2001). In the case of the symbiosome, such a process could operate due to the acidic pH of the symbiosome space and the high concentrations of ammonium that accumulate during active nitrogen fixation (Streeter 1989) (Figure 4.1.2). Entry of  $\text{NH}_4^+$  into the more alkaline plant cytosol would result in loss of a proton generating  $\text{NH}_3$  which could reenter the symbiosome space, possibly through nodulin 26. The result would be a net transport of a proton from the symbiosome space to the cytosol which would dissipate the proton motive force generated by the symbiosome membrane  $\text{H}^+$ -ATPase (Udvardi and Day 1989), and lead to hydrolysis of ATP and futile cycling. As stated above, the interaction of nodulin 26 with GS<sub>1</sub> could facilitate rapid  $\text{NH}_4^+$  assimilation, preventing its accumulation in the cytosol. The maintenance of low cytosolic concentrations of  $\text{NH}_4^+$ , which are estimated to be 50-fold lower than the  $\text{NH}_4^+$  concentration in nitrogen-fixing symbiosomes (Streeter 1989), would prevent potential futile cycling.

Another potential level of complexity in the nodulin 26/GS interaction comes from the observation that both binding partners are subject to

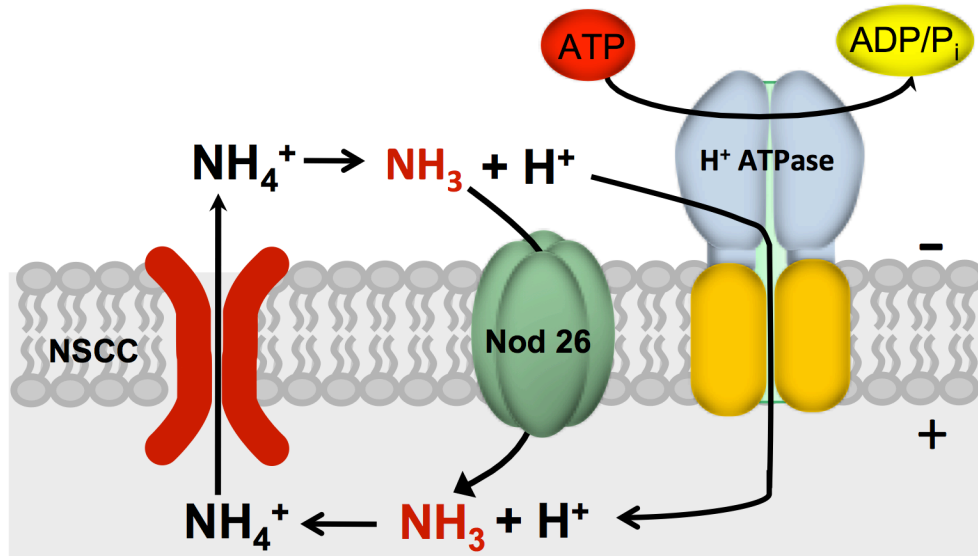


**Figure 4.1.2: Futile cycle prevention by nodulin 26/GS interaction.**

A potential mechanism for ammonia futile cycling through the symbiosome membrane is shown. The symbiosome membrane is energized by an H<sup>+</sup>-ATPase which generates a proton gradient by pumping H<sup>+</sup> into the symbiosome space (Udvardi and Day 1989). When the symbiosome membrane is hyperpolarized, the NSCC is activated which directionally transports NH<sub>4</sub><sup>+</sup> into the cytosolic compartment (Tyerman et al. 1995). Since the cytosol is more alkaline than the symbiosome space, NH<sub>4</sub><sup>+</sup> can release a H<sup>+</sup> with NH<sub>3</sub> potentially reentering the symbiosome space through nodulin 26. Maintenance of cytosolic NH<sub>4</sub><sup>+</sup> levels at low concentrations by rapid assimilation via GS would be one approach to prevent this potential metabolite cycling.

posttranslational phosphorylation (Finnemann and Schjoerring 2000; Lima et al. 2006b; Weaver et al. 1991; Weaver and Roberts 1992). In the case of nodulin 26 the unique site of phosphorylation is ser 262 (Weaver and Roberts 1992), which resides in the C-terminal domain which is the site of GS interaction. Ser 262 phosphorylation is catalyzed by a calcium-dependent protein kinase that is localized to the symbiosome membrane (Weaver et al. 1991). Nodulin 26 phosphorylation is developmentally regulated, becoming apparent at the onset of nitrogen fixation, and maintained at steady-state levels throughout the N<sub>2</sub>-fixing portion of the nodule lifespan (Guenther et al. 2003). In addition, the phosphorylation is increased by osmotic stress signals (Guenther et al. 2003) which may reflect the regulation of nodulin 26 transport act as part of an osmoregulatory response. Phosphorylation of nodulin 26 also affects the transport selectivity of the channel, with phosphorylation stimulating the aquaporin activity of nodulin 26 (Guenther et al. 2003) while dephosphorylation appears to stimulate the ammoniaporin activity (Niemietz and Tyerman 2000; Hwang and Roberts, unpublished results). At the peptide binding level, phosphorylation of ser262 appears to exert minor effect on nodulin 26 association with GS<sub>1</sub>. Thus, while phosphorylation of nodulin 26 affects transport activity in response to developmental and environmental cues, it does not appear to influence GS<sub>1</sub> association. Whether GS<sub>1</sub> association affects nodulin 26 activity or its ability to be phosphorylated *in vivo* remains unresolved.

Cytosolic GS<sub>1</sub> is also a target for posttranslational phosphorylation by various protein kinases in plant tissues phosphorylation (Engelsberger and Schulze 2012; Finnemann and Schjoerring 2000; Li et al. 2006; Lima et al. 2006a; b; Melo-Oliveira et al. 1996; Rose et al. 2012), with phosphorylation potentially leading to interaction with other proteins including 14-3-3 proteins (Finnemann et al. 2000) and other unidentified phosphoproteins (Lima et al. 2006b). The interplay between phosphorylation, GS regulation, and interaction with nodulin 26 and other potential regulatory targets, and the effects of these on nitrogen fixation and assimilation in response to environmental cues, remains a topic for future investigation.

## **4.2. Regulation of glutamine synthetase by reversible oxidation**

Given its central role in nitrogen metabolism, it is of no surprise that glutamine synthetase from different plants has been shown to be regulated at the transcriptional level, as well as at the posttranslational level by phosphorylation (Becker et al. 1992; Edwards and Coruzzi 1989; Elmlinger et al. 1994; Engelsberger and Schulze 2012; Finnemann and Schjoerring 2000; Li et al. 2006; Lima et al. 2006a; b; Melo-Oliveira et al. 1996; Miao et al. 1991; Migge et al. 1998; Morey et al. 2002; Reiland et al. 2009; Riedel et al. 2001; Rose et al. 2012; Seabra et al. 2013; Simonovic and Anderson 2008; Tingey et al. 1988). The results of the present work support a potential role of reversible disulfide oxidation as an additional level of isoform-specific regulation of soybean nodule glutamine synthetases. We have shown that two GS<sub>1</sub> isoforms from soybean



root nodule (GS<sub>1</sub>β1 and GS<sub>1</sub>γ1) have different oligomeric structures that are proposed to result in differential susceptibility to disulfide regulation. GS<sub>1</sub>γ is dodecamer that undergoes oxidation which results in the formation of an inter subunit disulfide bond between cys92 and cys159 leading to its inhibition. In contrast the decameric GS<sub>1</sub>β1 is less susceptible to oxidation.

Various studies have shown that GS is an oligomeric enzyme (Stewart et al. 1980) in which the N-terminal beta-grasp domain of one monomer forms an active site with the C-terminal catalytic domain of adjacent monomer. Although catalytic residues are conserved among GS proteins from prokaryotes to eukaryotes, they adopt distinct oligomeric structures. Prokaryotic GSI is the best characterized form of this enzyme family and several atomic structures of GSI have been determined (Almassy et al. 1986; Gill and Eisenberg 2001; Gill et al. 2002; Yamashita et al. 1989). In each case GSI forms a dodecamer consisting of two stacked hexameric rings. In contrast, the oligomeric structures of eukaryotic GSII are variable and controversial (reviewed in Betti et al. 2012). In early low-resolution electron microscopic and biochemical studies, it was believed that eukaryotic GS<sub>1</sub> is an octamer in which two tetrameric rings are stacked together to make one octamer of GS (Boksha et al. 2002; Llorca et al. 2006; Mcparland et al. 1976; Pushkin et al. 1985; Pushkin et al. 1981; Stewart et al. 1980; Tsuprun et al. 1987). The crystal structure of the cytosolic GS1a isoform from maize revealed a decameric structure formed by stacking of two pentameric rings held together by hydrophobic interactions (Unno et al. 2006). In

decameric homology models of soybean GS<sub>1</sub> in the present work, the proposed intersubunit distance between cys92 and cys159 is between 11-12 Å. The ability of GS<sub>1</sub>γ1 to assume a dodecameric structure, presumably forming two stacked hexameric rings, may position these cysteine pairs in closer proximity or in a conformation that increases their susceptibility to oxidation. The increased susceptibility of GS<sub>1</sub>γ to this reversible modification suggests that this could be a mechanism for selective thiol regulation of this isoform class in the microaerobic nitrogen fixing nodules.

#### **4.3. Potential role of thiol regulation in nodule GS function**

The reversible formation of disulfide bonds catalyzed by glutathione or thioredoxin is a common mechanism of enzyme regulation (Meyer et al. 2009) referred to as thiol-based signaling which was first characterized in plants (Wouters et al. 2011). Redox regulation has been shown in many mammalian proteins including Ca<sup>2+</sup>-ATPase, Ras-related GTPase, phosphorylase β kinase and the voltage-dependent anion channel protein (Aram et al. 2010; Heo and Campbell 2005; Matsunaga et al. 2003; Yuan et al. 1994). Plant proteins, such as fructose1,6 bisphosphatase, phosphoribulokinase, protein phosphatases ABI1 and ABI2 are also targets for regulation by redox state (Jacquot et al. 2002; Meinhard and Grill 2001). Thiol based redox proteins are found to be involved in abscisic acid, methyl jasmonate and ethylene signaling in guard cells of *Brassica napus* plant (Desikan et al. 2005; Zhu et al. 2014). The best example of thiol regulation of glutamine synthetase comes from the light-dependent regulation of

the plastidic GS<sub>2</sub> isoform. GS<sub>2</sub> is involved in the reassimilation of photorespiratory ammonium (Orea et al. 2002; Walls-grove et al. 1987). These two processes are proposed to be linked through regulatory proteins such as thioredoxins and ferredoxin/thioredoxin reductase (Choi et al. 1999). Two specific cysteine residues from *Canavalia lineata* GS<sub>2</sub> are found to be involved in oxidative inactivation that can be reversed by incubation with a reducing agent (Choi et al. 1999). Spinach GS<sub>2</sub> has been shown to interact with immobilized thioredoxin (Motohashi et al. 2001). Reducing agents such as reduced glutathione are shown to have a positive effect on GS<sub>2</sub> activity and thermal stability, suggesting thiol regulation of GS<sub>2</sub> (Betti et al. 2006). This mode of regulation is proposed to be mediated by light-dependent changes in the redox state of the chloroplast, which in turn regulates a number of enzymes through thioredoxin-based disulfide bond formation and reduction.

Redox changes and thiol-based redox signaling are known to play important roles in the legume-rhizobium symbiosis (Chang et al. 2009; del Giudice et al. 2011; Jamet et al. 2007; Marino et al. 2011; Marino et al. 2012; Meilhoc et al. 2011; Pauly et al. 2006; Puppo et al. 2013; Ramu et al. 2002; Rubio et al. 2004; Santos et al. 2001). Various transcription factors involved in symbiosis are induced in response to reactive oxygen species (ROS) production (Andrio et al. 2013). Also various metabolic proteins from *Medicago truncatula* nodule are found to be regulated by sulfenylation, a thiol modification suggesting the role of oxidation in functioning of symbiosis (Oger et al. 2012; Puppo et al.

2013). H<sub>2</sub>O<sub>2</sub> producing NADPH oxidase is highly expressed in the microaerobic nitrogen-fixing zone of *Medicago truncatula* nodules and is required for proper functioning of nodule (Marino et al. 2011). Thioredoxin which is one of the important antioxidant present in the nodules is known to have many protein targets in soybean nodule including nodulin-35, a subunit of uricase enzyme that synthesizes ureides, a transport form of fixed nitrogen in soybean nodules (Du et al. 2010). All these finding suggest that redox regulation of proteins play important role in proper functioning of nodules.

The production of ROS responsible for oxidative modification of proteins increases under abiotic and biotic stress conditions in plants (Moller et al. 2007). It has been shown that natural senescence as well as abiotic stress, leading to a decrease in nitrogen fixation rates in nodules, is correlated to a decrease in antioxidant defense resulting in redox imbalance due to increased production of ROS (Escuredo et al. 1996; Evans et al. 1999; Gogorcena et al. 1997; Gogorcena et al. 1995; Jebara et al. 2005; Marino et al. 2007; Matamoros et al. 1999a; Matamoros et al. 1999b; Naya et al. 2007). Environmental stresses such as salt stress, drought stress, and dark stress have been reported to down regulate the enzymes involved in carbon supply to the bacteroids (Galvez et al. 2005; Gogorcena et al. 1997; Lopez et al. 2008). It has been proposed that the reduced carbon fixation leads to increased oxidative stress and a decrease in nitrogen fixation in nodules (Galvez et al. 2005; Matamoros et al. 1999a). Pea nodules treated with paraquat show biological responses that are similar to those

observed under environmental stress, indicating a likely involvement of redox modifications in the perception of environmental stress in pea nodules (Marino et al. 2006). Findings that sucrose synthase, involved in sucrose metabolism in nodules, is downregulated transcriptionally as well as posttranslationally by the cellular redox state under limiting conditions of carbon supply point towards the involvement of redox regulation of carbon metabolism in nodules (Marino et al. 2008). In those stress conditions, a mode of action for ROS is modification of cysteine residues either by disulfide bond formation or sulfenylation which alters the activity of proteins (Wouters et al. 2011).

What metabolic functions might be regulated by reversible disulfide bond formation in GS<sub>1</sub>γ1? A possible clue comes from the work of Melo et al. (2011) who have investigated a separate oxidative reaction, tyrosine nitration in the regulation of GS1a in *Medicago truncatula* nodules. According to their proposed model, nitrogen radicals produced by the reaction of nitric oxide with superoxide radicals is responsible for the inhibition of GS1a through tyrosine nitration. In the absence of active GS, the metabolic flow of glutamate diverts from ammonia assimilation to glutamine towards synthesis of glutathione (Melo et al. 2011; Silva and Carvalho 2013). A similar role can be proposed for soybean GS<sub>1</sub>γ1 where its differential regulation by oxidation in response to environmental stress or changing redox status in the nodule may be involved in maintaining the antioxidant status in nodules by regulating glutathione production (Figure 4.3.1). Under normal physiological conditions, GS assimilates ammonia to produce

glutamine. Glutamine is further utilized by GOGST to produce glutamate, which is further utilized by GS for ammonia assimilation as well as for production of glutathione (GSH). As plants are stressed under biotic or abiotic conditions, ROS produced inactivates GS thereby diverting the flow of glutamate to favor GSH production. Increased GSH helps alleviate ROS as well as reactivate the oxidized GS to bring back the normal physiological conditions.

While this model represents a starting point, it still does not address why there is a need for separate isoforms of GS<sub>1</sub> with differential sensitivity to oxidation. Q-PCR and two dimensional electrophoresis analysis have shown that the GS<sub>1</sub>γ isoforms are not the predominant GS present in soybean nodules. This raises a question as to the significance of GS<sub>1</sub>γ isoforms in ammonia assimilation and overall nitrogen metabolism and physiology in nodules. Although it is known that GS<sub>1</sub>β and GS<sub>1</sub>γ isoforms are expressed in nodules, their expression pattern in different cell types within the nodule is not known. Examples from Arabidopsis show that GS<sub>1</sub> isoforms expressed in roots exhibit cell-specific expression (GLN1-1 in epidermal cells, GLN1-2 in pericycle cells, GLN1-3 in vascular cells and GLN1-4 is in pericycle cells) reflecting cell specific metabolic functions (Ishiyama et al. 2004b). Compartmentalization of GS<sub>1</sub> isoforms was also observed in *Oryza sativa* (Ishiyama et al. 2004a). The soybean nodule represents a complex organ with distinct cell and tissue architecture and function. Nitrogen fixation takes place within the microaerobic nitrogen fixation zone at the core of the nodule, but a number of other cell types with distinct metabolic

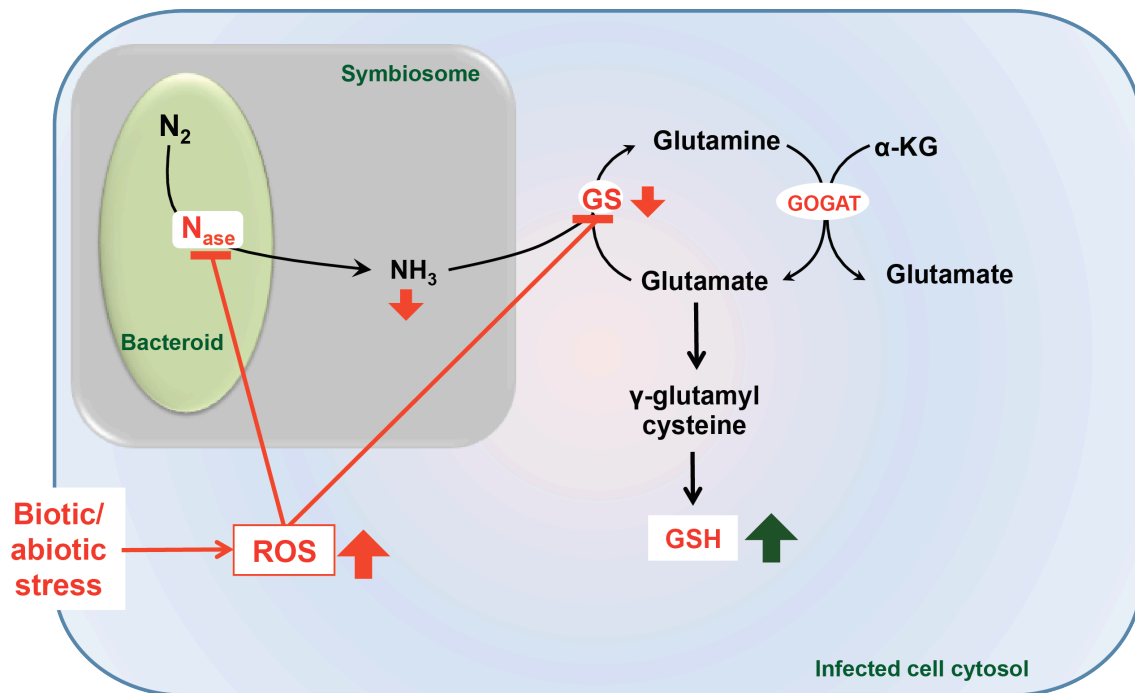


**Figure 4.3.1: Proposed model to integrate the oxidative regulation of GS within the context of root nodule metabolism.** Under normal physiological conditions (shown in black arrows),  $NH_3$  from bacteroids is assimilated by  $GS_1$  in the cytosol of infected cell. Glutamate required for  $GS$  function as well as production of glutathione ( $GSH$ ) is produced by  $GOGAT$ . Under stress conditions (shown in red arrows), reactive oxygen species ( $ROS$ ) produced in nodules inhibit  $GS$ . Inhibition of  $GS$  diverts glutamate flow towards synthesis of  $GSH$  which ultimately plays important role in alleviating the  $ROS$ .

functions that support nodule function also exist. Our working hypothesis for future investigation is that GS<sub>1</sub>γ isoforms may play a more selective role as redox sensors in the nodules, serving to regulate metabolic flow in response to environmental stress and changing redox/metabolic conditions.



## LIST OF REFERENCES

Almassy RJ, Janson CA, Hamlin R, Xuong NH, Eisenberg D (1986) Novel subunit subunit interactions in the structure of glutamine synthetase. *Nature* 323: 304-309

Andrio E, Marino D, Marmeys A, de Segonzac MD, Damiani I, Genre A, Huguet S, Frendo P, Puppo A, Pauly N (2013) Hydrogen peroxide-regulated genes in the *Medicago truncatula*-*Sinorhizobium meliloti* symbiosis. *The New Phytologist* 198: 179-189

Antunes F, Aguilar M, Pineda M, Sodek L (2008) Nitrogen stress and the expression of asparagine synthetase in roots and nodules of soybean (*Glycine max*). *Physiologia Plantarum* 133: 736-743

Aram L, Geula S, Arbel N, Shoshan-Barmatz V (2010) VDAC1 cysteine residues: topology and function in channel activity and apoptosis. *Biochemical Journal* 429: 613-614

Atkins CA (1987) Metabolism and translocation of fixed nitrogen in the nodulated legume. *Plant and Soil* 100: 157-169

Barnett MJ, Fisher RF (2006) Global gene expression in the rhizobial–legume symbiosis. *Symbiosis* 42: 1-24

Becker TW, Caboche M, Carrayol E, Hirel B (1992) Nucleotide sequence of a tobacco cDNA encoding plastidic glutamine synthetase and light inducibility,

organ specificity and diurnal rhythmicity in the expression of the corresponding genes of tobacco and tomato. *Plant Molecular Biology* 19: 367-379

Beijerinck MW (1901) On different forms of hereditary variation of microbes. *Proceedings of the Koninklijke Akademie Van Wetenschappen Te Amsterdam* 3: 352-365

Bennett MJ, Lightfoot DA, Cullimore JV (1989) cDNA sequence and differential expression of the gene encoding the glutamine synthetase  $\gamma$  polypeptide of *Phaseolus vulgaris* L. *Plant Molecular Biology* 12: 553-565

Bernard SM, Habash DZ (2009) The importance of cytosolic glutamine synthetase in nitrogen assimilation and recycling. *The New Phytologist* 182: 608-620

Bernard SM, Moller ALB, Dionisio G, Kichey T, Jahn TP, Dubois F, Baudo M, Lopes MS, Terce-Laforge T, Foyer CH, Parry MAJ, Forde BG, Araus JL, Hirel B, Schjoerring JK, Habash DZ (2008) Gene expression, cellular localisation and function of glutamine synthetase isozymes in wheat (*Triticum aestivum* L.). *Plant Molecular Biology* 67: 89-105

Betti M, Arondeguy T, Marquez AJ (2006) Molecular analysis of two mutants from *Lotus japonicus* deficient in plastidic glutamine synthetase: functional properties of purified GLN2 enzymes. *Planta* 224: 1068-1079

Betti M, Garcia-Calderon M, Perez-Delgado CM, Credali A, Estivill G, Galvan F, Vega JM, Marquez AJ (2012) Glutamine synthetase in legumes: recent advances in enzyme structure and functional genomics. *International Journal of Molecular Sciences* 13: 7994-8024

Blackwell RD, Murray AJS, Lea PJ (1987) Inhibition of Photosynthesis in Barley with Decreased Levels of Chloroplastic Glutamine-Synthetase Activity. *Journal of Experimental Botany* 38: 1799-1809

Boksha IS, Schonfeld HJ, Langen H, Muller F, Tereshkina EB, Burbaeva GS (2002) Glutamine synthetase isolated from human brain: Octameric structure and homology of partial primary structure with human liver glutamine synthetase. *Biochemistry-Moscow* 67: 1012-1020

Bradford MM (1976) A rapid and sensitive method for the quantitation of microgram quantities of protein utilizing the principle of protein-dye binding. *Analytical Biochemistry* 72: 248-254

Brewin NJ (1991) Development of the legume root nodule. *Annual Review of Cell Biology* 7: 191-226

Britto DT, Kronzucker HJ (2002)  $\text{NH}_4^+$  toxicity in higher plants: a critical review. *Journal of Plant Physiology* 159: 567-584

Britto DT, Siddiqi MY, Glass ADM, Kronzucker HJ (2001) Futile transmembrane  $\text{NH}_4^+$  cycling: A cellular hypothesis to explain ammonium toxicity in plants.

Proceedings of the National Academy of Sciences of the United States of America 98: 4255-4258

Broghammer A, Krusell L, Blaise M, Sauer J, Sullivan JT, Maolanon N, Vinther M, Lorentzen A, Madsen EB, Jensen KJ, Roepstorff P, Thirup S, Ronson CW, Thygesen MB, Stougaard J (2012) Legume receptors perceive the rhizobial lipochitin oligosaccharide signal molecules by direct binding. Proceedings of the National Academy of Sciences of the United States of America 109: 13859-13864

Brugiere N, Dubois F, Limami AM, Lelandais M, Roux Y, Sangwan RS, Hirel B (1999) Glutamine synthetase in the phloem plays a major role in controlling proline production. Plant Cell 11: 1995-2011

Buist G, Steen A, Kok J, Kuipers OP (2008) LysM, a widely distributed protein motif for binding to (peptido)glycans. Molecular microbiology 68: 838-847

Canovas FM, Avila C, Canton FR, Canas RA, de la Torre F (2007) Ammonium assimilation and amino acid metabolism in conifers. Journal of Experimental Botany 58: 2307-2318

Cardenas L, Thomas-Oates JE, Nava N, Lopez-Lara IM, Hepler PK, Quinto C (2003) The role of nod factor substituents in actin cytoskeleton rearrangements in *Phaseolus vulgaris*. Molecular Plant-Microbe Interactions 16: 326-334

Catalano CM, Lane WS, Sherrier DJ (2004) Biochemical characterization of symbiosome membrane proteins from *Medicago truncatula* root nodules.

Electrophoresis 25: 519-531

Chang C, Damiani I, Puppo A, Frendo P (2009) Redox changes during the legume-rhizobium symbiosis. Molecular Plant 2: 370-377

Choi YA, Kim SG, Kwon YM (1999) The plastidic glutamine synthetase activity is directly modulated by means of redox change at two unique cysteine residues.

Plant Science 149: 175-182

Dam J, Schuck P (2004) Calculating sedimentation coefficient distributions by direct modeling of sedimentation velocity concentration profiles. Methods in

Enzymology 384: 185-212

Day DA, Poole PS, Tyerman SD, Rosendahl L (2001) Ammonia and amino acid transport across symbiotic membranes in nitrogen-fixing legume nodules.

Cellular and Molecular Life Sciences 58: 61-71

Dean RM, Rivers RL, Zeidel ML, Roberts DM (1999) purification and functional reconstitution of soybean nodulin 26. An aquaporin with water and glycerol

transport properties. Biochemistry 38: 347-353

del Giudice J, Cam Y, Damiani I, Fung-Chat F, Meilhoc E, Bruand C, Brouquisse R, Puppo A, Boscari A (2011) Nitric oxide is required for an optimal

establishment of the *Medicago truncatula*-*Sinorhizobium meliloti* symbiosis. The New Phytologist 191: 405-417

Denarie J, Debelle F, Prome JC (1996) Rhizobium lipo-chitooligosaccharide nodulation factors: signaling molecules mediating recognition and morphogenesis. Annual Review of Biochemistry 65: 503-535

Desikan R, Hancock JT, Bright J, Harrison J, Weir L, Hooley R, Neill SJ (2005) A role for ETR1 in hydrogen peroxide signaling in stomatal guard cells. Plant Physiology 137: 831-834

Dixon R, Kahn D (2004) Genetic regulation of biological nitrogen fixation. Nature Reviews Microbiology 2: 621-631

Downie JA (1998) Functions of rhizobial nodulation genes. In: Spaink HP, Kondorosi A, Hooykaas PJJ (eds) The *Rhizobiaceae*: Molecular biology of model plant-associated bacteria, pp 387-402

Downie JA, Walker SA (1999) Plant responses to nodulation factors. Current Opinion in Plant Biology 2: 483-489

Du H, Kim S, Nam KH, Lee MS, Son O, Lee SH, Cheon CI (2010) Identification of uricase as a potential target of plant thioredoxin: Implication in the regulation of nodule development. Biochemical and Biophysical Research Communications 397: 22-26

Eady RR, Postgate JR (1974) Nitrogenase. Nature 249: 805-810

Edwards JW, Coruzzi GM (1989) Photorespiration and light act in concert to regulate the expression of the nuclear gene for chloroplast glutamine synthetase.

Plant Cell 1: 241-248

Edwards JW, Walker EL, Coruzzi GM (1990) Cell-specific expression in transgenic plants reveals nonoverlapping roles for chloroplast and cytosolic glutamine-synthetase. Proceedings of the National Academy of Sciences of the United States of America 87: 3459-3463

Ehrhardt DW, Wais R, Long SR (1996) Calcium spiking in plant root hairs responding to Rhizobium nodulation signals. Cell 85: 673-681

Eisenberg D, Gill HS, Pfluegl GMU, Rotstein SH (2000) Structure-function relationships of glutamine synthetases. Biochimica Et Biophysica Acta-Protein Structure and Molecular Enzymology 1477: 122-145

Elmlinger MW, Bolle C, Batschauer A, Oelmuller R, Mohr H (1994) Coaction of blue light and light absorbed by phytochrome in control of glutamine synthetase gene expression in scots pine (*Pinus Sylvestris* L) seedlings. Planta 192: 189-194

Emons AM, Mulder B (2000) Nodulation factors trigger an increase of fine bundles of subapical actin filaments in Vicia root hairs: Implications for root hair curling around bacteria. Biology of Plant-Microbe Interactions, Vol 2: 272-276



Engelsberger WR, Schulze WX (2012) Nitrate and ammonium lead to distinct global dynamic phosphorylation patterns when resupplied to nitrogen-starved *Arabidopsis* seedlings. *The Plant Journal* 69: 978-995

Escuredo PR, Minchin FR, Gogorcena Y, IturbeOrmaetxe I, Klucas RV, Becana M (1996) Involvement of activated oxygen in nitrate-induced senescence of pea root modules. *Plant Physiology* 110: 1187-1195

Eskew DL, Jiang Q, Caetano-Anolles G, Gresshoff PM (1993) Kinetics of Nodule Development in Glycine soja. *Plant Physiology* 103: 1139-1145

Esseling JJ, Lhuissier FGP, Emons AMC (2003) Nod factor-induced root hair curling: Continuous polar growth towards the point of nod factor application. *Plant Physiology* 132: 1982-1988

Evans PJ, Gallesi D, Mathieu C, Hernandez NJ, de Felipe N, Halliwell B, Puppo A (1999) Oxidative stress occurs during soybean nodule senescence. *Planta* 208: 73-79

Fan J, Fariss RN, G. PA, Slingsby C, Sandilands A, Quinlan R, Wistow G, Chepelinsky AB (2005) Specific interaction between lens MIP/Aquaporin-0 and two members of the gamma-crystallin family. *Molecular Vision* 11: 76-87

Faucher C, Camut S, Denarie J, Truchet G (1989) The *nodH* and *nodQ* host range genes of *Rhizobium meliloti* behave as avirulence genes in *R.*

*leguminosarum* bv *viciae* and determine changes in the production of plant-specific extracellular signals. *Molecular Plant-Microbe Interactions* 2: 291-300

Finnemann J, Schjoerring JK (2000) Post-translational regulation of cytosolic glutamine synthetase by reversible phosphorylation and 14-3-3 protein interaction. *The Plant Journal* 24: 171-181

Forde BG, Day HM, Turton JF, Wen-jun S, Cullimore JV, Oliver JE (1989) Two glutamine synthetase genes from *Phaseolus vulgaris* L. display contrasting developmental and spatial patterns of expression in transgenic *Lotus corniculatus* plants. *Plant Cell* 1: 391-401

Forde BG, Lea PJ (2007) Glutamate in plants: metabolism, regulation, and signalling. *Journal of Experimental Botany* 58: 2339-2358

Forde G, Woodall J (1995) Glutamine synthetase in higher plants. *Amino Acids and their Derivatives in Higher Plants*. Cambridge University Press, Cambridge, pp 1-18

Fortin MG, Morrison NA, Verma DP (1987) Nodulin-26, a peribacteroid membrane nodulin is expressed independently of the development of the peribacteroid compartment. *Nucleic Acids Research* 15: 813-824

Fortin MG, Zelechowska M, Verma DP (1985) Specific targeting of membrane nodulins to the bacteroid-enclosing compartment in soybean nodules. *The EMBO Journal* 4: 3041-3046

Franche C, Lindstrom K, Elmerich C (2009) Nitrogen-fixing bacteria associated with leguminous and non-leguminous plants. *Plant and Soil* 321: 35-59

Fu D, Libson A, Miercke LJW, Weitzman C, Nollert P, Krucinski J, Stroud RM (2000) Structure of a glycerol-conducting channel and the basis for its selectivity. *Science* 290: 481-486

Gage DJ (2004) Infection and invasion of roots by symbiotic, nitrogen-fixing rhizobia during nodulation of temperate legumes. *Microbiology and Molecular Biology Reviews* 68: 280-300

Galvez L, Gonzalez EM, Arrese-Igor C (2005) Evidence for carbon flux shortage and strong carbon/nitrogen interactions in pea nodules at early stages of water stress. *Journal of Experimental Botany* 56: 2551-2561

Gawronski JD, Benson DR (2004) Microtiter assay for glutamine synthetase biosynthetic activity using inorganic phosphate detection. *Analytical Biochemistry* 327: 114-118

Gebhardt C, Oliver JE, Forde BG, Saarelainen R, Mifflin BJ (1986) Primary structure and differential expression of glutamine synthetase genes in nodules, roots and leaves of *Phaseolus vulgaris*. *The EMBO Journal* 5: 1429-1435

Geurts R, Fedorova E, Bisseling T (2005) Nod factor signaling genes and their function in the early stages of *Rhizobium* infection. *Current Opinion in Plant Biology* 8: 346-352

Gill HS, Eisenberg D (2001) The crystal structure of phosphinothricin in the active site of glutamine synthetase illuminates the mechanism of enzymatic inhibition.

Biochemistry 40: 1903-1912

Gill HS, Pfluegl GMU, Eisenberg D (2002) Multicopy crystallographic refinement of a relaxed glutamine synthetase from *Mycobacterium tuberculosis* highlights flexible loops in the enzymatic mechanism and its regulation. Biochemistry 41:

9863-9872

Girsch SJ, Perecchia C (1991) Calmodulin interacts with a C-terminus peptide from the lens membrane protein MIP26. Current Eye Research 10: 839-849

Gogorcena Y, Gordon AJ, Escuredo PR, Minchin FR, Witty JF, Moran JF, Becana M (1997) N<sub>2</sub> fixation, carbon metabolism, and oxidative damage in nodules of dark-stressed common bean plants. Plant Physiology 113: 1193-1201

Gogorcena Y, Iturbe-Ormaetxe I, Escuredo PR, Becana M (1995) Antioxidant defenses against activated oxygen in pea nodules subjected to water stress.

Plant Physiology 108: 753-759

Goodall AJ, Kumar P, Tobin AK (2013) Identification and expression analyses of cytosolic glutamine synthetase genes in barley (*Hordeum vulgare* L.). Plant and

Cell Physiology 54: 492-505

Goodman HJK, Woods DR (1993) Cloning and nucleotide sequence of the *Butyrivibrio fibrisolvens* gene encoding a type III glutamine synthetase. Journal of General Microbiology 139: 1487-1493

Graham PH, Vance CP (2000) Nitrogen fixation in perspective: an overview of research and extension needs. Field Crops Research 65: 93-106

Graham PH, Vance CP (2003) Legumes: Importance and constraints to greater use. Plant Physiology 131: 872-877

Gruber N, Galloway JN (2008) An Earth-system perspective of the global nitrogen cycle. Nature 451: 293-296

Guenther JF, Chanmanivone N, Galetovic MP, Wallace IS, Cobb JA, Roberts DM (2003) Phosphorylation of soybean nodulin 26 on serine 262 enhances water permeability and is regulated developmentally and by osmotic signals. Plant Cell 15: 981-991

Gutierrez RA (2012) Systems biology for enhanced plant nitrogen nutrition. Science 336: 1673-1675

Harper JF, Harmon A (2005) Plants, symbiosis and parasites: A calcium signalling connection. Nature Reviews Molecular Cell Biology 6: 555-566

Harries WEC, Akhavan D, Miercke LJW, Khademi S, Stroud RM (2004) The channel architecture of aquaporin 0 at a 2.2-Å resolution. Proceedings of the National Academy of Sciences United States of America 101: 14045-14050

He YX, Gui L, Liu YZ, Du Y, Zhou YY, Li P, Zhou CZ (2009) Crystal structure of *Saccharomyces cerevisiae* glutamine synthetase Gln1 suggests a nanotube-like supramolecular assembly. *Proteins-Structure Function and Bioinformatics* 76: 249-254

Heo J, Campbell SL (2005) Mechanism of redox-mediated guanine nucleotide exchange on redox-active rho GTPases. *Journal of Biological Chemistry* 280: 31003-31010

Herridge DF, Peoples MB, Boddey RM (2008) Global inputs of biological nitrogen fixation in agricultural systems. *Plant and Soil* 311: 1-18

Hirel B, Gadal P (1980) Glutamine Synthetase in Rice: A comparative study of the enzymes from roots and leaves. *Plant Physiology* 66: 619-623

Horvath B, Kondorosi E, John M, Schmidt J, Torok I, Gyorgypal Z, Barabas I, Wieneke U, Schell J, Kondorosi A (1986) Organization, structure and symbiotic function of *Rhizobium meliloti* nodulation genes determining host specificity for alfalfa. *Cell* 46: 335-343

Hu YL, Ribbe MW (2011) Biosynthesis of the metalloclusters of molybdenum nitrogenase. *Microbiology and Molecular Biology Reviews* 75: 664-677

Hwang JH, Ellingson SR, Roberts DM (2010) Ammonia permeability of the soybean nodulin 26 channel. *FEBS Letters* 584: 4339-4343

Igarashi RY, Seefeldt LC (2003) Nitrogen fixation: The mechanism of the Mo-dependent nitrogenase. *Critical Reviews in Biochemistry and Molecular Biology* 38: 351-384

Ireland RJ, Lea PJ (1999) The enzymes of glutamine, glutamate, asparagine, and aspartate metabolism. *Plant Amino Acids, Biochemistry and Biotechnology*. Marcel Dekker Inc., New York, pp 49-109

Ishiyama K, Inoue E, Tabuchi M, Yamaya T, Takahashi H (2004a) Biochemical background and compartmentalized functions of cytosolic glutamine synthetase for active ammonium assimilation in rice roots. *Plant and Cell Physiology* 45: 1640-1647

Ishiyama K, Inoue E, Watanabe-Takahashi A, Obara M, Yamaya T, Takahashi H (2004b) Kinetic properties and ammonium-dependent regulation of cytosolic isoenzymes of glutamine synthetase in *Arabidopsis*. *The Journal of Biological Chemistry* 279: 16598-16605

Ishiyama K, Inoue E, Watanabe-Takahashi A, Obara M, Yamaya T, Takahashi H (2004c) Nitrogen-dependent regulation of cytosolic glutamine synthetase in *Arabidopsis* roots. *Plant and Cell Physiology* 45: S98-S98

Jacquot JP, Rouhier N, Gelhaye E (2002) Redox control by dithiol-disulfide exchange in plants - I. The chloroplastic systems. *Annals of the New York Academy of Sciences* 973: 508-519

Jamet A, Mandon K, Puppo A, Herouart D (2007) H<sub>2</sub>O<sub>2</sub> is required for optimal establishment of the *Medicago sativa*/*Sinorhizobium meliloti* symbiosis. Journal of Bacteriology 189: 8741-8745

Jebara S, Jebara M, Limam F, Aouani ME (2005) Changes in ascorbate peroxidase, catalase, guaiacol peroxidase and superoxide dismutase activities in common bean (*Phaseolus vulgaris*) nodules under salt stress. Journal of Plant Physiology 162: 929-936

Kereszt A, Mergaert P, Kondorosi E (2011) Bacteroid development in legume nodules: Evolution of mutual benefit or of sacrificial victims? Molecular Plant-Microbe Interactions 24: 1300-1309

Kerppola TK (2008) Bimolecular fluorescence complementation: Visualization of molecular interactions in living cells. Methods in Cell Biology 85: 431-470

Kiang CH (2001) Single-particle study of protein assembly. Physical Review E 64

Kondorosi E, Banfalvi Z, Kondorosi A (1984) Physical and genetic analysis of a symbiotic region of *Rhizobium meliloti*: Identification of nodulation genes. Molecular and General Genetics 193: 445-452

Kosuta S, Hazledine S, Sun J, Miwa H, Morris RJ, Downie JA, Oldroyd GE (2008) Differential and chaotic calcium signatures in the symbiosis signaling pathway of legumes. Proceedings of the National Academy of Sciences of the United States of America 105: 9823-9828



Kozaki A, Takeba G (1996) Photorespiration protects C3 plants from photooxidation. *Nature* 384: 557-560

Krajewski WW, Collins R, Holmberg-Schiavone L, Jones TA, Karlberg T, Mowbray SL (2008) Crystal structures of mammalian glutamine synthetases illustrate substrate-induced conformational changes and provide opportunities for drug and herbicide design. *Journal of Molecular Biology* 375: 217-228

Laemmli UK (1970) Cleavage of structural proteins during the assembly of the head of bacteriophage T4. *Nature* 227: 680-685

Lam HM, Coschigano KT, Oliveira IC, Melo-Oliveira R, Coruzzi GM (1996) The molecular genetics of nitrogen assimilation into amino acids in higher plants. *Annual Review of Plant Physiology and Plant Molecular Biology* 47: 569-593

Lara M, Cullimore JV, Lea PJ, Miflin BJ, Johnston AWB, Lamb JW (1983) Appearance of a novel form of plant glutamine synthetase during nodule development in *Phaseolus vulgaris* L. *Planta* 157: 254-258

Legocki RP, Verma DPS (1980) Identification of nodule-specific host proteins (nodulins) involved in the development of rhizobium-legume symbiosis. *Cell* 20: 153-163

Levy J, Bres C, Geurts R, Chalhoub B, Kulikova O, Duc G, Journet EP, Ane JM, Lauber E, Bisseling T, Denarie J, Rosenberg C, Debelle F (2004) A putative  $\text{Ca}^{2+}$

and calmodulin-dependent protein kinase required for bacterial and fungal symbioses. *Science* 303: 1361-1364

Li J-F, Nebenfuhr A (2007) Organelle targeting of myosin XI is mediated by two globular tail subdomains with separate cargo binding sites. *The Journal of Biological Chemistry* 282: 20593-20602

Li MG, Villemur R, Hussey PJ, Silflow CD, Gantt JS, Snustad DP (1993) Differential expression of 6 glutamine synthetase genes in *Zea Mays*. *Plant Molecular Biology* 23: 401-407

Li RJ, Hua W, Lu YT (2006) *Arabidopsis* cytosolic glutamine synthetase AtGLN1;1 is a potential substrate of AtCRK3 involved in leaf senescence. *Biochemical and Biophysical Research Communications* 342: 119-126

Liaw SH, Eisenberg D (1994) Structural model for the reaction mechanism of glutamine synthetase, based on 5 crystal-structures of enzyme-substrate complexes. *Biochemistry* 33: 675-681

Libault M, Thibivilliers S, Bilgin DD, Radwan O, Benitez M, Clough SJ, Stacey G (2008) Identification of four soybean reference genes for gene expression normalization. *Plant Genome* 1: 44-54

Lima L, Seabra A, Melo P, Cullimore J, Carvalho H (2006a) Phosphorylation and subsequent interaction with 14-3-3 proteins regulate plastid glutamine synthetase in *Medicago truncatula*. *Planta* 223: 558-567

Lima L, Seabra A, Melo P, Cullimore J, Carvalho H (2006b) Post-translational regulation of cytosolic glutamine synthetase of *Medicago truncatula*. Journal of Experimental Botany 57: 2751-2761

Liu B-F, Liang JJ (2008) Confocal fluorescence microscopy study of interaction between lens MIP26/AQP0 and crystallins in living cells. Journal of Cellular Biochemistry 104: 51-58

Llorca O, Betti M, Gonzalez JM, Valencia A, Marquez AJ, Valpuesta JM (2006) The three-dimensional structure of an eukaryotic glutamine synthetase: Functional implications of its oligomeric structure. Journal of Structural Biology 156: 469-479

Long SR (1989) Rhizobium-legume nodulation: Life together in the underground. Cell 56: 203-214

Lopez M, Herrera-Cervera JA, Iribarne C, Tejera NA, Lluch C (2008) Growth and nitrogen fixation in *Lotus japonicus* and *Medicago truncatula* under NaCl stress: nodule carbon metabolism. Journal of Plant Physiology 165: 641-650

Marino D, Andrio E, Danchin EG, Oger E, Gucciardo S, Lambert A, Puppo A, Pauly N (2011) A *Medicago truncatula* NADPH oxidase is involved in symbiotic nodule functioning. The New Phytologist 189: 580-592

Marino D, Dunand C, Puppo A, Pauly N (2012) A burst of plant NADPH oxidases. Trends in Plant Science 17: 9-15

Marino D, Frendo P, Ladrera R, Zabalza A, Puppo A, Arrese-Igor C, Gonzalez EM (2007) Nitrogen fixation control under drought stress. Localized or systemic? *Plant Physiology* 143: 1968-1974

Marino D, Gonzalez EM, Arrese-Igor C (2006) Drought effects on carbon and nitrogen metabolism of pea nodules can be mimicked by paraquat: Evidence for the occurrence of two regulation pathways under oxidative stresses. *Journal of Experimental Botany* 57: 665-673

Marino D, Hohnjec N, Kuster H, Moran JF, Gonzalez EM, Arrese-Igor C (2008) Evidence for transcriptional and post-translational regulation of sucrose synthase in pea nodules by the cellular redox state. *Molecular Plant-Microbe Interaction* 21: 622-630

Marquez AJ, Betti M, Garcia-Calderon M, Pal'ove-Balang P, Diaz P, Monza J (2005) Nitrate assimilation in *Lotus japonicus*. *Journal of Experimental Botany* 56: 1741-1749

Martin A, Lee J, Kichey T, Gerentes D, Zivy M, Tatout C, Dubois F, Balliau T, Valot B, Davanture M, Terce-Laforgue T, Quillere I, Coque M, Gallais A, Gonzalez-Moro MB, Bethencourt L, Habash DZ, Lea PJ, Charcosset A, Perez P, Murigneux A, Sakakibara H, Edwards KJ, Hirel B (2006) Two cytosolic glutamine synthetase isoforms of maize are specifically involved in the control of grain production. *The Plant Cell* 18: 3252-3274

Martinez E, Romero D, Palacios R (1990) The *Rhizobium* genome. Critical Reviews in Plant Sciences 9: 59-93

Masclaux C, Valadier MH, Brugiére N, Morot-Gaudry JF, Hirel B (2000) Characterization of the sink/source transition in tobacco ( *Nicotiana tabacum* L.) shoots in relation to nitrogen management and leaf senescence. Planta 211: 510-518

Masclaux-Daubresse C, Reisdorf-Cren M, Pageau K, Lelandais M, Grandjean O, Kronenberger J, Valadier MH, Feraud M, Jougllet T, Suzuki A (2006) Glutamine synthetase-glutamate synthase pathway and glutamate dehydrogenase play distinct roles in the sink-source nitrogen cycle in tobacco. Plant Physiology 140: 444-456

Matamoros MA, Baird LM, Escuredo PR, Dalton DA, Minchin FR, Iturbe-Ormaetxe I, Rubio MC, Moran JF, Gordon AJ, Becana M (1999a) Stress-induced legume root nodule senescence. Physiological, biochemical, and structural alterations. Plant Physiology 121: 97-112

Matamoros MA, Moran JF, Iturbe-Ormaetxe I, Rubio MC, Becana M (1999b) Glutathione and homoglutathione synthesis in legume root nodules. Plant Physiology 121: 879-888

Matsunaga S, Inashima S, Yamada T, Watanabe H, Hazama T, Wada M (2003) Oxidation of sarcoplasmic reticulum  $\text{Ca}^{2+}$ -ATPase induced by high-intensity exercise. Pflugers Archiv-European Journal of Physiology 446: 394-399

McNally SF, Hirel B, Gadal P, Mann AF, Stewart GR (1983) Glutamine synthetases of higher plants : Evidence for a specific isoform content related to their possible physiological role and their compartmentation within the leaf. *Plant Physiology* 72: 22-25

Mcparland RH, Guevara JG, Becker RR, Evans HJ (1976) Purification and properties of glutamine synthetase from cytosol of soybean root nodules. *Biochemical Journal* 153: 597-606

Meilhoc E, Boscari A, Bruand C, Puppo A, Brouquisse R (2011) Nitric oxide in legume–rhizobium symbiosis. *Plant Science* 181: 573-581

Meinhard M, Grill E (2001) Hydrogen peroxide is a regulator of ABI1, a protein phosphatase 2C from *Arabidopsis*. *Febs Letters* 508: 443-446

Melo PM, Lima LM, Santos IM, Carvalho HG, Cullimore JV (2003) Expression of the plastid-located glutamine synthetase of *Medicago truncatula*. Accumulation of the precursor in root nodules reveals an in vivo control at the level of protein import into plastids. *Plant Physiology* 132: 390-399

Melo PM, Silva LS, Ribeiro I, Seabra AR, Carvalho HG (2011) Glutamine synthetase is a molecular target of nitric oxide in root nodules of *Medicago truncatula* and is regulated by tyrosine nitration. *Plant Physiology* 157: 1505-1517

Melo-Oliveira R, Oliveira IC, Coruzzi GM (1996) *Arabidopsis* mutant analysis and gene regulation define a nonredundant role for glutamate dehydrogenase in

nitrogen assimilation. Proceedings of the National Academy of Sciences of the United States of America 93: 4718-4723

Meyer Y, Buchanan BB, Vignols F, Reichheld JP (2009) Thioredoxins and glutaredoxins: Unifying elements in redox biology. Annual Review of Genetics 43: 335-367

Miao GH, Hirel B, Marsolier MC, Ridge RW, Verma DPS (1991) Ammonia-regulated expression of a soybean gene encoding cytosolic glutamine synthetase in transgenic *Lotus corniculatus*. Plant Cell 3: 11-22

Miflin BJ, Habash DZ (2002) The role of glutamine synthetase and glutamate dehydrogenase in nitrogen assimilation and possibilities for improvement in the nitrogen utilization of crops. Journal of Experimental Botany 53: 979-987

Miflin BJ, Lea PJ (1980) Ammonia assimilation. In: Miflin BJ (ed) The Biochemistry of Plants. Academic Press, New York, pp 169-202

Migge A, Carrayol E, Hirel B, Lohmann M, Meya G, Becker TW (1998) Regulation of the subunit composition of plastidic glutamine synthetase of the wild-type and of the phytochrome-deficient aurea mutant of tomato by blue/UV-A- or by UV-B-light. Plant Molecular Biology 37: 689-700

Miller JB, Oldroyd GED (2012) The role of diffusible signals in the establishment of rhizobial and mycorrhizal symbioses. Signaling and Communication in Plant Symbiosis: 1-30

Minet R, Villie F, Marcollet M, Meynial-Denis D, Cynober L (1997) Measurement of glutamine synthetase activity in rat muscle by a colorimetric assay. *Clinica Chimica Acta* 268: 121-132

Mitra RM, Gleason CA, Edwards A, Hadfield J, Downie JA, Oldroyd GED, Long SR (2004) A  $\text{Ca}^{2+}$ /calmodulin-dependent protein kinase required for symbiotic nodule development: Gene identification by transcript-based cloning. *Proceedings of the National Academy of Sciences of the United States of America* 101: 4701-4705

Moller IM, Jensen PE, Hansson A (2007) Oxidative modifications to cellular components in plants. *Annual Review of Plant Biology* 58: 459-481

Morey KJ, Ortega JL, Sengupta-Gopalan C (2002) Cytosolic glutamine synthetase in soybean is encoded by a multigene family, and the members are regulated in an organ-specific and developmental manner. *Plant Physiology* 128: 182-193

Motohashi K, Kondoh A, Stumpp MT, Hisabori T (2001) Comprehensive survey of proteins targeted by chloroplast thioredoxin. *Proceedings of the National Academy of Sciences United States of America* 98: 11224-11229

Mouritzen P, Rosendahl L (1997) Identification of a transport mechanism for  $\text{NH}_4^+$  in symbiosome membrane of pea root nodules. *Plant Physiology* 115: 519-526



Mulder L, Lefebvre B, Cullimore J, Imberty A (2006) LysM domains of *Medicago truncatula* NFP protein involved in Nod factor perception. Glycosylation state, molecular modeling and docking of chitooligosaccharides and Nod factors.

Glycobiology 16: 801-809

Naya L, Ladrera R, Ramos J, Gonzalez EM, Arrese-Igor C, Minchin FR, Becana M (2007) The response of carbon metabolism and antioxidant defenses of alfalfa nodules to drought stress and to the subsequent recovery of plants. Plant

Physiology 144: 1104-1114

Niemietz CM, Tyerman SD (2000) Channel-mediated permeation of ammonia gas through the peribacteroid membrane of soybean nodules. FEBS Letters 465:

110-114

Noda Y, Horikawa S, Furukawa T, Hirai K, Katayama Y, Asai T, Kuwahara M, Katagiri K, Kinashi T, Hattori M, Minato N, Sasaki S (2004a) Aquaporin-2 trafficking is regulated by PDZ-domain containing protein SPA-1. FEBS Letters

568: 139-145

Noda Y, Horikawa S, Katayama Y, Sasaki S (2004b) Water channel aquaporin-2 directly binds to actin. Biochemical and Biophysical Research Communications

322: 740-745

Noda Y, Sasaki S (2005) Trafficking mechanism of water channel aquaporin-2.

Biology of the Cell 97: 885-892

Nogueira ED, Olivares FL, Japiassu JC, Vilar C, Vinagre F, Baldani JI, Hemerly AS (2005) Characterization of glutamine synthetase genes in sugarcane genotypes with different rates of biological nitrogen fixation. *Plant Science* 169: 819-832

Obermeyer G, Tyerman SD (2005)  $\text{NH}_4^+$  currents across the peribacteroid membrane of soybean. Macroscopic and microscopic properties, inhibition by  $\text{Mg}^{2+}$ , and temperature dependence indicate a subpico Siemens channel finely regulated by divalent cations. *Plant Physiology* 139: 1015-1029

Obrdlik P, El-Bakkoury M, Hamacher T, Cappellaro C, Vilarino C, Fleischer C, Ellerbrok H, Kamuzinzi R, Ledent V, Blaudez D, Sanders D, Revuelta JL, Boles E, Andre B, Frommer WB (2004)  $\text{K}^+$  channel interactions detected by a genetic system optimized for systematic studies of membrane protein interactions. *Proceedings of the National Academy of Sciences of the United States of America* 101: 12242-12247

Oger E, Marino D, Guigonis JM, Pauly N, Puppo A (2012) Sulfenylated proteins in the *Medicago truncatula*-*Sinorhizobium meliloti* symbiosis. *Journal of Proteomics* 75: 4102-4113

Ohyama T, Minagawa R, Ishikawa S, Yamamoto M, Hung NVP, Ohtake N, Sueyoshi K, Sato T, Nagumo Y, Takahashi Y (2013) Soybean seed production and nitrogen nutrition

Oldroyd GE (2013) Speak, friend, and enter: Signalling systems that promote beneficial symbiotic associations in plants. *Nature Reviews Microbiology* 11: 252-263

Oldroyd GE, Downie JA (2008) Coordinating nodule morphogenesis with rhizobial infection in legumes. *Annual Review of Plant Biology* 59: 519-546

Oldroyd GE, Murray JD, Poole PS, Downie JA (2011) The rules of engagement in the legume-rhizobial symbiosis. *Annual Review of Genetics* 45: 119-144

Oldroyd GED, Downie JA (2004) Calcium, kinases and nodulation signalling in legumes. *Nature Reviews Molecular Cell Biology* 5: 566-576

Orea A, Pajuelo P, Pajuelo E, Quidiello C, Romero JM, Marquez AJ (2002) Isolation of photorespiratory mutants from *Lotus japonicus* deficient in glutamine synthetase. *Physiologia Plantarum* 115: 352-361

Ott T, van Dongen JT, Gunther C, Krusell L, Desbrosses G, Vigeolas H, Bock V, Czechowski T, Geigenberger P, Udvardi MK (2005) Symbiotic leghemoglobins are crucial for nitrogen fixation in legume root nodules but not for general plant growth and development. *Current Biology* 15: 531-535

Ou yang L-J, Whelan J, Weaver CD, Roberts DM, Day DA (1991) Protein phosphorylation stimulates the rate of malate uptake across the peribacteroid membrane of soybean nodules. *FEBS Letters* 293: 188-190

Ou Yang LJ, Udvardi MK, Day DA (1990) Specificity and regulation of the dicarboxylate carrier on the peribacteroid membrane of soybean nodules. *Planta* 182: 437-444

Pauly N, Pucciariello C, Mandon K, Innocenti G, Jamet A, Baudouin E, Herouart D, Frendo P, Puppo A (2006) Reactive oxygen and nitrogen species and glutathione: Key players in the legume-*Rhizobium* symbiosis. *Journal of Experimental Botany* 57: 1769-1776

Perret X, Staehelin C, Broughton WJ (2000) Molecular basis of symbiotic promiscuity. *Microbiology and Molecular Biology Reviews* 64: 180-201

Pfaffl MW (2001) A new mathematical model for relative quantification in real-time RT-PCR. *Nucleic Acids Research* 29

Pierre O, Engler G, Hopkins J, Brau F, Boncompagni E, Herouart D (2013) Peribacteroid space acidification: A marker of mature bacteroid functioning in *Medicago truncatula* nodules. *Plant Cell and Environment* 36: 2059-2070

Postgate J (1998) Nitrogen Fixation. Nitrogen Fixation. Cambridge University Press, UK

Postgate JR (1982) Biological nitrogen fixation: Fundamentals. *Philosophical Transactions of the Royal Society of London Series B-Biological Sciences* 296: 375-385

- Puppo A, Pauly N, Boscari A, Mandon K, Brouquisse R (2013) Hydrogen peroxide and nitric oxide: Key regulators of the legume-*Rhizobium* and mycorrhizal symbioses. *Antioxidants & Redox Signaling* 18: 2202-2219
- Pushkin AV, Antoniuk LP, Solovieva NA, Shubin VV, Evstigneeva ZG, Kretovich WL, Cherednikova TV, Tsuprun VL, Zograf ON, Kiselev NA (1985) Glutamine synthetases of pea leaf and seed cytosol. Structure and properties. *Biochimica Et Biophysica Acta* 828: 336-350
- Pushkin AV, Tsuprun VL, Dzhokharidze TZ, Evstigneeva ZG, Kretovich WL (1981) Glutamine synthetase from the pumpkin leaf cytosol. *Biochimica Et Biophysica Acta* 662: 160-162
- Radutoiu S, Madsen LH, Madsen EB, Jurkiewicz A, Fukai E, Quistgaard EM, Albrechtsen AS, James EK, Thirup S, Stougaard J (2007) LysM domains mediate lipochitin-oligosaccharide recognition and *Nfr* genes extend the symbiotic host range. *The EMBO Journal* 26: 3923-3935
- Ramu SK, Peng HM, Cook DR (2002) Nod factor induction of reactive oxygen species production is correlated with expression of the early nodulin gene *rip1* in *Medicago truncatula*. *Molecular Plant-Microbe Interactions* 15: 522-528
- Rathbun EA, Naldrett MJ, Brewin NJ (2002) Identification of a family of extensin-like glycoproteins in the lumen of rhizobium-induced infection threads in pea root nodules. *Molecular Plant-Microbe Interactions* 15: 350-359

- Reiland S, Messerli G, Baerenfaller K, Gerrits B, Endler A, Grossmann J, Gruissem W, Baginsky S (2009) Large-scale *Arabidopsis* phosphoproteome profiling reveals novel chloroplast kinase substrates and phosphorylation networks. *Plant Physiology* 150: 889-903
- Reyes JC, Florencio FJ (1994) Transcription of glutamine synthetase genes (*glnA* and *glnN*) from the cyanobacterium *Synechocystis* sp. Strain PCC 6803 is differently regulated in response to nitrogen availability. *Journal of Bacteriology* 176: 1260-1267
- Ridge RW, Rolfe BG (1985) *Rhizobium* sp. Degradation of legume root hair cell wall at the site of infection thread origin. *Applied And Environmental Microbiology* 50: 717-720
- Riedel J, Tischner R, Mack G (2001) The chloroplastic glutamine synthetase (GS-2) of tobacco is phosphorylated and associated with 14-3-3 proteins inside the chloroplast. *Planta* 213: 396-401
- Rivers RL, Dean RM, Chandy G, Hall JE, Roberts DM, Zeidel ML (1997) Functional analysis of nodulin 26, an aquaporin in soybean root nodule symbiosomes. *Journal of Biological Chemistry* 272: 16256-16261
- Roberts DM, Tyerman SD (2002) Voltage-dependent cation channels permeable to  $\text{NH}_4^+$ ,  $\text{K}^+$ , and  $\text{Ca}^{2+}$  in the symbiosome membrane of the model legume *Lotus japonicus*. *Plant Physiology* 128: 370-378

Roche P, Debelle F, Maillet F, Lerouge P, Faucher C, Truchet G, Denarie J, Prome JC (1991) Molecular basis of symbiotic host specificity in *Rhizobium meliloti* *nodH* and *nodPQ* genes encode the sulfation of lipo-oligosaccharide signals. *Cell* 67: 1131-1143

Rose CM, Venkateshwaran M, Volkening JD, Grimsrud PA, Maeda J, Bailey DJ, Park K, Howes-Podoll M, den Os D, Yeun LH, Westphall MS, Sussman MR, Ane JM, Coon JJ (2012) Rapid phosphoproteomic and transcriptomic changes in the rhizobia-legume symbiosis. *Molecular & Cellular Proteomics* 11: 724-744

Rose LKM, Wang Z, Magrath GN, Hazard ES, Hildebrandt JD, Schey KL (2008) Aquaporin 0-calmodulin interaction and the effect of aquaporin 0 phosphorylation. *Biochemistry* 47: 339-347

Roth E, Jeon K, Stacey G (1988) Homology in endosymbiotic systems: The term 'symbiosome.'. In: R. Palacios, Verma DPS (eds) *Molecular Genetics of Plant Microbe Interactions*. American Phytopathological Society, St. Paul, MN, pp 220-225

Rubio MC, James EK, Clemente MR, Bucciarelli B, Fedorova M, Vance CP, Becana M (2004) Localization of superoxide dismutases and hydrogen peroxide in legume root nodules. *Molecular Plant-Microbe Interaction* 17: 1294-1305

Sakamoto A, Ogawa M, Masumura T, Shibata D, Takeba G, Tanaka K, Fujii S (1989) Three cDNA sequences coding for glutamine synthetase polypeptides in *Oryza sativa* L. *Plant Molecular Biology* 13: 611-614

Sakurai N, Hayakawa T, Nakamura T, Yamaya T (1996) Changes in the cellular localization of cytosolic glutamine synthetase protein in vascular bundles of rice leaves at various stages of development. *Planta* 200: 306-311

Sambrook J, Fritsch EF, Maniatis T (2001) Preparation and transformation of competent *E coli*. In: Chris N (ed) *Molecular Cloning: A Laboratory Manual*. Cold Spring Harbor Laboratory Press, Cold Spring Harbor Laboratory Press, NY, pp 82 - 83

Sanchez E, Avila-Quezada G, Gardea AA, Munoz E, Ruiz JM, Romero L (2009) Nitrogen metabolism in roots and leaves of green bean plants exposed to different phosphorus doses. *Phyton-International Journal of Experimental Botany* 78: 11-16

Sandal NN, Marcker KA (1988) Soybean nodulin 26 is homologous to the major intrinsic protein of the bovine lens fiber membrane. *Nucleic Acids Research* 16: 9347

Santos R, Herouart D, Sigaud S, Touati D, Puppo A (2001) Oxidative burst in alfalfa-*Sinorhizobium meliloti* symbiotic interaction. *Molecular Plant-Microbe Interactions* 14: 86-89

Schmittgen TD, Livak KJ (2008) Analyzing real-time PCR data by the comparative C-T method. *Nature Protocols* 3: 1101-1108



Schuck P (2000) Size-distribution analysis of macromolecules by sedimentation velocity ultracentrifugation and Lamm equation modeling. *Biophysical Journal* 78: 1606-1619

Seabra AR, Carvalho H, Pereira PJB (2009) Crystallization and preliminary crystallographic characterization of glutamine synthetase from *Medicago truncatula*. *Acta Crystallographica Section F-Structural Biology and Crystallization Communications* 65: 1309-1312

Seabra AR, Silva LS, Carvalho HG (2013) Novel aspects of glutamine synthetase (GS) regulation revealed by a detailed expression analysis of the entire GS gene family of *Medicago truncatula* under different physiological conditions. *BMC Plant Biology* 13

Sedlak J, Lindsay RH (1968) Estimation of total, protein-bound, and nonprotein sulfhydryl groups in tissue with Ellman's reagent. *Analytical Biochemistry* 25: 192-205

Seefeldt LC, Hoffman BM, Dean DR (2009) Mechanism of Mo-dependent nitrogenase. *Annual Review of Biochemistry* 78: 701-722

Shi ZD, Karki RG, Oishi S, Worthy KM, Bindu LK, Dharmawardana PG, Nicklaus MC, Bottaro DP, Fisher RJ, Burke TR (2005) Utilization of a nitrobenzoxadiazole (NBD) fluorophore in the design of a Grb2 SH2 domain-binding peptide mimetic. *Bioorganic & Medicinal Chemistry Letters* 15: 1385-1388

Sieberer BJ, Ketelaar T, Esseling JJ, Emons AM (2005) Microtubules guide root hair tip growth. *The New Phytologist* 167: 711-719

Sielberer BJ, Timmers ACJ, Emons AMC (2005) Nod factors alter the microtubule cytoskeleton in *Medicago truncatula* root hairs to allow root hair reorientation. *Molecular Plant-Microbe Interactions* 18: 1195-1204

Silva L, Carvalho H (2013) Possible role of glutamine synthetase in the NO signaling response in root nodules by contributing to the antioxidant defenses. *Frontiers in Plant Science* 4: 372

Simonovic AD, Anderson MD (2008) Light modulates activity and expression of glutamine synthetase isoforms in maize seedling roots. *Archives of Biological Sciences* 60: 649-660

Sivasankar S, Oaks A (1996) Nitrate assimilation in higher plants: The effect of metabolites and light. *Plant Physiology and Biochemistry* 34: 609-620

Sloan DJ, Hellinga HW (1998) Structure-based engineering of environmentally sensitive fluorophores for monitoring protein-protein interactions. *Protein Engineering* 11: 819-823

Socolow RH (1999) Nitrogen management and the future of food: Lessons from the management of energy and carbon. *Proceedings of the National Academy of Sciences of the United States of America* 96: 6001-6008

- Southern JA, Parker JR, Woods DR (1986) Expression and purification of glutamine synthetase cloned from *Bacteroides fragilis*. *Journal of General Microbiology* 132: 2827-2835
- Stal LJ, Severin I, Bolhuis H (2010) The ecology of nitrogen fixation in cyanobacterial mats. *Advances in Experimental Medicine and Biology* 675: 31-45
- Stanford AC, Larsen K, Barker DG, Cullimore JV (1993) Differential expression within the glutamine synthetase gene family of the model legume *Medicago truncatula*. *Plant Physiology* 103: 73-81
- Stewart GR, Mann AF, Fentem PA (1980) Enzymes of glutamate formation: Glutamate dehydrogenase, glutamine synthetase, and glutamate synthase. In: Mifflin BJ (ed) *The Biochemistry of Plants*. Academic Press, New York, pp 271-327
- Stitt M (1999) Nitrate regulation of metabolism and growth. *Current Opinion in Plant Biology* 2: 178-186
- Streeter JG (1989) Estimation of ammonium concentration in the cytosol of soybean nodules. *Plant Physiology* 90: 779-782
- Stroud RM, Fu DX, Libson A, Nollert P, Weitzman C, Miercke L, Krucinski J (2001) Structure of a glycerol conducting channel and the basis for its selectivity. *Biophysical Journal* 80: 246A-247A

Sui H, Han B-G, Lee JK, Walian P, Jap BK (2001) Structural basis of water-specific transport through the AQP1 water channel. *Nature* 414: 872-878

Swarbreck SM, Defoin-Platel M, Hindle M, Saqi M, Habash DZ (2011) New perspectives on glutamine synthetase in grasses. *Journal of Experimental Botany* 62: 1511-1522

Tabuchi M, Abiko T, Yamaya T (2007) Assimilation of ammonium ions and reutilization of nitrogen in rice (*Oryza sativa* L.). *Journal of Experimental Botany* 58: 2319-2327

Tabuchi M, Sugiyama K, Ishiyama K, Inoue E, Sato T, Takahashi H, Yamaya T (2005) Severe reduction in growth rate and grain filling of rice mutants lacking OsGS1;1, a cytosolic glutamine synthetase1;1. *Plant Journal* 42: 641-651

Teixeira J, Pereira S, Canovas F, Salema R (2005) Glutamine synthetase of potato (*Solanum tuberosum* L. cv. Désirée) plants: cell- and organ-specific expression and differential developmental regulation reveal specific roles in nitrogen assimilation and mobilization. *Journal of Experimental Botany* 56: 663-671

Temple SJ, Heard J, Ganter G, Dunn K, Sengupta-Gopalan C (1995) Characterization of a nodule-enhanced glutamine synthetase from alfalfa: Nucleotide sequence, *in situ* localization, and transcript analysis. *Molecular Plant-Microbe Interaction* 8: 218-227

Temple SJ, Kunjibettu S, Roche D, Sengupta-Gopalan C (1996) Total glutamine synthetase activity during soybean nodule development is controlled at the level of transcription and holoprotein turnover. *Plant Physiology* 112: 1723-1733

Timmers ACJ, Auriac MC, Truchet G (1999) Refined analysis of early symbiotic steps of the *Rhizobium-Medicago* interaction in relationship with microtubular cytoskeleton rearrangements. *Development* 126: 3617-3628

Tingey SV, Tsai FY, Edwards JW, Walker EL, Coruzzi GM (1988) Chloroplast and cytosolic glutamine synthetase are encoded by homologous nuclear genes which are differentially expressed in vivo. *Journal of Biological Chemistry* 263: 9651-9657

Tingey SV, Walker EL, Coruzzi GM (1987) Glutamine synthetase genes of pea encode distinct polypeptides which are differentially expressed in leaves, roots and nodules. *The EMBO Journal* 6: 1-9

Törnroth-Horsefield S, Yi W, Hedfalk K, Johanson U, Karlsson M, Tajkhorshid E, Neutze R, Kjellbom P (2006) Structural mechanism of plant aquaporin gating. *Nature* 439: 688-694

Tsuprun VL, Zograf ON, Orlova EV, Kiselev NA, Pushkin AV, Shiffelova GE, Solovieva NA, Evstigneeva ZG, Kretovich WL (1987) Electron microscopy of multiple forms of glutamine synthetase from bacteroids and the cytosol of yellow lupin root nodules. *Biochimica Et Biophysica Acta* 913: 368-376

Turgeon BG, Bauer WD (1985) Ultrastructure of infection-thread development during the infection of soybean by *Rhizobium japonicum*. *Planta* 163: 328-349

Tyerman SD, Whitehead LF, Day DA (1995) A channel-like transporter for  $\text{NH}_4^+$  on the symbiotic interface of  $\text{N}_2$ -fixing plants. *Nature* 378: 629-632

Udvardi M, Lister D, Day D (1991) ATPase activity and anion transport across the peribacteroid membrane of isolated soybean symbiosomes. *Archives of Microbiology* 156: 362-366

Udvardi M, Poole PS (2013) Transport and metabolism in legume-rhizobia symbioses. *Annual Review of Plant Biology* 64: 781-805

Udvardi MK, Day DA (1989) Electrogenic ATPase activity on the peribacteroid membrane of soybean (*Glycine max* L.) root nodules. *Plant Physiology* 90: 982-987

Udvardi MK, Day DA (1990) Ammonia (c-methylamine) transport across the bacteroid and peribacteroid membranes of soybean root nodules. *Plant Physiology* 94: 71-76

Udvardi MK, Day DA (1997) Metabolite transport across symbiotic membranes of legume nodules. *Annual Review of Plant Physiology and Plant Molecular Biology* 48: 493-525

Udvardi MK, Price GD, Gresshoff PM, Day DA (1988) A dicarboxylate transporter on the peribacteroid membrane of soybean nodules. *FEBS Letters* 231: 36-40

Unno H, Uchida T, Sugawara H, Kurisu G, Sugiyama T, Yamaya T, Sakakibara H, Hase T, Kusunoki M (2006) Atomic structure of plant glutamine synthetase: a key enzyme for plant productivity. *Journal of Biological Chemistry* 281: 29287-29296

van Rooyen JM, Abratt VR, Sewell BT (2006) Three-dimensional structure of a type III glutamine synthetase by single-particle reconstruction. *Journal of Molecular Biology* 361: 796-810

Vance CP, Gantt JS (1992) Control of nitrogen and carbon metabolism in root nodules. *Physiologia Plantarum* 85: 266-274

Verma DPS, Hong ZL (1996) Biogenesis of the peribacteroid membrane in root nodules. *Trends in Microbiology* 4: 364-368

Vessey JK, Pawlowski K, Bergman B (2005) Root-based N<sub>2</sub>-fixing symbioses: Legumes, actinorhizal plants, *Parasponia* sp and cycads. *Plant and Soil* 274: 51-78

Wagner SC (2011) Biological Nitrogen Fixation. *Nature Education Knowledge* 3:15-18

Walker JM (2009) The bicinchoninic acid (BCA) assay for protein quantitation. *Protein Protocols Handbook*, Third Edition: 11-15

Wallace IS, Choi W-G, Roberts DM (2006) The structure, function and regulation of the nodulin 26-like intrinsic protein family of plant aquaglyceroporins. *Biochim Biophys Acta - Biomembranes* 1758: 1165-1175

Wallace IS, Roberts DM (2004) Homology modeling of representative subfamilies of arabidopsis major intrinsic proteins. Classification based on the aromatic/arginine selectivity filter. *Plant Physiology* 135: 1059-1068

Walls-grove RM, Turner JC, Hall NP, Kendall AC, Bright SWJ (1987) Barley mutants lacking chloroplast glutamine synthetase - Biochemical and genetic analysis. *Plant Physiology* 83: 155-158

Wang Y, Schulten K, Tajkhorshid E (2005) What makes an aquaporin a glycerol channel? A comparative study of AqpZ and GlpF. *Structure* 13: 1107-1118

Weaver C, Shomer N, Louis C, Roberts D (1994) Nodulin 26, a nodule-specific symbiosome membrane protein from soybean, is an ion channel. *Journal of Biological Chemistry* 269: 17858-17862

Weaver CD, Crombie B, Stacey G, Roberts DM (1991) Calcium-dependent phosphorylation of symbiosome membrane proteins from nitrogen-fixing soybean nodules : Evidence for phosphorylation of nodulin-26. *Plant Physiology* 95: 222-227



Weaver CD, Roberts DM (1992) Determination of the site of phosphorylation of nodulin 26 by the calcium-dependent protein kinase from soybean nodules.

Biochemistry 31: 8954-8959

White J, Prell J, James EK, Poole P (2007) Nutrient sharing between symbionts.

Plant Physiology 144: 604-614

Whitehead LF, Day DA, Tyerman SD (1998) Divalent cation gating of an ammonium permeable channel in the symbiotic membrane from soybean nodules. The Plant Journal 16: 313-324

Whitehead LF, Tyerman SD, Day DA (2001) Polyamines as potential regulators of nutrient exchange across the peribacteroid membrane in soybean root nodules. Functional Plant Biology 28: 677-683

Woodall J, Forde BG (1996) Glutamine synthetase polypeptides in the roots of 55 legume species in relation to their climatic origin and the partitioning of nitrate assimilation. Plant Cell and Environment 19: 848-858

Wouters MA, Iismaa S, Fan SW, Haworth NL (2011) Thiol-based redox signalling: Rust never sleeps. International Journal of Biochemistry & Cell Biology 43: 1079-1085

Yamashita MM, Almasy RJ, Janson CA, Cascio D, Eisenberg D (1989) Refined atomic model of glutamine synthetase at 3.5Å resolution. Journal of Biological Chemistry 264: 17681-17690

Yang ZY, Danyal K, Seefeldt LC (2011) Mechanism of Mo-dependent nitrogenase. Nitrogen Fixation: Methods in Molecular Biology 766: 9-29

Yu XS, Jiang JX (2004) Interaction of major intrinsic protein (aquaporin-0) with fiber connexins in lens development. Journal of Cell Science 117: 871-880

Yu XS, Yin X, Lafer EM, Jiang JX (2005) Developmental regulation of the direct interaction between the intracellular loop of connexin 45.6 and the C terminus of major intrinsic protein (aquaporin-0). The Journal of Biological Chemistry 280: 22081-22090

Yuan CJ, Huang CYF, Graves DJ (1994) Oxidation and site-directed mutagenesis of the sulfhydryl groups of a truncated gamma catalytic subunit of phosphorylase-kinase. Functional and structural effects. Journal of Biological Chemistry 269: 24367-24373

Zhu MM, Zhu N, Song WY, Harmon AC, Assmann SM, Chen SX (2014) Thiol-based redox proteins in abscisic acid and methyl jasmonate signaling in *Brassica napus* guard cells. Plant Journal 78: 491-515

## **VITA**

Pintu D Masalkar was born in Pune, Maharashtra, India on 4<sup>th</sup> April, 1979. He started his graduate studies in the University of Pune in 1997 and secured Bachelor of Science degree in Microbiology in 2000. He continued his graduate studies in the University of Pune and secured Master of Science degree in 2004 in the field of Medical Biochemistry. After graduation, he worked as a biochemist in Poona Hospital and Research Center, Pune for 1 year and then moved on to work as a lecturer in MIMER Medical College, Talegaon Dabhade, for another 6 months.

He joined the University of Tennessee, Knoxville in January 2007 to pursue his Doctoral studies in the field of protein biochemistry. He joined Dr. Daniel Roberts laboratory at the University of Tennessee, Knoxville in May 2007 and started his work on cytosolic glutamine synthetase isoforms from soybean root nodules. His research contributed towards understanding the functional significance and regulation of glutamine synthetase isoforms from soybean root nodules.